Investigation of Changes in Glucose Homeostasis by Modulating Endothelial Permeability

Thanh Q. Dang

A thesis submitted to the Faculty of Graduate Studies in fulfillment of the requirements for the degree of

Master of Science

Graduate Program in Biology

York University

Toronto, Ontario

August 2017

Abstract

Altered permeability of the endothelial barrier in a variety of tissues has implications both in disease pathogenesis and treatment. Glucocorticoids are potent mediators of endothelial permeability and this forms the basis for their heavily-prescribed use as medications to treat ocular disease. However, the effect of glucocorticoids on endothelial barriers elsewhere in the body is less well-studied. Here we investigated glucocorticoid-mediated changes in endothelial flux of Adiponectin (Ad), a hormone with a critical role in diabetes. First, we used monolayers of endothelial cells in vitro and found that the glucocorticoid dexamethasone increased transendothelial electrical resistance and reduced permeability of polyethylene glycol (PEG, molecular weight 4000kDa). Dexamethasone reduced flux of Ad from the apical to basolateral side, measured both by ELISA and Western blotting. We then examined a diabetic rat model induced by treatment with exogenous corticosterone, which was characterized by glucose intolerance and hyperinsulinemia

Acknowledgements

I would like to express my appreciation to my principle supervisor Dr. Gary Sweeney, and co-supervisor Dr. Scott Kelly. Without their constant support this work would not have been possible. Thank you to Dr. Helen Chasiotis for mentoring me since the very first day I joined the lab.

Furthermore, I would like to express my gratitude to my committee members and advisor: Dr. Tara Haas, Dr. Rolando Ceddia, Dr. Robert Tsushima, and Dr. Michael Riddell for their time and support in the discussion and revision of my thesis.

Lastly, thank you to all past and current Sweeney Lab members. A special thank you to Stephanie Han, Dr. Amos Song, Michelle Prioriello, Diane Kishi, Dr. Subrata Chakrabarti, and Nanyoung Yoon for your help with the experiments for this project. Finally, thank you Esther Rai for editing my thesis.

Table of contents

List of Figures

Chapter 2- Study 1: Transendothelial movement of adiponectin is restricted by glucocorticoids

Chapter 3- Study 2: Modification of endothelium tightness by iron & the effects of iron on glucose metabolism

List of abbreviations

3-(4,55-Dimethylthiazol-2-yl)-2,5- Diphenyltetrazolium Bromide	MTT
5' AMP-activated protein kinase or AMPK	AMPK
Activator protein 1	AP-1
Acyl- coenzyme A	Acyl- CoA
Adaptor protein, phosphotyrosine interacting with PH domain and leucine zipper	APPL
Adenosine triphosphate	ATP
Adiponectin	Ad
Adiponectin receptor	AdipoR
Adipose	adipo
Beta cell	β - cells
Body mass index	BMI
c-Jun amino- terminal kinases	JNK
cAMP response element-binding protein	CREB
Carbon dioxide	CO2
Carnitine palmitoyltransferase I	CPT1
Comprehensive Lab Animal Monitoring System	CLAMS
Cortisone	Cort
Cyan fluorescent protein	CFP
Cyclic AMP-dependent transcription factor	ATF3
Dexamethasone	Dex
Dimethyl sulfoxide	DMSO

enzyme-linked immunosorbent assay	ELISA
Epididymal	epi
Extracellular signal–regulated kinases	ERK
Fatty-acid-binding protein 3	FABP3
Ferroportin	FPN
G- protein- coupled receptor	GPR40
Gastrocnemius muscle	Gastroc
Globular adiponectin	gAd
Glucocorticoid	GC
Glucocorticoid receptor	GR
Glucocorticoid response elements	GRE
Glucose Tolerance Test	GTT
Glycogen synthase kinase 3	GSK3β
Hemojuvelin	HJV
Hereditary hemochromatosis	HH
High Fat	HF
High molecular weight	HMW
Human Dermal Microvascular Endothelial Cells	HDMEC
Human embryonic kidney	HEK
Human hemochromatosis	HFE
Hydrogen Peroxide	H_2O_2
Inhibitor kappa B kinase	IKK
Insulin	Ins

Insulin receptor substrade-1	IRS- 1
Insulin receptor substrate-2	IRS-2
Insulin Tolerance Test	ITT
Insulin- like growth factor 1	IGF- 1
Insulin-regulated glucose transporter	GLUT4
Interleukin-6	IL-6
Iron overload	IO
Iron response element	IRE
Knockout	KO
Ligand-activated nuclear hormone receptor alpha/ gamma	PPARα/γ
Low molecular weight	LMW
Mammalian target of rapamycin	mTOR
Metabolic syndrome	MetS
Middle molecular weight	MMW
Mitogen- activated protein kinases	MAPK
Mothers against decapentaplegic	SMAD
Non Tf- bound iron	NTBI
Non- esterified fatty acids	NEFA
Nuclear factor kappa-light-chain-enhancer of activated B cells	NFkb
Nuclear factor of activated T-cells	NFAT
Nuclear factor- kB	NF-kB
Obese mice	db/ db
Oxidative stress	OS

Oxygen	O2
Palmitoytransferase- 1	CPT-1
Peritoneal	peri
Peroxisome proliferator activated receptor y	PPARy
Phen Green SK	PGSK
Phosphate-buffered saline	PBS
Phosphatidylinositol-3-OH kinase	PI3K
Phospho-Protein Kinase β (Thr308)	pAkt
Phosphoenolpyruvate carboxykinase	PEPCK
Phosphorylation	p
Phosphotyrosine-binding domain	PTB
PI(d)K/ protein kinase-β	PKB
polyacrylamide gel electrophoresis	PAGE
Protein kinase c	PKC
Reactive oxygen species	ROS
Respiratory Exchange Ratio	RER
Retinol- binding protein-4	RBP4
Six transmembrane protein of prostate 2	STAMPS
Soleus	Sol
Subcutaneous fat	Subcu
Tf receptor	TfR1
Thiazolidinedione	TZD
Tibialis anterior muscle	TA

Tight junction	TJ
Transferrin	Tf
Tumor necrosis factor α	TNF- α
Visceral fat	Vis
Wild- type	WT

Chapter 1: Review of Literature

1.1 Diabetes introduction

1.1.1 Types of diabetes and their prevalence

Diabetes mellitus is a chronic disease that is a major global health concern due to its increasing prevalence. Statistics generated by the Canadian Diabetes Cost Model estimated that diabetes affected approximately 3.4 million Canadians in 2015 (an estimated 9.3% of Canadian population). Moreover, the model projected an increase to 5 million patients by 2025, which accounts for approximately 12.1% of the population. From a national survey of individuals aged 20 years and older, nearly 5.7 million individuals (22.1% population) are at risk of developing diabetes, and the number is projected to increase to 6.4 million (23.2%) by 2025.

Diabetes has significant impacts on government funding. In 1999, the Canadian Diabetes Strategy (CDS) was created with an initial funding of $115 million for 5 years to focus on diabetes awareness programs. However, in 2005, the government increased its budget by 80% to $18 million per year (Leung, 2016). The budget increase focused on expanding public education of diabetes prevention and management of its complications. Another diabetes-related policy and program at the federal level focuses on increasing awareness of diabetes among the First Nations people, since they are considered as high-risk communities. The initial funding of $58 million for a period of five years from 1999-2004 was expanded to $190 million for 2010-2015 (Leung, 2016). The funds mentioned above exclude costs that are associated with treatment of long-term complications of diabetes. People with diabetes are three times more likely to be hospitalized than those with cardiovascular disease, at a 12 times greater risk for end-stage renal disease, and a 20 times

greater risk for lower limb amputation when compared to the general population (Booth and Cheng, 2013).

As of late 2015, research from the University of Toronto School of Public Health indicated that each diabetic patient costs the healthcare system about $16000 over eight years as compared to approximately $6000 for people who do not have diabetes (Rosella et al., 2016). Therefore, the expenditure for diabetic care has a significant monetary impact on the Canadian health care system.

1.1.2 Metabolic Syndrome

Metabolic syndrome (MetS) is a common and complex disorder clustering hypertension, obesity, dyslipidemia, and insulin resistance. Diabetes mellitus is the most common and widely studied metabolic syndrome. Diabetes mellitus is characterized by an alteration in carbohydrate metabolism leading to hyperglycemia with symptoms that include polyuria, polydipsia, and weight loss. There are 2 main types of diabetes: type 1 and type 2 diabetes mellitus. Type 1 diabetes caused by destruction of pancreatic β cells, resulting in disrupted and ultimately deficient insulin secretion. Type 2 diabetes is characterized by insulin resistance, which is initially compensated for by increased insulin secretion but ultimately β cell failure occurs leading to hyperglycemia. In addition to type 1 and 2 diabetes, gestational diabetes occurs during pregnancy when the body naturally becomes more resistant to insulin. Gestational diabetes is not permanent, and blood sugar will typically returns to normal after birth. However, gestational diabetes can potentially increase the risk of type 2 diabetes in the future.

Type 2 diabetes is the most prevalent type of diabetes, accounting for nearly 90% of the diabetic population worldwide. There are many risk factors for type 2 diabetes

including pregnancy, genetics (defects in insulin secretion), age, race, diet, and lack of physical activity. However, the best predictor for type 2 diabetes is obesity. The number of obese individuals is growing at an alarming rate. From a Canadian government survey of the population aged 18 years and older between 2003 and 2014, approximately 8.2 million (62%) men and 6.1 million (46%) women had an increased health risk due to excess body weight. The number of obese individuals had increased from 57% in men and 41% in women prior to the 2003 survey (Shields, 2006). Notably, excessive visceral obesity is closely associated with the rising incidence of type 2 diabetes (Ford, 2005; Yusuf et al., 2005).

1.2 **Diabetes pathophysiology**

1.2.1 Proposed mechanisms responsible for development of diabetes (whole body)

As mentioned above, obesity is a key risk factor for the emergence of type 2 diabetes. Adipose tissue regulates glucose metabolism by releasing various adipokines. In association with obesity, retinol-binding protein-4 (RBP4) is released and induces insulin resistance through reduced phosphatidylinositol-3-OH kinase (PI3K) signalling in muscles and enhanced glucose production in the liver by increased expression of the glyconeogenic enzyme phosphoenolpyruvate carboxykinase (PEPCK) (Yang et al., 2005). Studies have shown an increased release of tumour necrosis factor α (TNF-α), interleukin-6 (IL-6), and monocyte chemoattractant protein-1 (MCP-1) from adipose tissue, which suggests macrophage infiltration might have a role in the development of insulin resistance (Fain et al., 2004; Wellen and Hotamisligil, 2005). Other studies have shown that macrophage infiltration into white adipose tissue is increased in association with obesity (Weisberg et al., 2003; Xu et al., 2003b).

The increase in non-esterified fatty acids (NEFA) levels observed in obesity and type 2 diabetes may be responsible for inducing insulin resistance and impairing β-cell function (Boden, 1997; Reaven et al., 1988). An increase in NEFA levels causes the intracellular accumulation of fatty acid metabolites such as fatty acyl-coenzyme A (fatty acyl-coA) and diacylglycerol (DAG), which activate a serine/threonine kinase cascade (*e.g.* protein kinase C) leading to phosphorylation of insulin receptor substrate-1 (IRS-1) and insulin receptor substrate-2 (IRS-2), preventing the receptors' ability to activate downstream signaling via PI3K. Hence, downstream insulin-receptor signaling is diminished (Shulman, 2000). Previous studies have shown that increased serine/threonine phosphorylation of IRS-1 and IRS-2 can significantly reduce their ability to interact with the insulin receptor, and impair insulin-induced tyrosine phosphorylation on the receptor β-subunit, affecting propagation of insulin signaling in Fao cells (Paz et al., 1997; Paz et al., 1996). Furthermore, NEFAs can also bind to the G-protein-coupled receptor GPR40 on the cell membrane to activate glucose-stimulated insulin secretion in β-cells, or generate fatty acyl-CoA and DAG, which will increase insulin levels through stimulating insulin granule exocytosis from β-cells (Itoh et al., 2003; Prentki et al., 2002).

β-cells are known for their ability to regulate insulin release, which ensures plasma glucose concentrations to remain within a healthy range. Increased levels of glucose induce insulin release from the secretory granules in the β-cells by increasing intracellular ATP (Wilcox, 2005). The adaptive response to insulin resistance involves changes in both function and mass of β-cells. Studies have demonstrated that obesity can alter β-cell function as well as cell volume. A study using mice fed on a high-fat diet (12 months) to induce obesity and insulin resistance has found an increase in islet size rather than new

islet formation to accommodate for increased secretory demand (Hull et al., 2005). Human studies have also suggested that obese individuals are prone to hypertrophy of existing β-cells rather than cell proliferation, with volume increasing around 50% (Butler et al., 2003; Kloppel et al., 1985). It has been proposed that activation of the insulin-like growth factor 1 (IGF-1) receptor leads to phosphorylation of IRS-2, and activation of PI3K/protein kinase-B (PKB/Akt) and Ras, leading to the activation of the mitogen-activated protein (MAP) kinases ERK-1/2. All of these pathways promote β-cell proliferation, tissue regeneration, and survival. In IRS-2 knockout mice, reintroduction of β-cell IRS-2 alone can increase β-cell replication and cell mass, hence reversing the diabetic phenotype. Therefore, the IGF-1 pathway is important for regulation of β-cell mass (Bernal-Mizrachi et al., 2001; Rhodes, 2005; Rui et al., 2001).

1.2.2 Skeletal muscle and glucose metabolism

Skeletal muscle has been identified as a major site for insulin-stimulated glucose disposal, and hence is a main locus of insulin resistance. Studies have shown that an intramuscular triglyceride pool exists within human skeletal muscle as a source of energy (Dagenais et al., 1976). Studies utilizing a high fat diet-fed rat model suggested that the increase in triglyceride storage within the muscles is clearly associated with impairment in insulin-stimulated glucose metabolism, as assessed by euglycemic clamp (Storlien et al., 1991). They concluded high triglyceride accumulation impaired insulin action.

The inability of adipose tissue to store excess energy results in elevated release of free fatty acids, causing metabolic dysregulation. The mitochondria have been postulated to be key regulators of insulin resistance development. Mitochondria are known for their role in energy production; it is the site of oxidative phosphorylation that couples the

electron transfer from respiratory substrates to oxygen with ATP synthesis. The respiratory chain involves four protein complexes on the inner mitochondrial membrane. Complexes I and II transfer electrons to ubiquinone, then to complex III, cytochrome c, complex IV, and finally to oxygen (Navarro and Boveris, 2007). There are several theories regarding the relationship between mitochondrial dysfunction and insulin resistance. Early studies in obese and insulin-resistant individuals have shown a mitochondrial dysfunction phenotype (Kelley et al., 1999). One study proposed that the loss of mitochondrial content or function resulted in insufficient fatty acid oxidation and excessive lipids in circulation, leading to an intracellular accumulation of fatty acyl-coA and DAG in skeletal muscles that interfere with insulin signalling (Lowell and Shulman, 2005). Further studies demonstrated that in type 2 diabetes patients, skeletal muscles exhibited lower respiratory chain activity due to the reduction in the expression of genes encoding mitochondrial enzyme subunits (Kelley et al., 2002; Mootha et al., 2003; Patti et al., 2003; Ritov et al., 2010).

1.2.3 Insulin signalling

The insulin receptor (IR) is a transmembrane glycoprotein belonging to the receptor tyrosine kinases family. It is composed of α- and β- subunits linked by disulfide bonds. The α-subunits serve as the extracellular binding site for insulin, whereas the β-subunits contain the insulin-regulated tyrosine kinase activity responsible for initiating the signalling cascade (Ullrich et al., 1986). The signalling pathway begins with the interaction between insulin and the α-subunit of the insulin receptor on the cell surface (Fig. 1). This interaction leads to the stimulation of tyrosine kinase activity on the receptor β-subunit. The phosphotyrosine-binding (PTB) domain of the insulin receptor substrate (IRS) recognizes the activation of IR, subsequently leading to the phosphorylation of tyrosine residues on

IRS. Phosphorylated IRS is recognized by the Src homology 2 (SH2) domain on the p85 regulatory subunit of PI3-kinase, further leading to the activation of PI3K. PI3K facilitates the translocation of the insulin-responsive glucose transporter (GLUT4) towards the plasma membrane. The link between PI3K and glucose transport is not completely understood. However, several studies suggest that PI3K activation is mediated by the recruitment and activation of 3-phosphoinositide-dependent kinases (PDK), and the subsequent phosphorylation of serine/threonine kinase (Akt). Akt has several downstream substrates including protein kinase C (PKC) and glycogen synthase kinase 3 (GSK3) (Bandyopadhyay et al., 1997; Bandyopadhyay et al., 1999). Furthermore, clinical studies have demonstrated obesity and type 2 diabetes both exhibit reduced IRS-1 tyrosine phosphorylation and reduced PI3K activity by inhibitor kappa B kinase (IKK) and c-Jun amino-terminal kinases (JNK) (Aguirre et al., 2000).

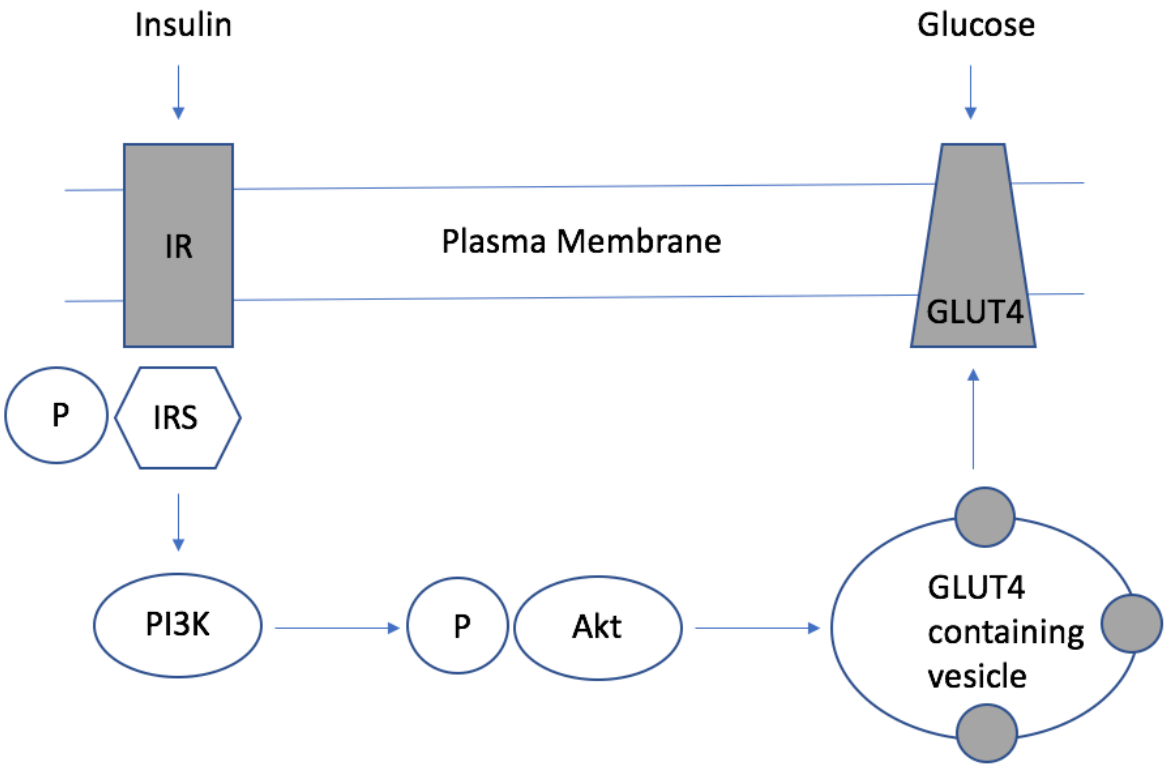

Figure 1: *Insulin signaling pathway in skeletal muscles. The signalling pathway begins with the interaction between insulin and the α-subunit of the insulin receptor on the cell surface (Fig. 1). The interactions lead to the stimulation of tyrosine kinase activity on the receptor β-subunit. The phosphotyrosine-binding (PTB) domain of the insulin receptor substrate (IRS) recognizes the activation of IR, subsequently leading to the phosphorylation of tyrosine residues on IRS. Phosphorylated IRS is recognized by the Src homology 2 (SH2) domain on the p85 regulatory subunit of PI3-kinase, further leading to the activation of PI3K. Through a series of additional steps, PI3K facilitates the translocation of the insulin-responsive glucose transporter (GLUT4) towards the plasma membrane.*

1.3 **Glucocorticoids**

1.3.1 Association of glucocorticoids with diabetes

Glucocorticoid (GC) is a natural hormone secreted by the adrenal cortex under the control of the neuroendocrine feedback system for the regulation of circadian rhythms and stress. Exposure to GCs in large amounts during treatment for disorders such as Cushing syndrome or mental stress induces insulin resistance (Buren and Eriksson, 2005; Ruzzin et al., 2005). Skeletal muscles, adipose tissue, and liver were found to be insulin resistant after GC treatment (Witchel and DeFranco, 2006)

1.3.2 GC receptor and control of energy homeostasis

The glucocorticoid receptor (GR) is crucial for the survival of mice, as GR knockout was found to be lethal (Cole et al., 1995). In the absence of a GR-ligand, this nuclear receptor stays within the cytosol as part of a multi-protein chaperone complex. Upon hormone binding, the GR translocates to the nucleus and binds directly to DNA at

glucocorticoid response elements (GREs) on target genes (Schoneveld et al., 2004). The concentration of GC in the blood generally rises during stress, fasting, conditions of decreased glucose uptake in muscles and fat, or during gluconeogenesis in the liver to maintain normal blood glucose levels (Makimura et al., 2003; Munck et al., 1984)

High levels of glucocorticoid were found in conditions of obesity, hypertension and impaired glucose homeostasis (Bjorntorp and Rosmond, 2000; Lemke et al., 2008). In fact, an increase in GR activity leads to lower protein and insulin synthesis in skeletal muscles (Vegiopoulos and Herzig, 2007). Studies from cultured muscle fibres treated with Dexamethasone (Dex) were found to have lower GLUT4 translocation, and reduced glycogen synthase activation, leading to the conclusion that Dex diminished glucose uptake under insulin-stimulated conditions (Dimitriadis et al., 1997; Weinstein et al., 1998)

1.3.3 Use of GC as an anti-inflammatory and immunosuppressive drug

Under normal conditions, GCs have the ability to inhibit inflammatory responses. GCs inhibit the vasodilation and vascular permeability that occurs during inflammation, and decreases leukocyte accumulation into the inflamed sites. The result is an acute reduction in inflammatory events (Perretti and Ahluwalia, 2000). Additionally, in the long term, GCs bind to the GR to regulate NF-κB and AP-1 transcription in leukocytes (Ashwell et al., 2000), or repress transcription of pro-inflammatory related cytokines, chemokines, and cell adhesion molecules that are involved in the initiation of the host inflammatory response (Smoak and Cidlowski, 2004).

1.3.4 Glucocorticoid-induced diabetes models

Rats injected with Dex were found to have decreased insulin-stimulated Akt phosphorylation at both Ser^{473} and Thr^{308} sites (Buren et al., 2008). In rat L6 myotubes

treated with Dex, a reduction in insulin receptor substrate (IRS-1) protein and PI3K/Akt signalling were also observed (Zheng et al., 2010).

Long term usage of GCs potentially lead to adverse side effects such as osteoporosis, chronic interstitial nephritis, retinopathy, and diabetes (Kessing et al., 2010; Perneger et al., 1994; Wolfe and Marmor, 2010; Yang et al., 2006). In senior patients, the risk of diabetes doubled after 1 year of exposure to GCs (Blackburn et al., 2002). Moreover, 38% of young people who are chronically treated with steroids have undergone regular monitoring for diabetes (Blackburn et al., 2002) (Panthakalam et al., 2004).

1.4 Iron and diabetes risk

1.4.1 Association between iron and metabolic syndrome

The connection between iron and metabolism is well established. To examine the link between iron and diabetes, a group of researchers generated human hemochromatosis protein knockout (HFE KO) mice, which exhibited impaired glucose-stimulated insulin secretion and increased β-cell apoptosis (Cooksey et al., 2004). The crosstalk between iron metabolism and diabetes has also been demonstrated by Tanner and Lienhard, who observed co-localization of transferrin receptors and glucose transporters on the membrane of adipocytes *in vitro*. Their study suggested that the regulation of iron occurs in parallel with its effects on glucose transport (Tanner and Lienhard, 1989). Increased iron storage is associated with the development of type 2 diabetes (Fernandez-Real et al., 2002). Ferritin is one of the key proteins regulating iron homeostasis and it is a widely used clinical biomarker of iron status. Clinical studies have shown that higher serum ferritin levels were found in patients with metabolic syndrome and insulin resistance. Thus, high iron level is

associated with increased risk of type 2 diabetes, suggesting it may be a prevalent cause of diabetes (Moreno et al., 2015)

Thalassemia is a disorder characterized by a deficiency in the β-globin subunit of hemoglobin. Patients become overloaded with iron from increased iron absorption, because the patients' body is unable to maintain normal erythrocyte levels in the blood to uptake the iron that is taken up by the gut (Weatherall, 1998). Clinical studies on thalassemia have also found that these patients have insulin deficiency and resistance, which may lead to a prediabetic state and the development of diabetes (Messina et al., 2002).

1.4.2 Iron homeostasis

Serum and tissue iron levels are regulated by hepcidin. Hepcidin promotes internalization and ubiquitin-mediated degradation of ferroportin (FPN), an iron exporter. Hepcidin therefore inhibits iron release and reduces circulating iron levels, but accumulates iron in tissues. The main source of iron for most cells is through the uptake of transfferin (Tf)-bound iron and its receptor (TfR1). Tf is a protein produced by the liver that binds to iron molecules. Tf enters and is redistributed to the cells via TfR1, which is internalized through clatherin-mediated endocytosis. The circulating ferric form of iron is released, and the Tf-TfR1 complex is recycled back to the cell membrane where the complex is separated. Hepcidin is not normally involved in the regulation of iron release unless Tf is saturated, leading to the formation of non Tf-bound iron (NTBI). When Tf is saturated and NTBI is formed, the free cellular iron is toxic and redox-active.

1.4.3 Iron overload in humans (e.g., Hereditary hemochromatosis)

Although type 2 diabetes is largely attributed to the obesity epidemic, the underlying genetic cause of this metabolic syndrome is unknown. Hereditary

hemochromatosis (HH) is an autosomal recessive disorder characterized by excess iron concentration in the body. The most common form of this disease is caused by a mutation in the HFE gene resulting in a C282Y substitution in the HFE protein. The HFE protein is responsible for iron metabolism by acting as an iron sensor for the body to regulate iron absorption in the small intestine, and the recycling of iron by macrophages (Feder et al., 1996). While HFE normally functions through the stimulation of hepcidin, a mutation in HFE causes a decline in hepcidin expression, resulting a higher than normal iron absorption (Nemeth et al., 2004). Mutation in HFE was thought to be an adaptive response in populations with an iron-deficient diet (Toomajian et al., 2003). Clinical studies have demonstrated HH patients cannot respond to increased insulin secretion demand primarily due to the β -cell pathology. In these patients, insulin sensitivity will improve after phlebotomy therapy to achieve iron depletion. Hence, these patients are at a higher risk to develop diabetes (Abraham et al., 2006; McClain et al., 2006).

1.4.4 Iron overload – animal models

An alteration in iron homeostasis allows uncontrolled iron entry to different organs, progressively leading to tissue damage and organ failure. To study this phenomenon, many laboratories have created a genetic knockout model of hemojuvelin (HJV), a membrane protein that acts as a co-receptor in the SMAD pathway to regulate hepcidin expression. Hepcidin is a key regulator of iron metabolism that works by binding to the iron export channel ferroportin, the resulting inhibition of iron transport results in an iron overload. Iron accumulation and morphological damage of the retina has been shown in mice with HJV deletion (Gnana-Prakasam et al., 2012). Moreover, a murine iron overload model was achieved by HJV deletion in combination with dietary iron supplement and iron injection.

It increased oxidative stress and myocardial fibrosis, resulting in heart disease (Das et al., 2015).

1.4.5 Iron overload and glucose metabolism

The liver is the major site of iron storage in the body as transferrin-bound iron is taken up by hepatocytes via TfR1. When excess iron is stored in the liver it interferes with glucose metabolism and causes hyperinsulinemia (Niederau et al., 1984). Insulin enhances the uptake of extracellular iron by inducing expression of TfRs at the cell surface, as well as down regulating the expression of hepcidin (Davis et al., 1986; Wang et al., 2014).

1.4.6 Physiological effects of iron

Iron is an essential nutrient that plays an important role as a cofactor for fuel oxidation and electron transport, as well as being required for normal cellular structure and functions such as cell growth and proliferation (Gozzelino and Arosio, 2016). However, excessive amounts of iron could be toxic if not carefully regulated. Iron, combined with Hydrogen Peroxide (H_2O_2), generates various Reactive Oxygen Species (ROS) through the Fenton reaction. This process causes oxidation of organic pollutants such as pesticides (Mirzaei et al., 2017). In rodent models, changes in iron homeostasis led to uncontrolled iron entry and deposition in skeletal muscles, and progressively caused insulin resistance, a key contributor to diabetes (Huang et al., 2011)

1.4.7 Cellular effects of iron

Oxidative stress has long been known to be a major causal factor for diabetes and its complications. For example, elevated ROS reduced metabolite clearance in patients with chronic renal failure (Toborek et al., 1992). Free radicals also disrupt tight junction (TJ) function by altering the cell-cell adherence properties of TJ proteins, and by inducing

reorganization of the actin filament network (Wichmann et al., 2015; Won et al., 2011). Another study suggested that iron overload in mice led to elevated ROS. Interestingly, iron overload was associated with decreased levels of TJ structural proteins occludin and zonula occludens 1 (ZO-1), and hence caused a disruption in TJ structure, resulting in increased permeability of hippocampal endothelial cells isolated from TFI-induced iron overloaded rats. Endothelial dysfunction contributes to the pathogenesis of atherosclerosis in diabetes (Handa et al., 2016; Won et al., 2011). Furthermore, previous research has found that inflammation coexisting with increased oxidative stress occurs in end-stage renal disease (Raj et al., 2005). ROS enters human skeletal muscles and activates an inflammatory cascade via activation of nuclear factor-kB (NF-κB), as well as upregulation of expression of various cytokines, including interleukin- 6 and 10 (IL- 6, 10) and TNF-α, in response to stimuli. The impaired glucose tolerance is associated with increased serum concentrations of these cytokines (Muller et al., 2002)

1.5 Adiponectin

1.5.1 Association of adiponectin with diabetes

The adipose tissue is an endocrine organ that secretes various adipokines to mediate metabolic effects (Valencak et al., 2017). Adiponectin (Ad) is one such adipokine, and its gene is located on a chromosome that has been identified as a diabetes-susceptible locus in genome-wide association studies (Mori et al., 2002; Vionnet et al., 2000). Hence, it is theorized to be a diabetes-related hormone. Ad is a 30kD protein that is primarily secreted by adipocytes and circulates abundantly in the blood stream at 3-30 μg/ml. The adiponectin protein must undergo post-translational modification before being secreted into the circulation (Dadson et al., 2011). Ad can exist as a full-length protein, or as a globular

fragment. The monomers can form trimers (low molecular weight (LMW) form), hexamers (medium molecular weight (MMW) form), and higher order oligomers (high molecular weight (HMW) form). The mixture of these different oligomeric forms is termed full length Ad (fAd). The globular form of Ad is generated during the posttranslational modification of fAd, and is smaller, consisting of the carboxyl-terminal domain, but it can also mediate biological effects (Dadson et al., 2011).

Many studies have recognized the role that a reduction in adiponectin action has in the metabolic syndrome and obesity-related diseases. The level of circulating adiponectin has an inverse relationship with BMI, plasma glucose, and serum triglycerides (Ouchi et al., 2011), and it is significantly reduced in obese/diabetic mice and humans (Hu et al., 1996; Yamauchi et al., 2001). Furthermore, Ad mRNA expression is down regulated in *db/db* obese diabetic mice (Hu et al., 1996). Thus, a reduction in circulating adiponectin levels is consistently observed in conditions associated with insulin resistance. Two main mechanisms that have been proposed for impaired adiponectin action in tissues are: 1) decrease circulating levels of adiponectin, or 2) reduced adiponectin sensitivity, both of which may promote inflammation in obesity and diabetic conditions, as adiponectin has potent anti-inflammatory effects (Yamauchi and Kadowaki, 2013).

1.5.2 Regulation of adiponectin production

Adiponectin is the product of the APM1 gene, which has been mapped to the human chromosome 3q27 locus, a diabetes-susceptible site. The gene is under transcriptional regulation by peroxisome proliferator activated receptor γ (PPARγ). It is a ligand-activated transcription factor belonging to the nuclear family of receptors. PPARγ deletion in mice reduces circulating adiponectin levels, hence diminishing adiponectin's antidiabetic and

cardioprotective effects. An increase in PPARγ activity increases adiponectin levels in the circulation. The most well-known and commonly used anti-diabetic drugs, such as rosiglitazone, belong to the thiazolidinedione (TZD) class of drugs. These drugs work to enhance insulin sensitivity and lower blood glucose levels by increasing adiponectin levels through PPARγ activation (Maeda et al., 2001). In contrast to PPARγ, cAMP response element-binding protein (CREB) has been identified as a repressor of adiponectin gene expression. This transcription factor is indirectly responsible for hyperglycemia and insulin resistance by down regulation of adiponectin through upregulation of ATF3, a gene repressor. (Kim et al., 2006). TNF-α is a pro-inflammatory cytokine that is known to suppress upstream adiponectin signalling through inhibition of PPARγ, and preventing SP-1 promotor binding, hence decreasing gene expression as well as reducing signalling cascades (Park et al., 2008).

1.5.3 Adiponectin signalling

The adiponectin signalling cascade is initiated by the interaction of circulating adiponectin with its transmembrane adiponectin receptor isoforms AdipoR1/R2. The receptors have seven transmembrane domains with an intracellular N-terminus and an extracellular C-terminus (Lee et al., 2008). It has been suggested that these receptors get phosphorylated at the tyrosine site and undergo conformational changes to initiate the signalling cascade. AdipoR1 is most abundant in the skeletal muscles and has a higher affinity for gAd as compared to fAd. The liver mainly expresses AdipoR2. Adaptor protein phosphotyrosine interacting with PH domain and leucine zippers 1 (APPL1) is an adaptor protein that interacts with the N-terminal intracellular domain of AdipoR1/R2 through its PTB domain (Lee et al., 2011). APPL1 has been shown to interact with the p110 catalytic

subunit and p85 regulatory subunit of PI3K, and also with Akt (Backer, 2010). Hence, APPL1 is a key adaptor protein responsible for the crosstalk between adiponectin and the insulin signalling pathway. Translocation of the glucose transporter GLUT4 to the cell surface was diminished in APPL1 knockdown in a skeletal muscle cell model (Dadson et al., 2011). Other than its role in mediating the insulin-sensitizing effects of adiponectin, the signalling cascades activated by APPL1 are also known for roles in cell proliferation, chromatin remodeling, and cell survival (Liu et al., 2017)

AMP-activated protein kinase (AMPK) is a downstream target of AdipoR/APPL1 signalling. AMPK belongs to the family of energy sensing enzymes that are activated by ATP depletion. Fatty acid uptake and oxidation is the primary energy source for cardiac cells, a process which is upregulated by Ad. Conversely, Ad also suppresses fatty acid synthesis through the activation of AMPK, p38 MAPK and PPARα. AMPK phosphorylation is critical for the activation of palmitoytransferase-1 (CPT-1), a mitochondrial outer membrane protein responsible for transporting long chain fatty acids (LCFAs) into the mitochondria. In its dephosphorylated and activated state, acetyl CoA carboxylase (ACC) produces malonyl-CoA, which inhibits CPT-1 activity and prevents the mitochondrial import of LCFAs. However, AMPK phosphorylates and deactivates ACC and releases the inhibition of CPT-1, allowing LCFAs to be transported into the mitochondria for oxidation (Yoon et al., 2006).

PPARα (a ligand-activated nuclear hormone receptor) controls the expression of a number of genes involved in mitochondrial β-oxidation such *ACO*, *CPT1*, and *FABP3* for the generation of energy from fatty acid oxidation in the liver, heart, kidney, and skeletal muscles (Rodriguez et al., 1994). Studies using PPARα knockout mice have demonstrated

defects in fatty acid oxidation, resulting in elevated plasma free fatty acid levels and hypothermia (Hashimoto et al., 2000; Kersten et al., 1999).

p38 mitogen-activated protein kinase p38 MAPK is activated by inflammatory cytokines and has an important role in initiating an immune response upon metabolic stress (e.g. muscle contraction, ischemia). These physiological conditions are similar to those associated with AMPK activation, suggesting possible crosstalk between the AMPK and p38 MAPK signalling pathways (Hayashi et al., 2000).

1.5.4 Physiological effects of adiponectin

The physiological significance of Ad as an insulin-sensitizing adipokine is well established. Although adipocytes are the main source of circulating Ad, several studies have now demonstrated the potential for Ad production by skeletal muscles (Liu et al., 2009). Since skeletal muscle is the main site for glucose disposal in the body, it makes sense for it to be an important peripheral target tissue for Ad to exert its metabolic effects, and indeed has proved to be a site of Ad's anti-diabetic action. Cultured mouse and rat skeletal muscle cells demonstrate enhanced glucose uptake with Ad treatment (Ceddia et al., 2005; Yamauchi et al., 2002). Furthermore, administration of Ad to ob/ob mice was shown to reverse hyperglycemia (Xu et al., 2003a)

1.6 Transport of hormones across vascular endothelium

1.6.1 Structure and function of vascular endothelium

A monolayer of endothelial cells lines the entire circulatory system of the body. This endothelium acts as a barrier which regulates the exchange of hormones, proteins, and small molecules between the vascular compartment and the interstitial space (Goddard and Iruela-Arispe, 2013; Pries and Kuebler, 2006). The actions of a hormone or nutrient on a

target tissue are implicitly dependent upon the ability of these factors to gain access to the target. Numerous studies have indicated that hormone and nutrient concentrations in blood differ from those surrounding cells on the tissue side of the blood vessel endothelium (Barrett et al., 2011; Bodenlenz et al., 2005; Chiu et al., 2009; Chiu et al., 2008; Herkner et al., 2003; Kolka et al., 2010; Maggs et al., 1995; Sjostrand et al., 1999; Yang et al., 1994). In this regard, it is our contention that the significance of the endothelium as a regulator of hormone and substrate access to target tissues is often underappreciated. Two distinct pathways can regulate endothelial permeability: 1) the transcellular pathway, where solutes are actively transported across the endothelium, primarily via caveolae-mediated transcytosis; or 2) the paracellular pathway, where solutes passively move through the intercellular space between adjacent endothelial cells.

1.6.2 Transcellular and paracellular transport

The transcellular movement of solutes involves energy-dependent trafficking of vesicles across the endothelium (Goddard and Iruela-Arispe, 2013). This often requires their recognition by receptors in caveolae on the luminal surface of the endothelium, though it may also involve vesiculo-vacuolar organelles, or occur via transcellular channels (Goddard and Iruela-Arispe, 2013). Caveolae are cholesterol- and sphingolipid-rich non-clathrin-coated pits, and are abundant in endothelial cells. After ligand binding to receptors in caveolae, dynamin-mediated endocytosis occurs, followed by vectorial transport and fusion of the vesicle with the basolateral plasma membrane, resulting in the release of contents by exocytosis (Goddard and Iruela-Arispe, 2013). As a general concept, transcellular vesicle trafficking is important in the transport of larger macromolecules

across the endothelium, since the paracellular route is typically restricted to passaging of solutes smaller than 3 nm in radius (Gunzel and Fromm, 2012; Gunzel and Yu, 2013).

The paracellular mode of transport across the endothelium depends upon concentration gradients between blood and interstitial fluid. One regulatory mechanism of paracellular movement involves tight junctions (TJs), which are composed of strands of transmembrane and cytosolic proteins that closely control paracellular flux and have been established to be important in regulating hormone transport (Gunzel and Yu, 2013; Kolka and Bergman, 2012; Kolka et al., 2010). As a component of the cell-cell junctions between endothelia, TJs provide a selective barrier to solute movement between cells (Gunzel and Fromm, 2012). The perm-selectivity of the TJ barrier is dependent on the variable assemblage of TJ proteins that comprise the complex. Proteins such as occludin, tricellulin, and claudins directly establish the TJ barrier and form the backbone of TJ strands while the cytosolic proteins, such as ZO-1, provide structural support to the TJ complex. The incorporation of specific TJ protein isoforms can enhance TJ barrier function (i.e., make TJs tighter) or form channels to increase TJ permeability (i.e., make TJs leakier) (Gunzel and Fromm, 2012). Importantly, skeletal muscle and heart vasculature have continuous endothelium with TJs between cells (Aird, 2007a, b). However, the liver and spleen have a discontinuous endothelium with large holes, which allow rapid equilibration of plasma with the underlying tissue (Aird, 2007a, b). It was suggested that this expedited exposure of the liver to plasma solute changes, due to its characteristic fenestrated endothelium, may partly explain its earlier susceptibility to insulin resistance (Braet and Wisse, 2002; Kim et al., 2003).

1.6.3 Endothelial dysfunction in diabetes

Impaired vascular endothelial function is an early marker for atherosclerosis, which causes cardiovascular complications. The concept of endothelial dysfunction in diabetes is well established (Ding and Triggle, 2010). However, this typically refers to vascular functions independent of transendothelial solute flux. The endothelium is also a dynamic interface that responds to various stimuli, and synthesizes and liberates vasoactive molecules such as nitric oxide, prostaglandins and endothelin. Accordingly, vascular complications in diabetes include outcomes occurring in large (atherosclerosis, cardiomyopathy) and small (retinopathy, nephropathy, neuropathy) vessels (Symons and Abel, 2013). We believe that diabetes-induced deleterious alterations in paracellular solute movement also represent a form of endothelial dysfunction which should be fully characterized to establish its physiological significance.

1.7 **Research objectives/ hypothesis & specific aims**

As described above, regulation of the permeability of the endothelial barrier is an important way in which hormone access to the target tissue is controlled. I hypothesized that targeting tight junctions to alter endothelial permeability could control adiponectin flux, and consequently its cellular and physiological functions. To test this hypothesis, the following objectives were established:

Objective 1: Test whether using glucocorticoids to increase tightness of endothelial tight junctions could restrict adiponectin flux and action.

Aim 1: Use the synthetic glucocorticoid Dex to modify Human Umbilical Vein Endothelial Cells (HUVEC) tightness and test for changes in permeability of adiponectin.

Aim 2: Test mechanisms underlying changes observed in Aim 1: examine changes in endothelial tight junction components using Western blot and mRNA. Examine adiponectin flux in HUVEC where claudin-7 expression was reduced using shRNA.

Aim 3: Determine the effect of glucocorticoid Corticosterone (Cort) on the expression of adiponectin, its receptors, and tight junction components in rats treated with Cort.

Objective 2: Investigate whether iron could change endothelium tightness and alter metabolism

Aim 1: Test whether iron directly modifies Human Dermal Microvascular Endothelial Cell (HDMEC) permeability and adiponectin flux.

Aim 2: Using a mouse model of iron overload, test whether insulin sensitivity and glucose clearance was altered.

Aim 3: Determine tissue-specific effects and molecular mechanisms responsible for changes in glucose metabolism and activity using comprehensive lab animal monitoring system and western blotting.

Statement of Contribution

Chapter 2: T. Dang contributed to planning and conducting experiments, except for the [^{3}H]PEG-4000 and real-time PCR experiments performed by H. Chasiotis. Samples from the animal model of diabetes induced by exogenous corticosterone were obtained from E. Dunford. This chapter was co-written by H. Chasiotis, edited by Dr. G. Sweeney, and is published in the *Journal of Endocrinology*.

Chapter 2: Study 1

Transendothelial movement of adiponectin is restricted by glucocorticoids

1.1 Abstract

Altered permeability of the endothelial barrier in a variety of tissues has implications both in disease pathogenesis and treatment. Glucocorticoids are potent mediators of endothelial permeability and this forms the basis for their heavily-prescribed use as medications to treat ocular disease. However, the effect of glucocorticoids on endothelial barriers elsewhere in the body is less well-studied. Here we investigated glucocorticoid-mediated changes in endothelial flux of Adiponectin (Ad), a hormone with a critical role in diabetes. First, we used monolayers of endothelial cells *in vitro* and found that the glucocorticoid dexamethasone increased transendothelial electrical resistance and reduced permeability of polyethylene glycol (PEG, molecular weight 4000kDa). Dexamethasone reduced flux of Ad from the apical to basolateral side, measured both by ELISA and Western blotting. We then examined a diabetic rat model induced by treatment with exogenous corticosterone, which was characterized by glucose intolerance and hyperinsulinemia. There was no change in circulating Ad but less Ad protein in skeletal muscle homogenates, despite slightly higher mRNA levels, in diabetic versus control

muscles. Dexamethasone-induced changes in Ad flux across endothelial monolayers were associated with alterations in the abundance of select claudin (CLDN) tight junction (TJ) proteins. shRNA-mediated knockdown of one such gene, *claudin-7*, in HUVEC resulted in decreased TEER and increased adiponectin flux, confirming the functional significance of Dex-induced changes in its expression. In conclusion, our study identifies glucocorticoid-mediated reductions in flux of Ad across endothelial monolayers *in vivo* and *in vitro*. This suggests that impaired Ad action in target tissues, as a consequence of reduced transendothelial flux, may contribute to the glucocorticoid-induced diabetic phenotype.

1.2 Introduction

As the primary barrier to the movement of circulating endocrine factors from the bloodstream to the interstitial space, the endothelium plays a critical role in hormone action (Kolka and Bergman, 2012; Yoon et al., 2014). Endothelial permeability can significantly impact hormone action by preventing or delaying access of the hormone to target tissues (Kolka and Bergman, 2012; Won et al., 2011). Transendothelial solute movement can occur via the transcellular pathway where solutes are transported across the endothelium cell membrane *or* via the paracellular pathway where solutes passively move through the intercellular space between adjacent endothelial cells (Yoon et al., 2014) .Previous work has shown that hormone and nutrient concentrations in blood differ from surrounding cells on the tissue side of the blood vessel endothelium (Barrett et al., 2011; Herkner et al., 2003; Yang et al., 1994).Of note, this has been best documented in the case of insulin where concentrations of the hormone are significantly lower in the target tissue than in the circulation (Kolka and Bergman, 2012).

Glucocorticoids are among the most commonly prescribed anti-inflammatory and immunosuppressive medications worldwide (Clark and Belvisi, 2012). They are also commonly used in oncology treatment (Lin and Wang, 2016) and for the treatment of macular edema and, more recently, retinopathy (Agarwal et al., 2015; Zhang et al., 2014). However, glucocorticoids have been shown to have potent effects on restricting endothelial transport (Felinski and Antonetti, 2005; Witt and Sandoval, 2014) and they contribute to the development of diabetes at least in part by increasing hepatic glucose production and reducing GLUT4 translocation in muscle (Beaudry et al., 2015) . Yet despite these observations, the potential importance of glucocorticoid-induced alterations in the transendothelial flux of circulating glucoregulatory hormones such as Ad is unclear.

Ad is one of the most abundant plasma proteins and exists in three different isoforms: low molecular weight (LMW; trimer), medium molecular weight (MMW; hexamer) and high molecular weight (HMW; oligomer) (Dadson et al., 2011). Ad has important and beneficial anti-diabetic, anti-inflammatory and cardioprotective actions (Arita et al., 2002; Dadson et al., 2011). Ad levels, in particular HMW, are decreased in obese individuals and this correlates with development of associated complications, including diabetes and cardiovascular disease (Kadowaki et al., 2006; Peters et al., 2013). Transendothelial movement of Ad across the blood-brain barrier (BBB) into cerebrospinal fluid (CSF) was studied and only LMW and MMW were found in the CSF, suggesting that passage of HMW complexes were restricted (Kubota et al., 2007; Kusminski et al., 2007; Neumeier et al., 2007). This may be functionally significant since HMW Ad is often considered to be the most biologically active and physiologically relevant form (Dadson et al., 2011; Nanayakkara et al., 2012). A recent study calculated the Stokes radii for the Ad

oligomers and found that endothelial barriers controlled Ad transport in a cell- and tissue-specific manner (Rutkowski et al., 2014). Thus, emerging evidence suggests that Ad action may be at least in part mediated by endothelial transport, although whether this is influenced by glucocorticoid-induced changes in transendothelial permeability remains unknown.

Given the large size of Ad multimers it seem likely that transendothelial Ad movement is an important variable in determining it presence within, and action on, target tissues. Therefore we hypothesized that glucocorticoid-induced alterations in transendothelial permeability will modulate the transendothelial movement of Ad. In this regard, the objective of this study was to examine how glucocorticoid treatment of a cultured endothelium influences Ad flux in association with changes in permeability and apical junction protein abundance as well as investigate Ad content within the skeletal muscle in a diabetic rat model induced by exogenous glucocorticoid treatment. The overall goal of this work was to significantly advance our understanding of the glucocorticoid-induced diabetic phenotype by determining whether Ad movement out of the circulatory system might play a role in its pathogenesis.

1.3 Material and Methods

1.3.1 *HUVEC cell culture and treatments*

Normal primary human umbilical vein endothelial cells (HUVECs; Pooled, PCS-100-013) were obtained from ATCC (Manassas, VA, USA) and grown at 37°C and 5% CO_2 on uncoated T75 flasks in vascular cell basal medium (ATCC, PCS-100-030) containing 10% fetal bovine serum (FBS), VEGF endothelial cell growth kit (ATCC, PCS-100-041) and treated with DEX using 2% FBS (both medium were prepared without hydrocortisone

hemisuccinate), 100 units/mL penicillin and 100 μg/mL streptomycin. Cells were kept frozen in medium containing 10% DMSO (Bio-Rad Laboratories Canada Ltd., Mississauga, ON, Canada). For experiments, passage 3 was used. Cells were counted using a haemocytometer and seeded onto permeable polyethylene terephthalate (PET) filters at the base of BD Falcon cell culture inserts (BD Biosciences, Mississauga, ON, Canada) at a density of 0.5 x 10^6 cells/insert.

Dexamethasone (DEX) was obtained from Sigma-Aldrich (Oakville, ON, Canada), and full-length Ad was produced in-house using a mammalian expression system (i.e. HEK 293 cells) according to methods described by (Wang et al., 2002; Xu et al., 2004). HUVECs were treated for 5 days with DEX (1 μM) starting 24 h after seeding cells into inserts, HUVECs were treated with DEX added to both apical and basolateral sides of inserts at concentrations indicated above

1.3.2 shRNA-mediated knockdown of claudin-7 in HUVEC

We used pGPU6/Neo-claudin-7 shRNA vector with target sequence (5'-GGCCATCAGATTGTCACAGAC-3') (GenePharma Co., Ltd., Shanghai, China). These were transfected into HUVEC using Lipofectamine™ 3000 Reagent (Invitrogen, Carlsbad, CA, USA) exactly according to manufacturer's protocol. Non-specific scrambed target sequence shRNA vector was used as control. Following selection with 50 ug/ml Neomycin (Sigma-Aldrich, Oakville, ON, CA) for 24 hours, cells were seeded onto inserts for analysis of TEER, examining adiponectin flux or preparation of cell lysates to confirm claudin-7 knock-down.

2.3.3 Transendothelial electrical resistance (TEER),and [^{3}H]PEG4000 and Adflux

TEER was measured daily using chopstick electrodes (STX-2) connected to an EVOM voltohmmeter (World Precision Instruments, Sarasota, FL, USA). As a measure of paracellular permeability, apical to basolateral flux rates of [^{3}H] polyethylene glycol at 1 μCi; 1 h flux(molecular mass 4000 Da; PEG-4000; PerkinElmer, Woodbridge, ON, Canada)or Ad (10 μg/mL; 24 h flux) to apical culture medium were determined across HUVEC endothelia. [^{3}H]PEG-4000 in basolateral culture medium was detected using a liquid scintillation counter, Ad was detected using a mouse Ad ELISA kit (Antibody Immunoassay Services, Hong Kong) or Western blot. Permeability measurements were expressed according to calculations previously outlined by (Wood et al., 1998).

2.3.4 Quantitative real-time PCR analysis

Total RNA was isolated from control and DEX-treated HUVECs and from soleus skeletal muscle using TRIzol Reagent . Extracted RNA was then treated with DNase I and first-strand cDNA was synthesized using SuperScript III reverse transcriptase and oligo(dT)$_{12\text{-}18}$ primers (Life Technologies Inc.,Manassas MA, USA). Quantitative real-time PCR (qRT-PCR) analyses were conducted using gene specific primers. SYBR Green I Supermix (Bio-Rad Laboratories Canada Ltd.Mississauga, ON, Canada) and a Chromo4 Detection System (CFB-3240; Bio-Rad Laboratories Canada Ltd.) Samples were run in duplicate. For all qRT-PCR analyses, TJ protein mRNA expression was normalized to GAPDH transcript abundance. For the expression profile, TJ protein transcripts were expressed relative to occludin mRNA. For TJ protein transcripts that were not detected in HUVECs, normal human adult kidney cDNA was obtained (BioChain Institute, Inc., Newark, CA, USA) and used as a positive control in qRT-PCR reactions. Agarose gel

electrophoresis verified single qRT-PCR products at predicted amplicon sizes from positive control reactions.

2.3.5 Animal model of diabetes induced by exogenous corticosterone treatment

We used a well-established hyperinsulinemic/hyperglycemic rodent model of chronic glucocorticoid treatment (Beaudry et al., 2013; Beaudry et al., 2015; D'Souza A et al., 2012; Shikatani et al., 2012; Shpilberg et al., 2012). Upon experiment cessation, the tibialis anterior (TA) and soleus skeletal muscles were excised and immediately frozen in liquid N_2 and kept at -80^{o}C until future analysis.

2.3.6 Measurement of hydraulic conductivity (Lp) in individually perfused rat mesenteric microvessel

Female Sprague-Dawley rats of 220 to 250 g (2 to 3 mo old, Sage Laboratory Animal, PA) were used for the experiments. All procedures and animal use were approved by the Animal Care and Use Committee at Pennsylvania State University. Inactin hydrate (Sigma) was used for anesthesia and given subcutaneously at 170 mg/kg body weight. Microvessel permeability was assessed by measuring Lp in individually perfused microvessels, which measures the volume of water flux across the microvessel wall. Details have been described previously (Yuan and He, 2012; Yuan et al., 2014).

2.3.7 Immunohistochemistry of Ad and dystrophin in skeletal muscle

Tibialis anterior (TA) from Control and CORT treated rats were cryostat sectioned (10 μm thick) for analysis of muscle Ad content. Sections were stained as previously described (Krause et al., 2008). Quantification was performed using Zen 2.0 software. The total Ad and dystrophin signal was determined bythe sum of red/green signal intensity obtained arbitrary values in the field of view. Diagram view intensity was recorded by the software

in form of histograms. Intracellular quantification was done on Ad images (without dystrophin), images were changed to 8-bits on Image and the arbitrary intensity was calculated as mean intensity per area.

2.3.8 Western blot analysis

Control and DEX-treated HUVECs, and L6 or H9C2 cells treated with HUVEC-conditioned medium and soleus skeletal muscle were lysed in sample buffer (80 mMTris-HCl (pH 6.8), 2% (w/v) SDS, 20% glycerol, 3.3% (v/v) β-mercaptoethanol 0.01% w/v bromophenol blue) containing protease and phosphatase inhibitors (3 mM EDTA, 10 uM E64, 1 mM Na_3VO_4, 1 μM leupeptin, 1 μM pepstatin A, 1 μM okadaic acid and 200 μM PMSF). Apical and basolateral HUVEC-conditioned media collected from Ad flux experiments were concentrated with Amicon Ultra-4 Centrifugal Filter Units with Ultracel-30 membranes (EMD Millipore, Billerica, MA, USA) and subjected to nondenaturing, nonreducing conditions to allow the analysis of the different forms of Ad (HMW >250 kDa, MMW ~180 kDa, and LMW ~90 kDa). Primary antibodies specific for the following proteins: T-cadherin (1:1000, R&D Systems), occludin (OCLN, 1:3000), tricellulin (TRIC, 1:3000), claudin-7 (CLDN-7, 1:500), CLDN-10 (1:800), CLDN-11 (1:1000), phospho-AMPKα (Thr172) (1:1000), phospho-p38 MAPK [pT180/pY182] (1:1000), Ad (1:1000),β-actin (1:1000). OCLN, TRIC, CLDN-7, CLDN-10 and phospho-p38 MAPK [pT180/pY182] antibodies were obtained from Life Technologies, CLDN-11 and Ad antibodies were purchased from EMD Millipore and Signalway Antibody (College Park, MD, USA) respectively, and phospho-AMPKα (Thr172) and β-actin antibodies were obtained from Cell Signaling Technology (New England Biolabs Ltd., Whitby, ON, CA). Protein detection using enhanced chemiluminescence (Bio-Rad) and quantification by

densitometry using ImageJ analysis software. TJ protein expression was normalized to β-actin, Tubulin protein abundance.

2.3.9 Statistical analysis

All data are expressed as mean values ± SEM. A one-way analysis of variance (ANOVA) followed by a Student-Newman-Keuls test was used to determine significant differences ($P \leq 0.05$) between groups. When appropriate, a Student's t-test was also used. All statistical analyses were conducted using Prism 5, Excel SigmaStat 3.5 softwares.

2.4 Results

2.4.1 Dexamethasone induces endothelial tightening and inhibits Ad movement across endothelial cell monolayers

We first investigated the effect of dexamethasone (DEX), a synthetic glucocorticoid, on tightness of an endothelial monolayer of HUVECs. Addition of DEX to culture media significantly elevated TEER (Fig. 1A) and correspondingly reduced the endothelial permeability of the paracellular transport marker [^{3}H]PEG-4000 (Fig. 1B). Similar trends regarding permeability were observed in microvessels of DEX-treated rats. DEX treatment (n = 4) did not cause a significant reduction in baseline Lp compared to normal control group (n = 6), but lowered the mean value from 1.5 ± 0.1 to 1.1 ± 0.2 ($\times 10^{-7}$ cm/s/cm H_2O). When each vessel was exposed to platelet activating factor (PAF, 10 nM) that is known to cause transient increases in Lp(Zhou and He, 2011), microvessels in DEX-treated rats showed significantly attenuated Lp response. The mean peak Lp value was reduced from 11.1 ± 1.8 (normal control) to 6.0 ± 0.4($\times 10^{-7}$ cm/s/cm H_2O, Figure 1C). We then assessed flux of Ad from the apical to basolateral side of HUVEC monolayer and found a reduced total amount of Ad in basolateral media after DEX treatment (Fig. 1D-F). When monitoring

absolute flux rates in control cells, Ad flux rate was 4.4 ± 0.12 cm s^{-1} x 10^{-9} which significantly decreased after DEX treatment to 3.2 ± 0.30cm s^{-1} x 10^{-9} (Fig. 1D). Following a 24 h flux period, Ad levels detected in basolateral media were 64.8 ± 5.7 ng/mL. Using Western blotting to examine various oligomeric forms of Ad LMW (~90 kDa), MMW (~180 kDa) and HMW (>250 kDa), we found that flux of all forms was reduced by DEX (Fig. 1E&F). Additionally, the functional activity of Ad appearing in basolateral media was confirmed by using this media to treat L6 skeletal muscle cells and H9C2 cells derived from rat heart ventricle. In both cell types the media increased AMPK phosphorylation (supplementary Figure 1A-B)

2.4.2 Dexamethasone treatment alters transcript and protein abundance of select TJ proteins in HUVEC monolayers

A tissue expression profile of transcripts encoding 26 TJ proteins in HUVECs revealed the presence of 15 (Fig. 2A). The most abundant transcript was found to be *CLDN-11*, while *CLDN-7, CLDN-12* and *ZO-1* exhibited relatively high abundance and *OCLN, TRIC, CLDN-10* and *CLDN-15* exhibited moderate levels of abundance (Fig 2A). Transcripts not detected in HUVECs included *CLDN-3, -4, -5, -8, -9, -16, -17, -18, -19, -23* and *-25* (Fig. 2A & Supplementary figure 1C). Human kidney cDNA was used as a positive control for transcripts that were not detected in HUVECs (Supplementary figure 1C). To explore the response of TJ proteins to DEX- treatment, we first compared mRNA abundance of expressed target genes in HUVECs. DEX increased *CLDN-6* mRNA abundance while *CLDN-2, -20, -22, -24* and *ZO-1* mRNA showed significant decreases (Fig. 2B). DEX treatment had no significant effect on mRNA encoding *OCLN*, *TRIC, CLDN-1, -7, -10, -11 -12* and *-15*(Fig. 2B). Following DEX treatment, the protein abundance of CLDN-1, -

7, -11 and ZO-1 was examined and found to be significantly upregulated following DEX treatment when compared to the control group (Fig. 2C, D). On the other hand, CLDN-10 protein levels were significantly decreased when compared with the expression in control conditions (Fig. 2C, D). In order to validate the functional significance of Dex-induced changes in expression of tight juntion proteins we used shRNA to target claudin-7 and this effectively reduced its expression by 71% on average (Fig. 3A). Furthermore, HUVEC with reduced levels of claudin-7 showed reduced TEER and a small but significant increase in flux of adiponectin from apical to basolateral side (Figs 3B-D).

2.4.3 Examination of changes in transcellular endothelial flux

The possible contribution of transcellular receptor-mediated Ad movement across HUVEC monolayers was then investigated by analysis of expression levels of three identified Ad receptors. Intracellular Ad content in these cells was detected, although at low level, and expression levels did not change significantly with DEX treatment (Fig. 4A). However, DEX significantly increased T-cadherin protein abundance (Fig. 4B), but had no effect on protein abundance of AdipoR1 and AdipoR2 (Fig. 4C).

2.4.4 Skeletal muscle Ad content in a rat model of exogenous glucocorticoid-induced diabetes

We then examined whether the increased endothelial cell barrier tightness observed after DEX treatment would be paralleled in a diabetic rodent model of chronic glucocorticoid exposure. As expected based on previously published work (D'Souza A et al., 2012; Shikatani et al., 2012; Shpilberg et al., 2012), two weeks of exogenous corticosterone (CORT) treatment resulted in severe fasting hyperinsulinemia and impaired glucose tolerance (Supp Fig 2A). In addition, CORT treatment caused mild/moderate

elevations in fasted blood glucose concentrations (5.12± 0.2 mM to 8.3 ± 1.88 mM, Supp Fig 2B) despite the significantly increased fasted insulin concentrations (0.76±0.25 ng/ml to 4.68±0.72 ng/ml , Supp Fig 2C). CORT treatment also caused a change in skeletal muscle fibre type composition; a switch from predominantly slow to fast-twitch skeletal muscle fibers, within the tibialis anterior muscle (Supp Fig 2D).

To explore whether CORT-treatment affects circulating Ad levels, we measured plasma Ad levels in these animals before CORT pellet implantation and at 7 days post pellet implantation, at 0800h. Circulating Ad levels were unaffected by CORT treatment (Fig 5. A). Interestingly, there was an apparent elevation in skeletal muscle Ad mRNA levels (Fig 5. B), yet Ad protein content was significantly reduced (Fig 5. C&D). Upon immunohistochemical analyses, we also observed that the total amount of Ad was decreased in skeletal muscle from the COR-treated rats versus control rats (Fig 5. E-H). Dystrophin, was used to assess the structural integrity of the skeletal muscle and was unaffected by CORT treatment. Representative images are shown (Fig 5. E) with quantification of the total and intracellular Ad signal (Fig 5. G-H). Since CORT-treatment is known to preferentially target fast-twitch skeletal muscle (Beaudry et al., 2015), representative images accordingly depict smaller IIb/x fiber area (Supp Fig. 2D) within the CORT-treated rats. CORT-treatment was also found to cause a significant reduction in individual myocyte size (Fig. 5F).

2.4.5 AdipoR abundance in a rat model of exogenous glucocorticoid-induced diabetes

Both Ad receptor isoforms (*AdipoR1* and *AdipoR2*) genes were expressed in rat soleus skeletal muscle and although an apparent increase in *AdipoR1* mRNA abundance was seen in the diabetic rat model, neither was significantly altered (Fig. 6 A,B). However,

a significantly increased level of ADIPO-R1 protein (approximately 3.4 fold compared to the control) was seen (Fig. 6F). There were no changes in ADIPO- R2 nor in T- Cadherin protein levels (Fig. 6E, G).

2.4.6 CORT treatment altered Tight Junction genes in rat soleus skeletal muscle after 2 weeks

We then measured changes in mRNA abundance of tight junction, *Cldn-1, -2, -3, -4,-5, -6, -7, -9, -10, -11, -12, -24,-14, -15, -19, -20, -22, -23* and *Ocln, T*ricand *Z0-1* were found to be no significant changes with in diabetic rat skeletal muscle (Fig. 6C), with only *Cldn -5, -10, -11, -22* significantly decreased (Fig. 6D).

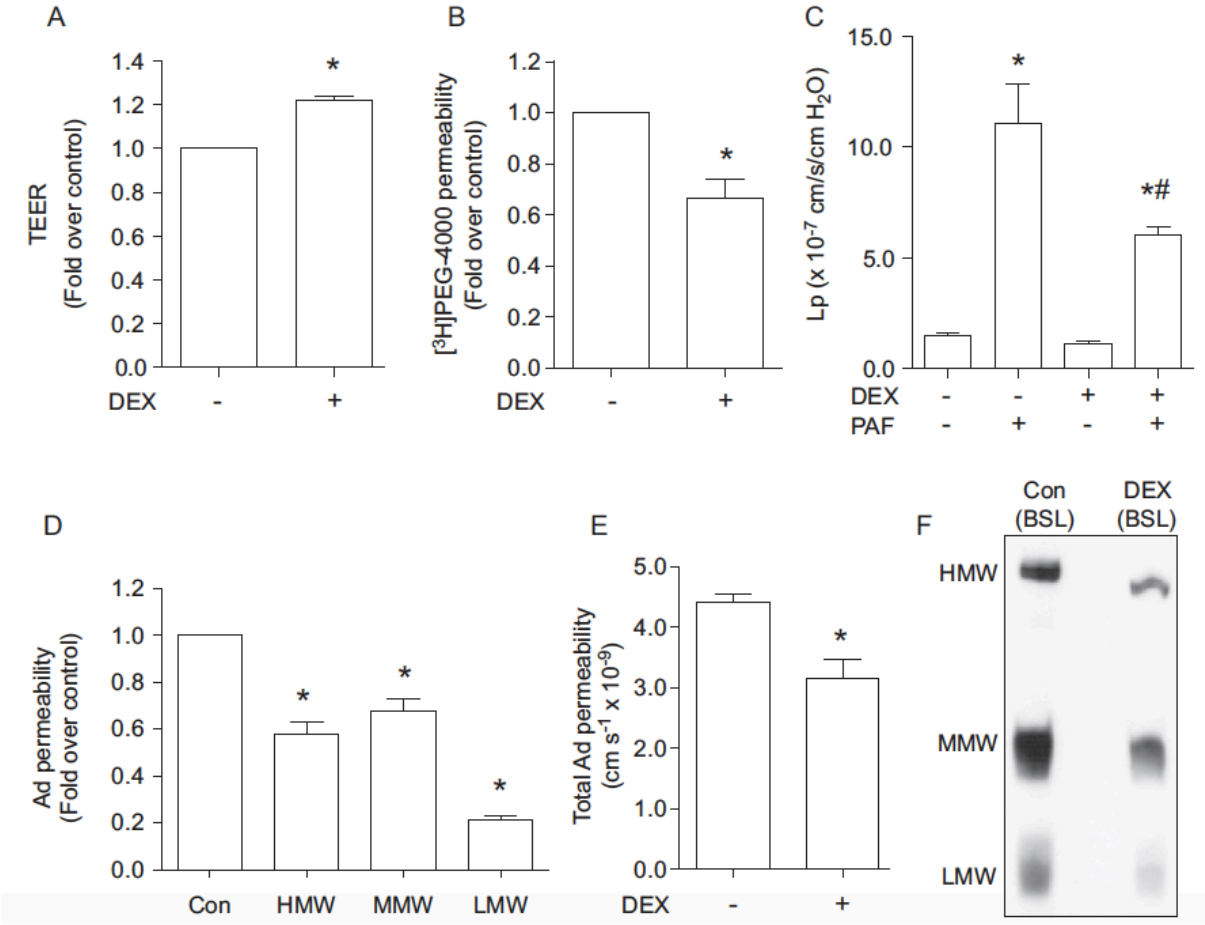

Figure 1: *Effects of DEX on permeability. HUVECs (Human Umbilical Vein Endothelial Cell) were seeded onto permeable polyethylene terephthalate (PET) filters and treated with or without 1μM of DEX every other day in both top and bottom of compartments. Tightness of the monolayer was measured on the 5th day of DEX treatment. A) Transendothelial Electrical Resistance (TEER). B) [^{3}H]PEG-4000 permeability across HUVEC monolayer. C) Measurements of hydraulic conductivity (Lp) in individually perfused mesenteric venulesfrom normal (n = 6) and Dex-treated(n = 4) rats. DEX treatment significantly attenuated the Lp responses to PAF that was known to cause transient increases inLp. D-F) 10 μg of full-length Ad was added onto the apical side. After 24 hrs, the medium on basolateral was collected. D) Total Ad amount was quantified using ELISA. E) The collected basolateral medium was concentrated and separated by PAGE. 3 forms of Ad are labeled as LMW (~90 kDa), MMW (~180 kDa), HMW (>250 kDa). F) Representative Western blot for full-length Ad flux across control and Dex-treated monolayers. Data are expressed as mean values ± SEM (n = 4-8). *Significant difference (P ≤ 0.05) from control (Con) group.*

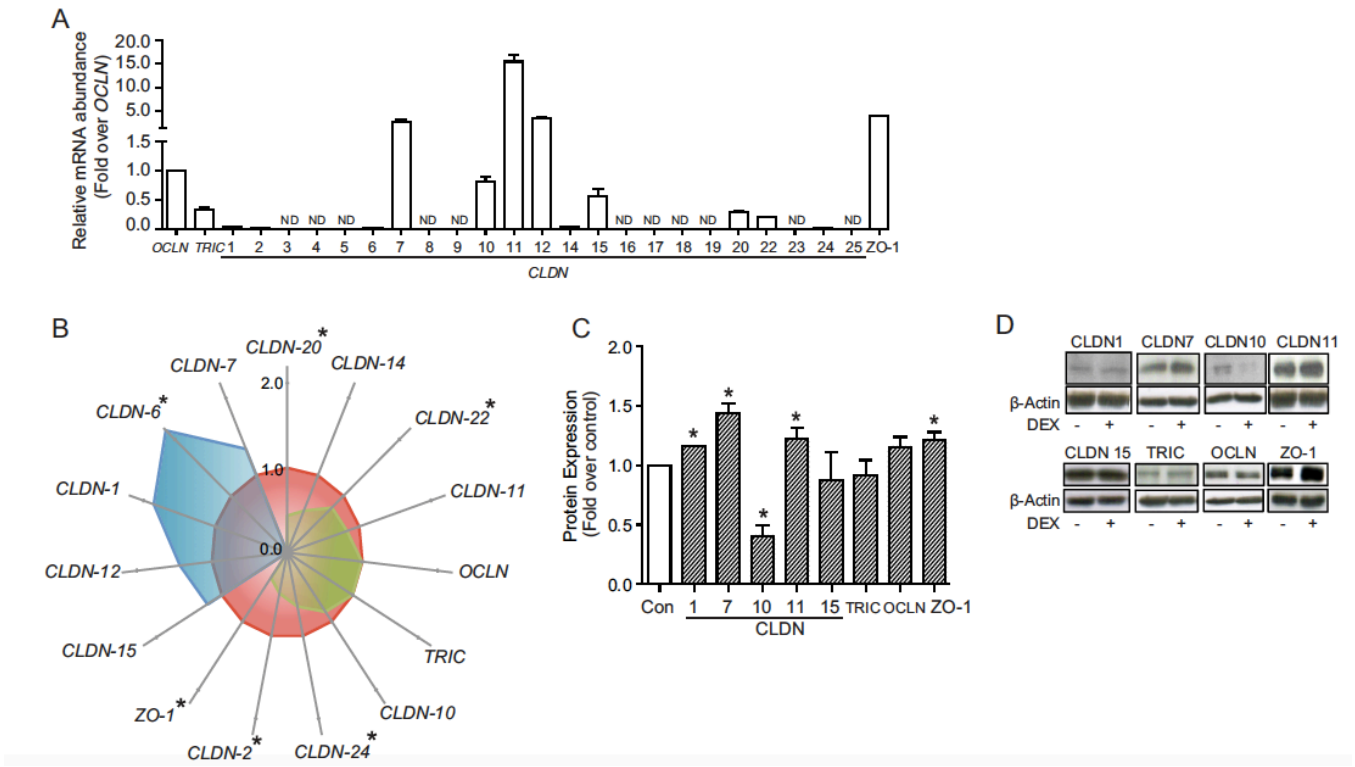

Figure 2: *Effect of DEX on Tight Junction Components. A) mRNA abundance by qRT-PCR analysis. HUVECs grown to confluence on permeable PET inserts. Total RNA was isolated from control cells on the 5th day. Transcript abundance was normalized to GAPDH and each gene examined was expressed relative to OCLN transcript abundance. B) TJ transcript levels in DEX-treated cells were normalized to GAPDH, and expressed relative to the control group (Blue - increasing compared to control; Green- decreasing compared to control). Data are expressed as mean values ± SEM (n = 3-5). C) Protein abundance in HUVECs grown on cell culture inserts. Protein abundance were normalized toβ-ACTIN, and expressed relative to the control group. D) Representative Western blots of CLDN- 1, -7, -10, -11, -15, TRI, OCC, Z0-1. Data are expressed as mean values ± SEM (n = 3-8). * indicates significant difference (P ≤ 0.05) from control (Con) group.*

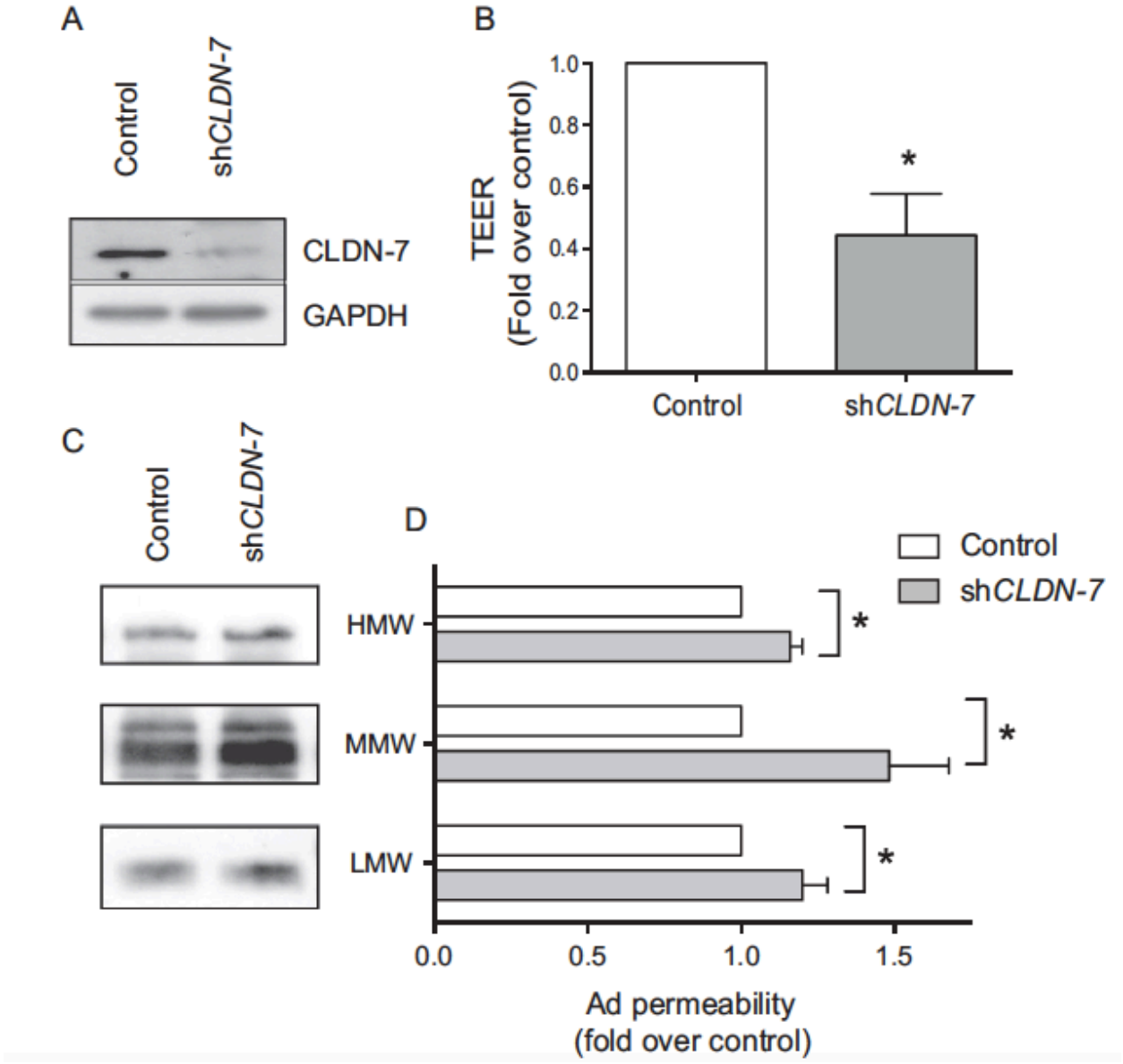

Figure 3: *Knockdown of claudin-7 alters transendothelial electrical resistance and adiponectin flux. We used shRNA to reduce levels of claudin-7 in HUVEC and average efficiency of knockdown was 71% with a representative Western blot shown in A. In cells transfected with scrambled (Control) or claudin-7 shRNA we then tested TEER (B) and flux of adiponectin with representative Western blot shown in C and quantitation in D. In B and D values are mean ± SEM (n = 3) and *indicates significant difference (P ≤ 0.05)*

from control group.

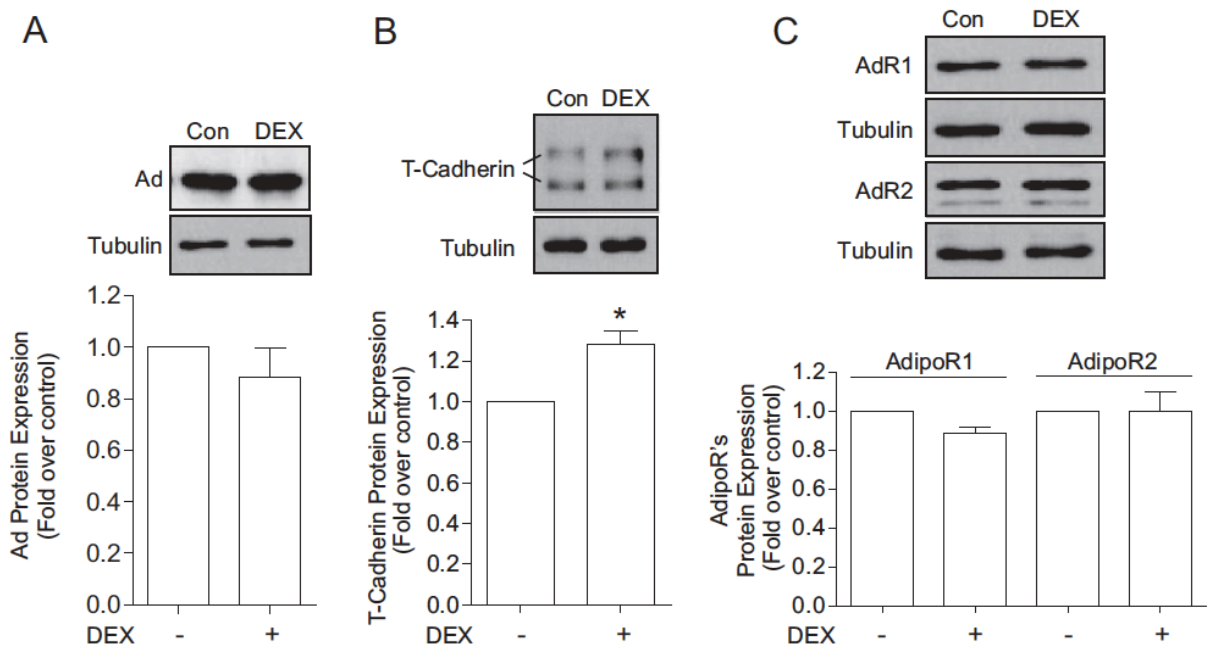

Figure 4: *Expression of Ad and its receptors in HUVEC. A) Ad expression in HUVECs treated with DEX after 5 days. B) T- CADHERIN expression in HUVECs with DEX treatment. C) ADIPO -R1/ -R2 expression in HUVECs. Data are expressed as mean values ± SEM (n = 3-6). *indicates significant difference (P ≤ 0.05) from control (Con) group.*

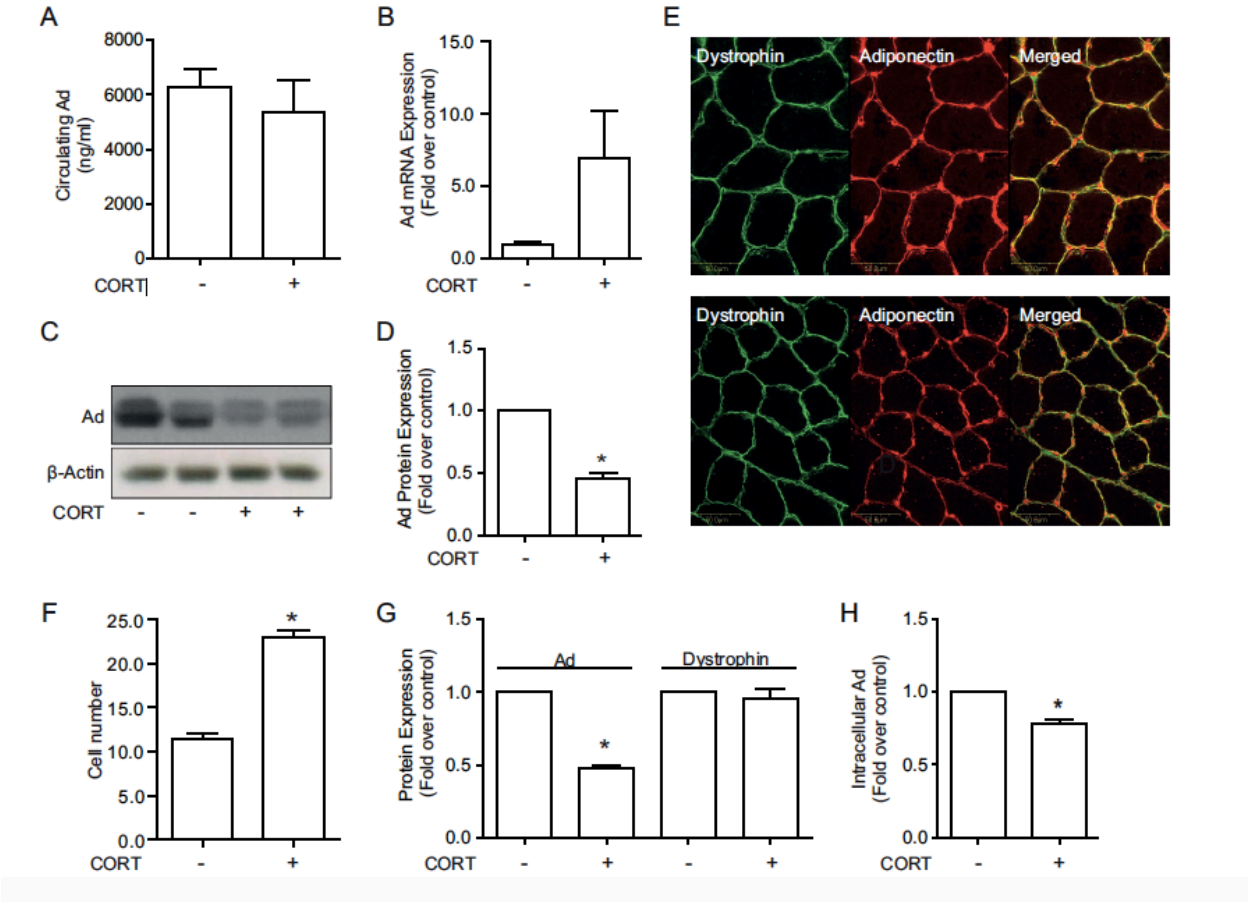

Figure 5: *Ad level in CORT treated animals. A) Using ELISA, circulating Ad was calculated in 1 week treated rat serum. B) Ad mRNA expression after 14 days of CORT. C&D) Representative Western blotting and quantitation of reduced Ad (~30 kDa) in soleus skeletal muscle. E) Immunohistochemical detection of dystrophin (green), Ad (red) in skeletal muscle isolated from rats after 2 weeks of CORT treatment, together with quantitation in F. G) Quantification of changes in intracellular Ad levels and H) cell number. Quantification of Ad shown as the intensity expressed per cell in arbitrary units and are expressed as mean values ± SEM (n = 3-5).* indicates significant difference (P ≤ 0.05) from control (Con) group.*

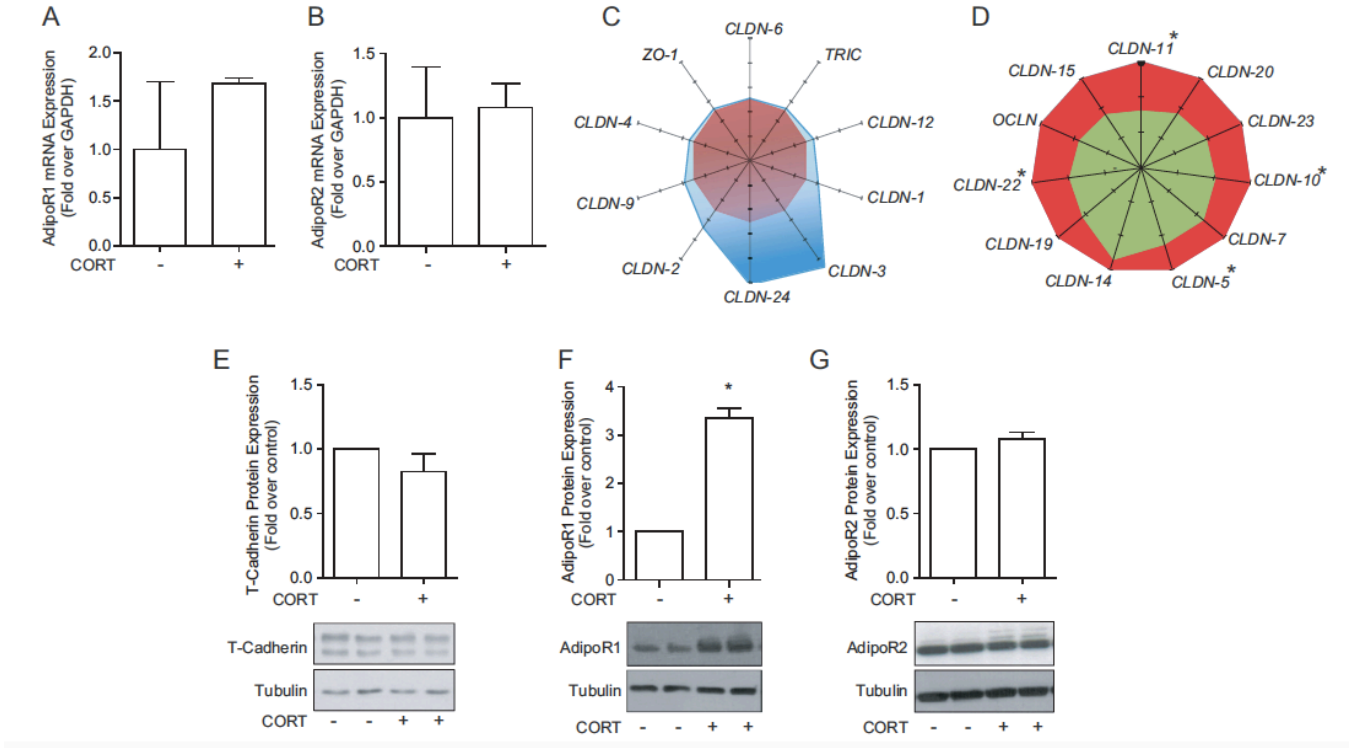

Figure 6: *Ad receptor expression in skeletal muscle. Rats were treated with CORT for 2 weeks. A,B) mRNA expression of Ad and its receptors after 14 days of CORT. Data are expressed as mean values ± SEM (n = 4-5). C-D) mRNA profile of tight junction in soleus skeletal muscle isolated from 2 weeks CORT- treated rats. mRNA abundance by qRT-PCR analysis. Transcript abundance was normalized to GAPDH mRNA abundance, and mRNA abundance for each gene examined was expressed relative to control group transcript abundance. Control group gene transcript were normalized to 1. C) mRNA profile of TJ that are increased after 2 weeks CORT treatment compared to control. Blue- CORT-treated, Red- Control. D) TJ genes that are decreased after 2 weeks of CORT treatment. . E- G) Protein expression in soleus. E) T- CADHERIN. F) Ad receptor 1. G) Ad receptor 2. Data are expressed as mean values ± SEM (n = 3). * indicates significant difference (P ≤ 0.05) from control group*

2.5 Discussion

Glucocorticoids are potential mediators of endothelium permeability. Our study was designed investigate the its influence on endothelium permeability and consequently the changes in Ad movement across the endothelium barrier and the underlying mechanism. More recently, a similar proposed mechanism for regulation of Ad action was suggested both by us and others (Rutkowski et al., 2014; Yoon et al., 2014). To the best of our knowledge, the regulation of this process by glucocorticoids had not been studied before. Our vitro model using DEX treated HUVEC and CORT treated rats to integrate the established observations that glucocorticoids can restrict paracellular transport across various endothelia (Keaney and Campbell, 2015; Rao et al., 2015; Rochfort and Cummins, 2015) with the fact that glucocorticoids, commonly prescribed medications, have numerous side effects, including insulin resistance and diabetes (Beaudry et al., 2015). Furthermore, we examined whether the emerging phenomenon that transendothelial movement of Ad may regulate the anti-diabetic effects of this hormone and whether this was regulated by glucocorticoids (Rutkowski et al., 2014; Yoon et al., 2014). Specifically, our approach involved the use of endothelial cell monolayers and individually perfused intact microvessels to examine whether glucocorticoid altered Ad flux was through reduced microvessel permeability. We also used a rat model of diabetes induced by exogenous glucocorticoid treatment to determine changes in Ad content in muscle as well as peripheral insulin sensitivity.

As indicated in the introduction, strong rationale for this work comes from previous studies with other circulating hormones, most notably insulin. Concentrations of insulin at

the cell surface have been shown to be very different from those observed in plasma in microdialysis experiments (Herkner et al., 2003; Sjostrand et al., 1999), direct interstitial sampling (Bodenlenz et al., 2005) and lymph measurements (Chiu et al., 2008; Yang et al., 1994). It was noted that insulin-mediated glucose uptake lagged behind the increase in plasma insulin (Freidenberg et al., 1994), whereas in cultured skeletal muscle cells, insulin-mediated glucose uptake occurs within 10 min (Somwar et al., 2001). The time delay seen in vivo (Freidenberg et al., 1994) reflects a delay in insulin access to the myocyte which is mediated in part via altered paracellular or transcellular endothelial transport. Thus, modification of access to skeletal muscle can have major effects on insulin action and metabolism, suggesting that reaching the interstitial space is the limiting factor for insulin-mediated glucose uptake (Kolka and Bergman, 2012). Indeed, delivery of insulin to the interstitial space has been shown to be altered by diet (Kubota et al., 2011).

We confirmed the ability of the synthetic glucocorticoid DEX to alter endothelial transport properties, in this case of HUVEC monolayers, as indicated by changes in TEER and PEG-4000. Similar effects were observed in DEX-treated rats, where we saw a significant reduction of permeability in rat mesenteric venules. We then showed that DEX reduced Ad flux across cultured endothelial monolayers by ELISA detection of total Ad content. Western blotting of Ad isoforms indicated that all three oligomeric forms of Ad (trimer, hexamer and oligomer) were reduced in basolateral media from DEX-treated cells, and although the magnitude of change was more evident in the case of LMW adiponectin, all isoforms were significantly altered and we do not believe this data infers a preferential restriction of LMW flux. This demonstration of restricted flux is important to establish

from several perspectives. First, many studies have suggested that oligomeric high molecular weight complexes of Ad are most tightly correlated with insulin resistance (Liu et al., 2007; Pajvani et al., 2004). Second, the concept that endothelial transport regulated Ad action was also proposed by a recent study which estimated the size of different Ad forms by calculating a Stokes radius (Rutkowski et al., 2014). The Stokes radii were 3.96 nm for trimeric Ad, 6.01 nm for hexameric Ad and 10.1 nm for various HMW oligomeric forms (Rutkowski et al., 2014) and these sizes are likely to be in the range that can be physically obstructed or facilitated by changes in endothelial cell tight junction size. Indeed, it was concluded that Ad bioavailability and action in target cells was attenuated under stressed conditions due to reduced trans-endothelial transport (Rutkowski et al., 2014). We concur that regulation of Ad flux across endothelium is particularly relevant since the target tissues where Ad mediates its physiological effects have a wide-range of endothelial permeability. Liver, for example has highly fenestrated endothelium that may permit the passage of HMW Ad, which has potent effects on hepatic metabolism. In contrast, the central effects of HMW Ad may be limited by its transport across the comparatively tighter blood brain barrier (Yoon et al., 2014).

The well-established effect of glucocorticoids to restrict endothelial transport has been proposed to be mediated via regulation of TJ and adherens junction (AJ) proteins (Blecharz et al., 2008; Felinski and Antonetti, 2005). Strands of transmembrane and cytosolic proteins form TJ and AJ complexes that regulate permeability between endothelial cells (Gunzel and Fromm, 2012). Functional characteristics of the vertebrate TJ complex are dependent on the variable assemblage of TJ proteins such as occludin

(OCLN), tricellulin (TRIC) and in particular, claudins (CLDNs) which directly establish the TJ barrier and form the backbone of TJ strands, while cytosolic ZO-1 and other cortical TJ proteins provide structural support to the TJ complex (Gunzel and Fromm, 2012). The CLDN superfamily consists of at least 27 isoforms in mammals and the incorporation of specific CLDN isoforms in TJs can modulate TJ barrier function by making the paracellular pathway tighter or leakier (Gunzel and Yu, 2013). The main observations in our study were increased CLDN-7 and decreased CLDN-10 protein abundance in HUVEC in response to DEX and these changes may underlie the functional properties of paracellular transport limiting Ad flux. Little is known about CLDN-7, although CLDN-7 knockout is lethal in murine models and it seems that CLDN-7 most likely facilitates anion movement across vertebrate epithelia. CLDN-7 was previously found to form a complex with the epithelial cell adhesion molecule (EpCAM) which enhanced cell-cell interaction (Krug et al., 2012; Verma and Molitoris, 2015) . We suggested that the functional role of CLDN-7 in our model is tightening of the endothelium in association with an increase in abundance, and that this may help to explain, in part, the restricted movement of Ad in DEX-treated HUVEC as well CORT-treated rats. Further supporting this idea, a reprevious studies which have found that CLDN-7 (-/-) can cause colonic inflammation and enhance the paracellular flux of small organic solutes (Tanaka et al., 2015), as well as observations that CLDN-7 (-/-) results in the presence of intercellular gaps below TJs and cell matrix loosening (Ding et al., 2012). Thus, we used shRNA to target claudin-7 in HUVEC and observed that this caused a decrease in TEER and increase in adiponectin flux across monolayers, further indicating an important mechanistic role for Dex-mediated changes in claudin-7 expression. Interestingly, another group found that NLRP3 inflammasome

promoted endothelial disruption via production of HMGB1 to disrupt the junctions and increased paracellular permeability (Chen et al., 2015). Finally, (Tatum et al., 2010) reported that urine Na(+), Cl(-), and K(+) were significantly increased in CLDN-7(-/-) mice compared with that of CLDN-7(+/+) mice. Taken together, the studies outlined above and our data indicate an important functional consequence for CLDN-7 reduction and compromised epithelial permeability as the result of tight junction disruption, and this supports the view that increased CDLN-7 abundance, as seen in these experiments, may contribute to endothelial tightening and reduced Ad flux.

In contrast, CLDN-10 isoforms in vertebrate epithelia have been described to impart both charge and size selective properties to the paracellular pathway. Previous studies investigated the role of CLDN-10 deficient mice using Cre-Lox found that serum phosphate concentration was 28% higher and serum Mg^{2+} concentration was almost two-fold higher in cKO mice compared with controls. However, the same study also found that CLDN-10 transports molecules in a charged selective manner (Breiderhoff et al., 2012). To the best of our knowledge, Ad is uncharged. Therefore, the transport of Ad is less likely to be affected by CLDN-10. Nevertheless, it would be very interesting to explore whether the consistent decrease in CLDN-10 observed in this study has a functional role in the modulation of Ad transport across the endothelium barrier.

In the glucocorticoid-induced diabetic rodent model used here, a decrease in CLDN-10 mRNA expression in skeletal muscle was also observed. Although changes in expression profiles of other tight junction proteins do not entirely match the changes in

HUVEC treated directly with DEX, this is not entirely surprising since there are multiple factors impinging upon tight junction protein expression in skeletal muscle tissue *in vivo*.

We believe that reduced paracellular transport is the main mechanism of reduced Ad flux observed, yet we also tested possible indicators of altered transendothelial flux (Yoon et al., 2014). In DEX-treated endothelial cells, there was no major change in ADIPO-R1 or ADIPO-R2 mRNA and protein expression, although in skeletal muscle homogenates, ADIPO-R1 protein expression levels increased significantly in CORT-treated animals. This may reflect a compensatory mechanism to reduced Ad availability in order to increase sensitivity to available Ad. We also observed that DEX increased expression of T-cadherin in HUVEC. T-cadherin has been identified as a non-functional receptor for Ad (Hug et al., 2004). This is in agreement with a previous study showing that DEX enhanced T-cadherin expression in human osteosarcoma cells (Bromhead et al., 2006). One possible interpretation of our finding is that binding to endothelial T-cadherin may trap Ad in the vasculature, as has recently been proposed (Matsuda et al., 2015).

We also investigated potential alterations in endothelial transport of Ad in a rodent model of glucocorticoid-induced diabetes (Shpilberg et al., 2012). In these rats, we found normal circulating Ad levels but significantly reduced total Ad protein content within skeletal muscle without an accompanying decrease in muscle Ad gene expression. This suggests less flux of Ad from circulation could be a contributory mechanism. Indeed, upon immunohistochemical analysis we found reduced Ad content in the interstitial space. Although not a direct comparison to the *in vitro* studies we used here, it suggests that skeletal muscle Ad availability, and thus action, may be limited in this animal model

possibly contributing to its diabetic phenotype (Beaudry et al., 2013; Beaudry et al., 2015; Beaudry et al., 2014; Shpilberg et al., 2012; Yoon et al., 2014).

In conclusion, our study indicates that glucocorticoid-mediated tightening can reduce flux of Ad across endothelial monolayers, and that this may be due to alterations in the expression profile of tight junction proteins. Furthermore, in a rat model of diabetes induced by exogenous glucocorticoids, we observed reduced interstitial and intracellular levels of Ad in skeletal muscle. Thus, we propose that reduced Ad action in target tissues, as a consequence of reduced endothelial flux from circulation to interstitial space, may contribute to the diabetic phenotype occurring after glucocorticoid treatment. Since glucocorticoids are one of the most commonly prescribed medications, our discovery of reduced Ad transport in response to glucocorticoids is a particularly important and novel finding with potentially far-reaching consequences.

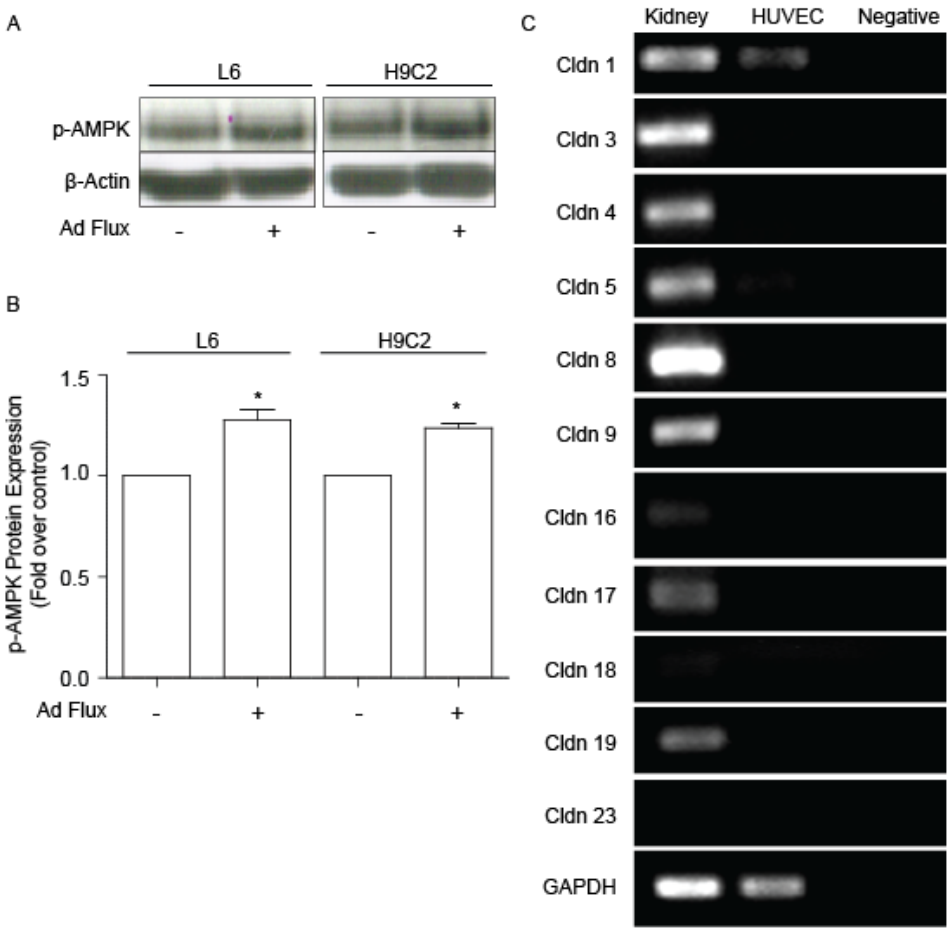

Supp. Figure 1: *A) Effect of treatment with HUVEC-conditioned basolateral medium from Ad flux experiments onp-AMPK and p-p38 MAPK phosphorylation in rat L6 and H9C2. Phosphorylated AMPK and p_p38 MAPK protein abundance was normalized to β-actin, and expressed relative to the corresponding time-matched control group. In (C), Western blots of p-AMPK, phospho-p38 MAPKare shown. Data are expressed as mean values ± SEM (n = 3). B) Non-detected genes in figure 1(C) was ran on 1% gel in order to confirm the absence. Human kidney was used as positive control. Data are expressed as mean values ± SEM (n = 3 - 16). *Significant difference (P ≤ 0.05) from control (Con) group.*

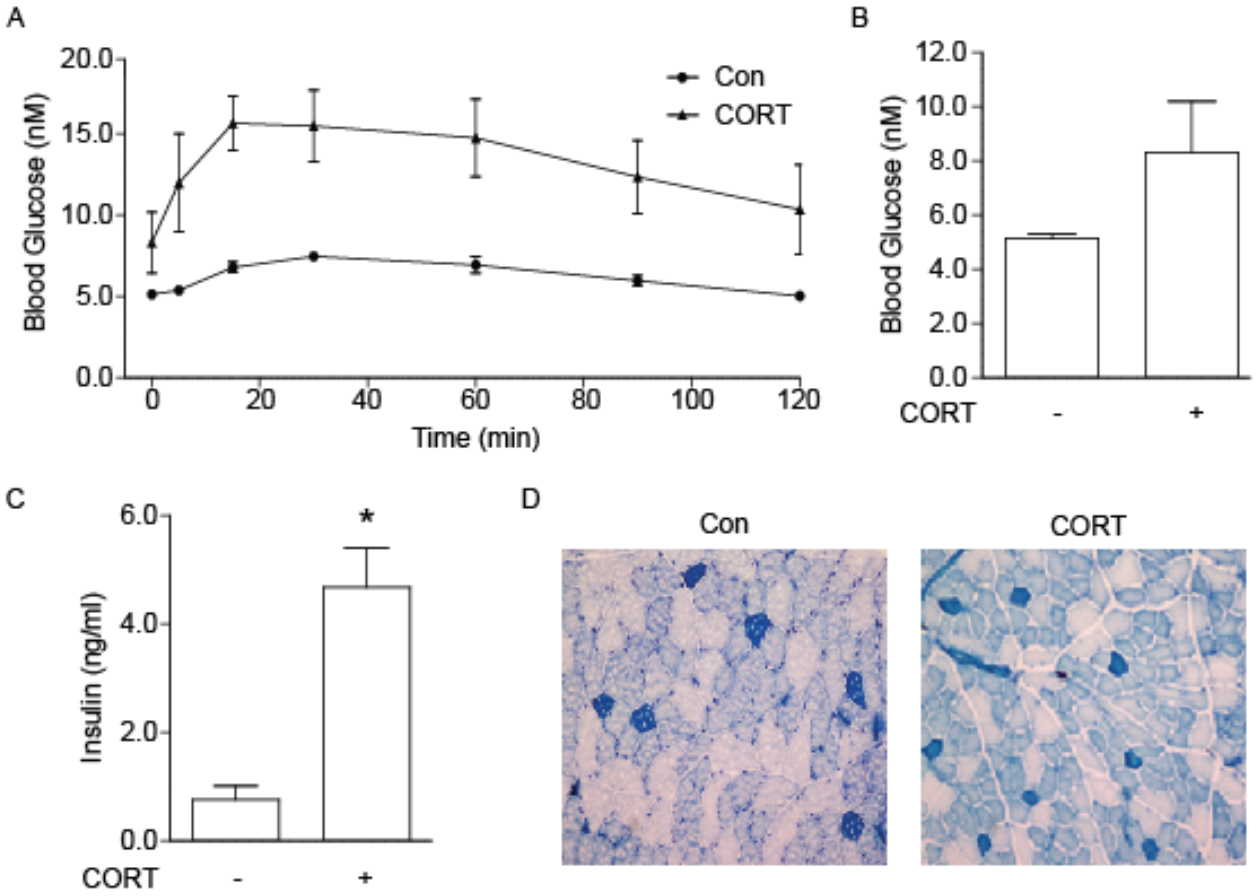

Supp. Figure 2: *Circulation of metabolites in CORT treated rats. A) Glucose tolerance in response to an oral glucose tolerance test (OGTT). B) Fasted blood glucose and C) fasted insulin concentrations measured at the onset of the OGTT after 12 days of CORT treatment. D) Representative images of the tibialis anterior (TA) depicting fiber type staining with Metachromatic myosin ATPase. Data are expressed as mean values ± SEM (n =5). *Significant difference (P ≤ 0.05) from control (Con) group.*

Copyright Permission

BIOSCIENTIFICA LTD. ORDER DETAILS

Sep 21, 2017

This Agreement between ("You") and BioScientifica Ltd. ("BioScientifica Ltd.") consists of your order details and the terms and conditions provided by BioScientifica Ltd. and Copyright Clearance Center.

Order Number	501300235
Order date	Aug 22, 2017
Licensed Content Publisher	BioScientifica Ltd.
Licensed Content Publication	Journal of Endocrinology
Licensed Content Title	Transendothelial movement of adiponectin is restricted by glucocorticoids
Licensed Content Author	Thanh Q Dang, Nanyoung Yoon, Helen Chasiotis et al.
Licensed Content Date	Aug 1, 2017
Licensed Content Volume	234
Licensed Content Issue	2
Type of Use	Thesis/Dissertation
Requestor type	Author of requested content
Format	Electronic
Portion	chapter/article
Rights for	Main product
Duration of use	0 - 5 years
Creation of copies for the disabled	no
With minor editing privileges	no
For distribution to	Canada
In the following language(s)	Original language of publication
With incidental promotional use	no

2.6 References

Agarwal A, Sarwar S, Sepah YJ & Nguyen QD 2015 What have we learnt about the management of diabetic macular edema in the antivascular endothelial growth factor and corticosteroid era? *Curr Opin Ophthalmol* **26** 177-183.

Arita Y, Kihara S, Ouchi N, Maeda K, Kuriyama H, Okamoto Y, Kumada M, Hotta K, Nishida M, Takahashi M, et al. 2002 Adipocyte-derived plasma protein adiponectin acts as a platelet-derived growth factor-BB-binding protein and regulates growth factor-induced common postreceptor signal in vascular smooth muscle cell. *Circulation* **105** 2893-2898.

Barrett EJ, Wang H, Upchurch CT & Liu Z 2011 Insulin regulates its own delivery to skeletal muscle by feed-forward actions on the vasculature. *Am J Physiol Endocrinol Metab* **301** E252-263.

Beaudry JL, D'Souza A M, Teich T, Tsushima R & Riddell MC 2013 Exogenous glucocorticoids and a high-fat diet cause severe hyperglycemia and hyperinsulinemia and limit islet glucose responsiveness in young male Sprague-Dawley rats. *Endocrinology* **154** 3197-3208.

Beaudry JL, Dunford EC, Leclair E, Mandel ER, Peckett AJ, Haas TL & Riddell MC 2015 Voluntary exercise improves metabolic profile in high-fat fed glucocorticoid-treated rats. *J Appl Physiol (1985)* **118** 1331-1343.

Beaudry JL, Dunford EC, Teich T, Zaharieva D, Hunt H, Belanoff JK & Riddell MC 2014 Effects of selective and non-selective glucocorticoid receptor II antagonists on rapid-onset diabetes in young rats. *PLoS One* **9** e91248.

Blecharz KG, Drenckhahn D & Forster CY 2008 Glucocorticoids increase VE-cadherin expression and cause cytoskeletal rearrangements in murine brain endothelial cEND cells. *J Cereb Blood Flow Metab* **28** 1139-1149.

Bodenlenz M, Schaupp LA, Druml T, Sommer R, Wutte A, Schaller HC, Sinner F, Wach P & Pieber TR 2005 Measurement of interstitial insulin in human adipose and muscle tissue under moderate hyperinsulinemia by means of direct interstitial access. *Am J Physiol Endocrinol Metab* **289** E296-300.

Breiderhoff T, Himmerkus N, Stuiver M, Mutig K, Will C, Meij IC, Bachmann S, Bleich M, Willnow TE & Muller D 2012 Deletion of claudin-10 (Cldn10) in the thick ascending limb impairs paracellular sodium permeability and leads to hypermagnesemia and nephrocalcinosis. *Proc Natl Acad Sci U S A* **109** 14241-14246.

Bromhead C, Miller JH & McDonald FJ 2006 Regulation of T-cadherin by hormones, glucocorticoid and EGF. *Gene* **374** 58-67.

Chen Y, Pitzer AL, Li X, Li PL, Wang L & Zhang Y 2015 Instigation of endothelial Nlrp3 inflammasome by adipokine visfatin promotes inter-endothelial junction disruption: role of HMGB1. *J Cell Mol Med* **19** 2715-2727.

Chiu JD, Richey JM, Harrison LN, Zuniga E, Kolka CM, Kirkman E, Ellmerer M & Bergman RN 2008 Direct administration of insulin into skeletal muscle reveals that the transport of insulin across the capillary endothelium limits the time course of insulin to activate glucose disposal. *Diabetes* **57** 828-835.

Clark AR & Belvisi MG 2012 Maps and legends: the quest for dissociated ligands of the glucocorticoid receptor. *Pharmacol Ther* **134** 54-67.

D'Souza A M, Beaudry JL, Szigiato AA, Trumble SJ, Snook LA, Bonen A, Giacca A & Riddell MC 2012 Consumption of a high-fat diet rapidly exacerbates the development of fatty liver disease that occurs with chronically elevated glucocorticoids. *Am J Physiol Gastrointest Liver Physiol* **302** G850-863.

Dadson K, Liu Y & Sweeney G 2011 Adiponectin action: a combination of endocrine and autocrine/paracrine effects. *Front Endocrinol (Lausanne)* **2** 62.

Ding L, Lu Z, Foreman O, Tatum R, Lu Q, Renegar R, Cao J & Chen YH 2012 Inflammation and disruption of the mucosal architecture in claudin-7-deficient mice. *Gastroenterology* **142** 305-315.

Felinski EA & Antonetti DA 2005 Glucocorticoid regulation of endothelial cell tight junction gene expression: novel treatments for diabetic retinopathy. *Curr Eye Res* **30** 949-957.

Freidenberg GR, Suter S, Henry RR, Nolan J, Reichart D & Olefsky JM 1994 Delayed onset of insulin activation of the insulin receptor kinase in vivo in human skeletal muscle. *Diabetes* **43** 118-126.

Gunzel D & Fromm M 2012 Claudins and other tight junction proteins. *Compr Physiol* **2** 1819-1852.

Gunzel D & Yu AS 2013 Claudins and the modulation of tight junction permeability. *Physiol Rev* **93** 525-569.

Herkner H, Klein N, Joukhadar C, Lackner E, Langenberger H, Frossard M, Bieglmayer C, Wagner O, Roden M & Muller M 2003 Transcapillary insulin transfer in human skeletal muscle. *Eur J Clin Invest* **33** 141-146.

Hug C, Wang J, Ahmad NS, Bogan JS, Tsao TS & Lodish HF 2004 T-cadherin is a receptor for hexameric and high-molecular-weight forms of Acrp30/adiponectin. *Proc Natl Acad Sci U S A* **101** 10308-10313.

Kadowaki T, Yamauchi T, Kubota N, Hara K, Ueki K & Tobe K 2006 Adiponectin and adiponectin receptors in insulin resistance, diabetes, and the metabolic syndrome. *J Clin Invest* **116** 1784-1792.

Keaney J & Campbell M 2015 The dynamic blood-brain barrier. *FEBS J* **282** 4067-4079.

Kolka CM & Bergman RN 2012 The barrier within: endothelial transport of hormones. *Physiology (Bethesda)* **27** 237-247.

Krause MP, Liu Y, Vu V, Chan L, Xu A, Riddell MC, Sweeney G & Hawke TJ 2008 Adiponectin is expressed by skeletal muscle fibers and influences muscle phenotype and function. *Am J Physiol Cell Physiol* **295** C203-212.

Krug SM, Gunzel D, Conrad MP, Lee IF, Amasheh S, Fromm M & Yu AS 2012 Charge-selective claudin channels. *Ann N Y Acad Sci* **1257** 20-28.

Kubota N, Yano W, Kubota T, Yamauchi T, Itoh S, Kumagai H, Kozono H, Takamoto I, Okamoto S, Shiuchi T, et al. 2007 Adiponectin stimulates AMP-activated protein kinase in the hypothalamus and increases food intake. *Cell Metab* **6** 55-68.

Kubota T, Kubota N, Kumagai H, Yamaguchi S, Kozono H, Takahashi T, Inoue M, Itoh S, Takamoto I, Sasako T, et al. 2011 Impaired insulin signaling in endothelial cells reduces insulin-induced glucose uptake by skeletal muscle. *Cell Metab* **13** 294-307.

Kusminski CM, McTernan PG, Schraw T, Kos K, O'Hare JP, Ahima R, Kumar S & Scherer PE 2007 Adiponectin complexes in human cerebrospinal fluid: distinct complex distribution from serum. *Diabetologia* **50** 634-642.

Lin KT & Wang LH 2016 New dimension of glucocorticoids in cancer treatment. *Steroids* **111** 84-88.

Liu Y, Retnakaran R, Hanley A, Tungtrongchitr R, Shaw C & Sweeney G 2007 Total and high molecular weight but not trimeric or hexameric forms of adiponectin correlate with markers of the metabolic syndrome and liver injury in Thai subjects. *J Clin Endocrinol Metab* **92** 4313-4318.

Matsuda K, Fujishima Y, Maeda N, Mori T, Hirata A, Sekimoto R, Tsushima Y, Masuda S, Yamaoka M, Inoue K, et al. 2015 Positive feedback regulation between adiponectin and T-cadherin impacts adiponectin levels in tissue and plasma of male mice. *Endocrinology* **156** 934-946.

Nanayakkara G, Kariharan T, Wang L, Zhong J & Amin R 2012 The cardio-protective signaling and mechanisms of adiponectin. *Am J Cardiovasc Dis* **2** 253-266.

Neumeier M, Weigert J, Buettner R, Wanninger J, Schaffler A, Muller AM, Killian S, Sauerbruch S, Schlachetzki F, Steinbrecher A, et al. 2007 Detection of adiponectin in cerebrospinal fluid in humans. *Am J Physiol Endocrinol Metab* **293** E965-969.

Ogilvie RW & Feeback DL 1990 A metachromatic dye-ATPase method for the simultaneous identification of skeletal muscle fiber types I, IIA, IIB and IIC. *Stain Technol* **65** 231-241.

Pajvani UB, Hawkins M, Combs TP, Rajala MW, Doebber T, Berger JP, Wagner JA, Wu M, Knopps A, Xiang AH, et al. 2004 Complex distribution, not absolute amount of adiponectin, correlates with thiazolidinedione-mediated improvement in insulin sensitivity. *J Biol Chem* **279** 12152-12162.

Peters KE, Beilby J, Cadby G, Warrington NM, Bruce DG, Davis WA, Davis TM, Wiltshire S, Knuiman M, McQuillan BM, et al. 2013 A comprehensive investigation of variants in genes encoding adiponectin (ADIPOQ) and its receptors (ADIPOR1/R2), and their association with serum adiponectin, type 2 diabetes, insulin resistance and the metabolic syndrome. *BMC Med Genet* **14** 15.

Rao A, Pandya V & Whaley-Connell A 2015 Obesity and insulin resistance in resistant hypertension: implications for the kidney. *Adv Chronic Kidney Dis* **22** 211-217.

Rochfort KD & Cummins PM 2015 The blood-brain barrier endothelium: a target for pro-inflammatory cytokines. *Biochem Soc Trans* **43** 702-706.

Rutkowski JM, Halberg N, Wang QA, Holland WL, Xia JY & Scherer PE 2014 Differential transendothelial transport of adiponectin complexes. *Cardiovasc Diabetol* **13** 47.

Shikatani EA, Trifonova A, Mandel ER, Liu ST, Roudier E, Krylova A, Szigiato A, Beaudry J, Riddell MC & Haas TL 2012 Inhibition of proliferation, migration and proteolysis contribute to corticosterone-mediated inhibition of angiogenesis. *PLoS One* **7** e46625.

Shpilberg Y, Beaudry JL, D'Souza A, Campbell JE, Peckett A & Riddell MC 2012 A rodent model of rapid-onset diabetes induced by glucocorticoids and high-fat feeding. *Dis Model Mech* **5** 671-680.

Sjostrand M, Holmang A & Lonnroth P 1999 Measurement of interstitial insulin in human muscle. *Am J Physiol* **276** E151-154.

Somwar R, Kim DY, Sweeney G, Huang C, Niu W, Lador C, Ramlal T & Klip A 2001 GLUT4 translocation precedes the stimulation of glucose uptake by insulin in muscle cells: potential activation of GLUT4 via p38 mitogen-activated protein kinase. *Biochem J* **359** 639-649.

Tanaka H, Takechi M, Kiyonari H, Shioi G, Tamura A & Tsukita S 2015 Intestinal deletion of Claudin-7 enhances paracellular organic solute flux and initiates colonic inflammation in mice. *Gut* **64** 1529-1538.

Tatum R, Zhang Y, Salleng K, Lu Z, Lin JJ, Lu Q, Jeansonne BG, Ding L & Chen YH 2010 Renal salt wasting and chronic dehydration in claudin-7-deficient mice. *Am J Physiol Renal Physiol* **298** F24-34.

Verma SK & Molitoris BA 2015 Renal endothelial injury and microvascular dysfunction in acute kidney injury. *Semin Nephrol* **35** 96-107.

Wang Y, Xu A, Knight C, Xu LY & Cooper GJ 2002 Hydroxylation and glycosylation of the four conserved lysine residues in the collagenous domain of adiponectin. Potential role in the modulation of its insulin-sensitizing activity. *J Biol Chem* **277** 19521-19529.

Witt KA & Sandoval KE 2014 Steroids and the blood-brain barrier: therapeutic implications. *Adv Pharmacol* **71** 361-390.

Won SM, Lee JH, Park UJ, Gwag J, Gwag BJ & Lee YB 2011 Iron mediates endothelial cell damage and blood-brain barrier opening in the hippocampus after transient forebrain ischemia in rats. *Exp Mol Med* **43** 121-128.

Wood CM, Gilmour KM, Perry SF, Part P & Walsh PJ 1998 Pulsatile urea excretion in gulf toadfish (Opsanus beta): evidence for activation of a specific facilitated diffusion transport system. *J Exp Biol* **201** 805-817.

Xu A, Yin S, Wong L, Chan KW & Lam KS 2004 Adiponectin ameliorates dyslipidemia induced by the human immunodeficiency virus protease inhibitor ritonavir in mice. *Endocrinology* **145** 487-494.

Yang YJ, Hope ID, Ader M & Bergman RN 1994 Importance of transcapillary insulin transport to dynamics of insulin action after intravenous glucose. *Am J Physiol* **266** E17-25.

Yoon N, Dang TQ, Chasiotis H, Kelly SP & Sweeney G 2014 Altered transendothelial transport of hormones as a contributor to diabetes. *Diabetes Metab J* **38** 92-99.

Yuan D & He P 2012 Vascular remodeling alters adhesion protein and cytoskeleton reactions to inflammatory stimuli resulting in enhanced permeability increases in rat venules. *J Appl Physiol (1985)* **113** 1110-1120.

Yuan D, Xu S & He P 2014 Enhanced permeability responses to inflammation in streptozotocin-induced diabetic rat venules: Rho-mediated alterations of actin cytoskeleton and VE-cadherin. *Am J Physiol Heart Circ Physiol* **307** H44-53.

Zhang X, Wang N, Schachat AP, Bao S & Gillies MC 2014 Glucocorticoids: structure, signaling and molecular mechanisms in the treatment of diabetic retinopathy and diabetic macular edema. *Curr Mol Med* **14** 376-384.

Zhou X & He P 2011 Temporal and spatial correlation of platelet-activating factor-induced increases in endothelial [Ca(2)(+)]i, nitric oxide, and gap formation in intact venules. *Am J Physiol Heart Circ Physiol* **301** H1788-1797.

Statement of Contribution

Chapter 3: T. Dang contributed to planning and conducting experiments, except for the Prussian blue staining which was done by Dr. Subrata. Micro- CT quantification was done by P. Tadi. Advice and instruction on using CLAMS was given by D. Kishi. This chapter was written by T. Dang and edited by Dr. G. Sweeney

Chapter 3: Study 2

Modification of endothelium tightness by iron & the effects of iron on glucose metabolism

3.1 Abstract

There is a strong, clinically-proven, link between iron overload and diabetes. Limiting tissue access to adiponectin by an alteration in paracellular permeability can affect glucose metabolism. Iron is a potential mediator of endothelium tightness. We hypothesized that iron restricts adiponectin access to target tissues via tightening of the endothelium, and hence will impair glucose clearance. First, we confirmed iron overload in HDMEC cells using fluorescent imaging of intracellular iron using PGSK dye, and further with an iron response element (IRE)-CFP reporter construct. We found that iron did not affect the endothelium tightness, despite inducing an elevation in ROS. To further elucidate iron's effect on whole-body metabolism, we established an iron overload mouse model that mimics a physiological condition of hemochromatosis. We *i.p.* injected mice 5 days per week for one month to test the effect of iron overload on glucose metabolism. We found iron deposits in various skeletal muscles, liver, and fat using intracellular iron imaging and Prussian blue assays. We performed glucose and insulin tolerance testing to show better glucose tolerance in iron overload mice. Then we used the Comprehensive Lab Animal Monitoring System (CLAMS) to characterize activity, but found no significant

change. Furthermore, we found upregulation of pAkt in gastrocnemius muscle, but no change in glycogen content in skeletal muscles or liver. In addition to that, visceral adiposity was diminished, correlating with reduced adiponectin production. However, circulating insulin was not affected. Lastly, the iron overload induced higher glucose excretion through urine. From our study, we found that the iron treatment did not have an effect on endothelium tightness and adiponectin transport in *vitro.* However, in our *in vivo* study, we found iron overload mice exhibit better glucose tolerance and higher Akt phosphorylation, indicative of increased insulin signalling. Our data suggest that the endothelium might not be the key target of iron in altering glucose metabolism. The improved glucose clearance resulted mainly from pAkt upregulation as well as constant glucose excretion.

3.2 Introduction

Excessive amounts of iron promote insulin resistance in mice, which greatly increases the risk for developing diabetes and its complications (Yu et al., 2015) The connections between iron and metabolism are well established. Hereditary hemochromatosis (HH) is an autosomal recessive disorder characterized by excess iron in the body. The most common form of this disease is caused by a mutation in the HFE gene resulting in a C282Y substitution in the HFE protein. The HFE protein is responsible for iron metabolism by acting as an iron sensor for the body, regulating iron absorption in the small intestine, and recycling of iron by macrophages (Feder et al., 1996). To support the link between iron and diabetes, a group of researchers found that HFE KO mice exhibit impaired glucose-stimulated insulin secretion and increased β- cell apoptosis (Cooksey et al., 2004). Furthermore, in thalassemia, a disorder characterized by a deficiency in the β-

globin subunit of hemoglobin, patients become iron-overloaded from increased iron absorption because the body is unable to maintain a normal level of erythrocytes in the blood to uptake the iron that gets into the circulation through the gut (Weatherall, 1998). Clinical studies on thalassemia patients have found that they have insulin deficiency and insulin resistance, which may lead to a prediabetic state and the development of full-blown diabetes (Messina et al., 2002).

The cross-talk between iron metabolism and diabetes has also been reported by Tanner and Lienhard, who observed co-localization of transferrin receptors with glucose transporters on the membrane of adipocytes *in vitro*. Their study suggested that the regulation of iron occurs in parallel with its effects on glucose transport (Tanner and Lienhard, 1989). Increased iron storage is associated with the development of type 2 diabetes (Fernandez-Real et al., 2002). Ferritin is one of the key proteins regulating iron homeostasis and is a widely used clinical biomarker of iron status. Clinical studies have shown that higher serum ferritin levels were found in patients with metabolic syndrome and insulin resistance. High iron levels are associated with increased risk of type 2 diabetes, and thus may be a prevalent cause of diabetes (Moreno et al., 2015)

Iron is also known for its effect on elevating oxidative stress, a major causative factor for diabetes and its complications. In addition to elevated ROS reducing metabolic clearance (Toborek et al., 1992), free radicals disrupt tight junction (TJ) function by altering cell-cell adherence of TJ proteins and causing reorganization of the actin filament network (Wichmann et al., 2015; Won et al., 2011). Previous work has suggested that iron overload in mice leads to elevated ROS. Interestingly, it was associated with decreased levels of the TJ structural proteins occludin and zonula occludens 1, and hence caused a

disruption in TJ structure. This resulted in increased permeability in hippocampal endothelial cells that were isolated from the TFI-induced iron overload rat model.

Endothelial dysfunction contributes to the pathogenesis of atherosclerosis, a complication of diabetes (Handa et al., 2016; Won et al., 2011). Furthermore, previous research found that inflammation coexisting with increased oxidative stress occurred in end-stage renal disease (Raj et al., 2005). ROS enter human skeletal muscles and activates an inflammatory cascade via activation of nuclear factor- kB (NF-kB), as well as upregulating the expression of various cytokines including interleukin-6, -10 (IL-6, -10) and tumor necrosis factor-α (TNF-α) in response to stimuli. Increased serum concentrations of these cytokines are associated with impaired glucose tolerance (Muller et al., 2002). A monolayer of endothelial cells lines the entire circulatory system of the body. This endothelium acts as a barrier that regulates the exchange of hormones, proteins and small molecules between the vascular compartment and the interstitial space (Goddard and Iruela-Arispe, 2013; Pries and Kuebler, 2006). The actions of a hormone or nutrient on a target tissue is implicitly dependent upon the ability of these factors to gain access to the target. Adiponectin is an important hormone to stimulate glucose clearance. Therefore, changing adiponectin access to the target tissue through altering permeability could alter glucose metabolism.

Based on previous literature, the goals of this study were first to examine whether excess iron treatment causes a change in ROS production (using CellRox red) leading to alterations in endothelium tightness, hence changing adiponectin movement by TEER and flux experiments *in vitro*. I have developed an iron overload model that mimics the pathological conditions of thalassemia and hemochromatosis to examine glucose

metabolism. I have used well-established methods both *in intro* and *in vivo* to confirm iron overload *i.e.,* intracellular iron, IRE-CFP construct, PGSK, and Prussian blue staining. To study whole body glucose metabolism, I used GTT and ITT to evaluate glucose clearance in iron overloaded mice. I also used CLAMS to characterize this new mouse model to evaluate respiration and ambulatory activity. Characterizing physical activity is important in this study as it can have a potential effect on glucose metabolism. I then examined Akt phosphorylation under insulin-stimulated conditions. Glucose to glycogen conversion rate was tested in liver and skeletal muscles using a glycogen content assay to evaluate whether this process contributes to changes in circulating glucose levels with iron overload. I further investigated circulating insulin and adiponectin levels as possible contributors to changes in circulating glucose using ELISA. Since adiponectin is mainly secreted by adipocytes, fat content was also evaluated by isolated fat weight and whole body micro-CT scan.

3.3 Materials and Methods

3.3.1 HDMEC culture and treatments

Human dermal microvascular endothelial cells (HDMECs) were obtained from ATCC (Manassas, VA, USA) and grown at 37°C and 5% CO_2 on uncoated T75 flasks in vascular cell basal medium (ATCC, PCS-100-030) containing 10% fetal bovine serum (FBS), VEGF endothelial cell growth kit without hydrocortisone hemisuccinate (ATCC, PCS-100-041), 100 units/mL penicillin, and 100 μg/mL streptomycin. Following two passages, cells were trypsinized and transferred to medium containing 10% dimethyl sulfoxide (DMSO), frozen as aliquots in liquid nitrogen and designated as HDMECs at passage 3 (P3). For experiments, P3 aliquots of HDMECs were quickly thawed, plated to uncoated T75 flasks, and grown to ~90% confluence in medium described above. Cells

were then trypsinated, pelleted by centrifugation (380 x g, 10 min) and gently resuspended in vascular cell basal medium containing 2% FBS, VEGF endothelial cell growth kit without hydrocortisone hemisuccinate, 100 units/mL penicillin, and 100 μg/mL streptomycin. Cells were counted using a haemocytometer and seeded onto permeable polyethylene terephthalate (PET) filters (0.9 cm^2 growth area; 0.4 μm pore size; 1.6 x $10^6/cm^2$ pore density) at the base of BD Falcon cell culture inserts (BD Biosciences, Mississauga, ON, Canada) at a density of 0.5 x 10^6 cells/insert. Inserts were held in BD Falcon 12-well companion plates with inserts (apical side) and companion wells (basolateral side) containing 1 mL of medium each.

3.3.2 Cell viability

HDMEC were seeded in a 96-well plate and incubated with MTT (3-(4,55-Dimethylthiazol-2-yl)-2,5-Diphenyltetrazolium Bromide) (Sigma, St. Louis, MO) dissolved in PBS for 5 hours at 37^0C. DMSO was used to dissolve the precipitate formazan during the incubation, and a Multiskan Spectrum Spectrophotometer (Thermo Electron Corp) was used to detect concentration at 550 nm.

3.3.3 IRE transfection

HDMEC were first transfected with the IRE-CFP construct (Dongiovanni et al., 2013) using Lipofectamine™ 3000 Reagent (Invitrogen, Carlsbad, CA, USA) according to the manufacturer's protocol, and then treated with iron. The fluorescent signal was normalized to the transfected-control group. Exposing the cells to iron increased CFP fluorescence. This was followed by selection with 50 ug/ ml Neomycin (Sigma-Aldrich, Oakville, ON, CA) for 24 hours.

3.3.4 Iron detection by immunofluorescence

Half an hour prior to the end of iron treatment, cells were treated with 250 μM ferrous sulfate ($FeSO_4$; Sigma, St. Louis, MO), 3 μM *Phen Green SK (PGSK) or* 5 μM of CellRox Deep Red reagent (Invitrogen, Waltham, MA). Cells were then fixed with 4% PFA (Sigma, St. Louis, MO) followed by quenching with 1% glycine, and permeabilized with 0.1% Triton X- 100 (Bioshop, Burlington, ON). A control group at each time point was included in fluorescence quantification.

3.3.5 Animal protocols

Wild type (WT) male C57BL6 mice (Jackson Laboratory, Bar ME) were purchased at 8 weeks of age and were housed for one week of acclimatization in the facilities prior to experimentation (12h/12h light/dark cycle). Intraperitoneal injection of 10 mg of iron dextran (Santa Cruz, Dallas, TX) per 25g body weight was injected on a 5 day/week schedule for a duration of 4 weeks with a total volume of 300 μL per injection. 10% dextrose (Sigma, St. Louis, MO) was injected as a placebo. All mice were given chow diet. Individual mice were kept in the comprehensive lab animal monitoring system (metabolic cage) for 3 days for measurement of metabolic parameters. Night time data were recorded between 7:00 PM and 6:00 AM, day time data collected between 7:00 AM and 6:00 PM. All experiments were approved by the Animal Care and Use Committee at York University.

3.3.6 Glucose and insulin tolerance test

Animals were fasted prior to tolerance testing (6 hrs for insulin tolerance test, 16 hours for glucose tolerance test). Mice were i.p. injected with glucose at 2g/kg of body weight. Blood glucose was recorded over a period of 120 minutes at times 0, 20, 30, 60 90, and 120 minutes post-injection. For the Insulin Tolerance Test (ITT), mice were i.p.

injected with insulin at 1 unit/kg of body weight. Blood glucose was recorded over a period of 80 minutes with 10 minutes intervals. Blood glucose was measured via saphenous vein bleed using a sterile needle (25G) and glucometer (Accu-Chek). Plasma was collected for analysis of adiponectin and insulin using ELISA kit (AIS, Hong Kong).

3.3.7 Intracellular Iron

Lysates were added to iron releasing agent (equal volume of 1M HCl and 4.5% $KMnO_4$) and incubated at 60^0C for 2 hours. After incubation, iron detection reagent (6.5mM ferrozine, 6.5mM neocuproine, 2.5M ammonium acetate, 1M ascorbic acid; Sigma, St. Louis, MO) was added to samples and incubated at room temperature for 30 minutes. A spectrophotometer was used to determine the iron concentration at 550 nm. A standard curve was generated, and the amount of iron was normalized to protein concentration of the lysate.

3.3.8 Prussian blue staining

Tissues were embedded with O.C.T. compound (VWR, Radnor, PA) for Perl's Prussian blue staining for localization of iron. Section of 5-microns thickness were treated with 5% HCl to liberate ferric ions, then treated with 5% potassium ferrocyanide to produce insoluble ferric ferrocyanide. Sections were then counterstained with neutral red using the method previously described (Khan et al., 2004).

3.3.9 Micro-CT quantification

Mice were anesthetized using 5% isoflurane for imaging by Bruker micro-CT. The threshold was established using whole mice to determine total body and fat volume using CT analysis software. Visceral fat was determined by manually highlighting the regions

inside the mouse around the organs. Subcutaneous fat was calculated by subtracting visceral fat from the total fat.

3.3.10 Glycogen content

Briefly, skeletal muscles and liver were digested in 1M KOH. pH of digested muscles was adjusted to 4.8 before addition of acetate buffer and 0.5 mg/ml amyloglucosidase. Subsequently, glycogen was hydrolyzed overnight at room temperate. A spectrophotometer was used to determine the glycogen concentration at 340 nm (Fediuc et al., 2006).

3.3.11 Western blot analysis

HDMEC were lysed in a buffer containing protease and phosphatase inhibitor cocktail tablets (Sigma, St. Louis, MO) then heated to 95°C for 10 min. Equal amounts of protein frome ach sample were resolved by SDS-PAGE, transferred to PVDF membrane, blocked with 3% bovine serum albumin (BSA) in wash buffer, and then incubated overnight at 4°C with primary antibodies specific for the following proteins: pAkt Thr^{308}, PEPCK, $pGSK^{Ser9}$. Antibodies were obtained from Cell Signaling Technology (New England Biolabs Ltd., Whitby, ON, CA). Protein expression was normalized to GAPDH protein abundance.

3.3.12 Statistical analysis

All data are expressed as mean values ± SEM (n), where n represents the number of independent experiments conducted, except in Fig. 3 where n represents the number of inserts sampled from 1 out of 3 independent experiments conducted with equivalent results. A two-way analysis of variance (ANOVA) test was used to determine significant differences ($p \leq 0.05$) between groups. When appropriate, a Student's t-test was also used.

All statistical analyses were conducted using Prism 6 software (GraphPad Software, La Jolla, California, USA).

3.4 Results

3.4.1 Iron overloaded HDMEC showed increased ROS but no change in adiponectin movement

To create an IO (iron-overload) endothelium model, we used 3-(4,5-dimethylthiazol-2-yl)-2,5-diphenyltetrazolium bromide (MTT) assay to determine the iron concentration at which the cells' viability will reduce significantly. MTT is a compound that gets reduced into a purple dye by AD(P)H-dependent oxidoreductase in a living cell. Therefore, a lower reading at OD_{550} nm indicates less cell viability, or conversely, more cell death. We found that starting from 500 uM treatment of iron for 48 hrs, the cell showed significantly reduced viability and 250 uM was therefore chosen for further experiments. 500 μM hydrogen peroxide was used as a positive control (fig. 1A). Furthermore, we found that iron accumulation was the highest in HDMEC after 48 hrs using the 250 uM treatment (fig. 1B).

To confirm iron has an effect in HDMEC, we transfected HDMEC with an Iron Response Element (IRE)-CFP (cyan fluorescent protein) fusion construct. IRE is a short stem-loop sequence that is found on the mRNA of ferritin (iron storage protein). High concentration of iron causes an increase in transcription and translation of CFP (Meehan and Connell, 2001). We then checked for green signal from the non-transfected, transfected control, and transfected cells treated with iron for 48 hrs (fig. 2A). The greater green fluorescent signal suggested the IRE was activated by the iron treatment, as the quantification showed an 3.6-times enhanced signal (fig. 2B). To further confirm iron did

accumulate inside HDMEC, we used PGSK, which is a fluorescent dye that accumulates intracellularly and gets quenched by iron. The green fluorescent signal was reduced by 3.5 times in the iron-treated group (fig. 2C), as confirmed by quantification (fig. 2D), showing that iron did accumulate inside the cells.

We hypothesized that iron could potentially alter endothelium tightness via reactive oxygen species (ROS) production. To confirm this theory, CellRox Red was used to detect ROS elevation induced by iron. It is a cell-permeant dye that is non-fluorescent in a reduced state, however, upon oxidation by ROS it exhibits fluorescence. We saw a significant, 1.46-time increase in ROS after 48 hrs of iron treatment (fig. 3A,B). As a functional effect of iron, we checked for transepithelial electrical resistance (TEER), an indicator of endothelium tightness. If the TEER decreased, it suggested that the endothelium is leakier and more hormones will able to access the tissue. After 48 hrs, the tightness of control HDMEC was determined to be 36.40 ± 2.14 $\Omega*cm^2$, while under iron treatment with tightness was 38.80 ± 2.56 $\Omega*cm^2$ (fig. 3C), hence there was no significant change in flux of fAd (fig. 3D,E.).

3.4.2 Iron Overload (IO) Mice Showed Enhanced Glucose Clearance and insulin signaling

As IO turned out to have no effect on endothelium tightness or Ad flux, we then further investigated how iron affects glucose metabolism in the whole body. To create an IO mouse model, we injected the mice with iron intraperiotneally five days per week for four weeks. After 4 weeks (10mg/ 25g body weight) of injection, we found circulating iron increased significantly from 16.08 ± 0.08 mM to 51.80 ± 6.0 mM (fig. 4A) in the iron-treated mice. In order to characterize this new mouse model, we used a glucose tolerance

test (GTT) to evaluate the ability of the mice to use glucose. We found that IO mice have improved glucose clearance, corresponding to a lower area under the curve (28%) compared to control mice (fig.4D,E). IO also exhibited better insulin sensitivity, as there was an approximate 23% reduction in the area under the curve from the insulin tolerance test compared to controls (fig. 4F,G).

As validation of this model, iron accumulation was also shown in various skeletal muscle tissues. In tibialis anterior muscle (TA), control mice displayed and iron concentration of 0.42 ± 0.024 mM/ug protein compared to 0.79 ± 0.13 mM/ug protein in IO mice (fig. 5A,B). Similar observations were made in gastrocnemius muscles (Gas), where control mice accumulated 0.34 ± 0.04mM/ug, whereas IO mice deposited 0.58 ± 0.054 mM/ug protein (fig. 5C,D). Furthermore, as compared to other skeletal muscles, soleus (sol) accumulated the least iron at 0.71 ± 0.043mM/ug protein, but this was still higher than the control mice at 0.57 ± 0.01 mM/ug protein (fig. 5E,F). The change in iron accumulation in muscles was further confirmed by Prussian blue histology from isolated muscles. Interestingly, we also found that control mice had a body weight of 24.67 ± 0.49 g, but weight was reduced to 21.67 ± 0.56 g after 4 weeks injection in the IO group (fig. 6A). Circulating adiponectin was reduced from 28.36 ± 1.16 ug/ml to 16.91 ± 0.56 ug/ml in the IO mice compared to control (fig. 6B) However, circulating insulin in control was 1.83± 0.01ng/ml and did not change significantly in the IO condition, reaching 1.84 ± 0.01 ng/ml (fig. 6C).

3.4.3 IO mice showed no change in activity

To further characterize this IO mouse model, activity level along with other metabolic parameters were measured using Comprehensive Lab Animal Monitoring System

(CLAMS) for a 3 day period. All mice had free access to food and water and were subjected to light-dark cycle.

The mice showed a characteristically higher CO2 elimination and O2 consumption at night, compared to the day (fig. 7A,B), as further quantified in fig. 7C,G, reflecting the normal nocturnal activity of mice. Thus, their respiratory exchange ratio was also higher at night (fig. 8A,B). IO mice were found to be less active (20%), and produced less heat as compared to the control mice (fig. 9A,B), as quantified in fig. 9C,D.

3.4.4 Effect of iron on skeletal muscles

There are various tissues responsible for glucose utilization; therefore we wanted to determine the tissue-specific effect and molecular mechanism responsible for the enhanced glucose tolerance observed in IO mice. We first looked at skeletal muscles since they are the main sites for glucose disposal. We isolated TA, gastro and sol and examined phosphorylation of Akt and GSK, downstream kinases of insulin receptor signaling (fig. 10). We found gastro had an increase in Akt phosphorylation under insulin-stimulated conditions (fig. 10B), as shown in a representative blot (fig. 10G).

The amount of glucose being converted into glycogen also could explain the IO mouse phenotype. However, there was no significant difference in glycogen content in tissues from IO mice as compared to the control group (fig. 11A-C)

3.4.5 Effect of iron on liver metabolism

The liver is an important metabolic organ and is the major site for iron storage. Iron concentration was quantified by intracellular iron assay showing control mice had 0.20 ± 0.02M/ug protein, which was increased significantly to 3.25 ± 0.49M/ug protein in the IO mice. Iron accumulation was further confirmed by Prussian blue staining (fig. 12A,B).

Corresponding to the iron accumulation, the liver enlarged from 0.93 ± 0.01 g to 1.9 ± 0.09 g with IO (Fig. 12C,D). Iron did not have an effect on the insulin signaling pathway, as shown by no change in insulin-stimulated Akt phosphorylation or PEPCK expression in the liver (Fig.12E,F). Furthermore, there was no significant difference in glycogen content in the livers isolated from IO mice (fig.11D)

3.4.6 Iron diminished fat content

To understand the cause of the lower body weight and body fat in IO mice, we examined their daily food intake and energy expenditure together. We isolated two different fat depots to study the change in fat composition in the IO condition. We isolated perirenal (peri) and epididymal (epi) fats to represent visceral fat. The weight for epi fat reduced from 0.39 ± 0.07 g to 0.02 ± 0.01 g (fig. 13B). Peri fat had an average weight of 0.15 ± 0.03 g (fig.13C) under control conditions, but could not be detected in the IO condition. Furthermore, weight of isolated fat from the inguinal region, representing subcutaneous fat (Sub), did not change; control mice weighed an average of 0.29 g ± 0.02 and this was not significantly changed in IO mice at 0.26 ± 0.03 g (fig. 13A). Since subcutaneous fat is another tissue that accumulates iron, we also quantified iron accumulation in this depot. Under control conditions sub fat had 0.67 ± 0.03 mM/ug protein, which was increased to 2.61 ± 0.36 mM/ug protein in IO (fig. 13D). This observation was also reflected in Prussian blue histology staining (fig. 13E). The reduction in fat is reflected in the computerized tomography (CT) scan (Fig. 13F) and body weight (Fig. 6A). Total body fat volume reduced from 717.6 ± 38.87 to 143.5 ± 22.96 mm^3 in IO (fig. 14B). Hence, total percentage body fat reduced from 10.60 ± 0.62 to 2.30 ± 0.36 in IO condition (fig. 14A). Quantification of the volume of each fat depot showed a reduction

of both subcutaneous fat (from 548.9 ± 29.55 mm^3 to 122.5 ± 19.36 mm^3) and visceral fat (from 168.7 ± 14.00 mm^3 to 20.99 ± 5.23 mm^3) in IO (fig.14C,D). Interestingly, on average per day IO mice had no difference in food consumption (4.66 ± 0.47 g) as compared to control mice (4.38 ± 0.83 g) (fig. 13G).

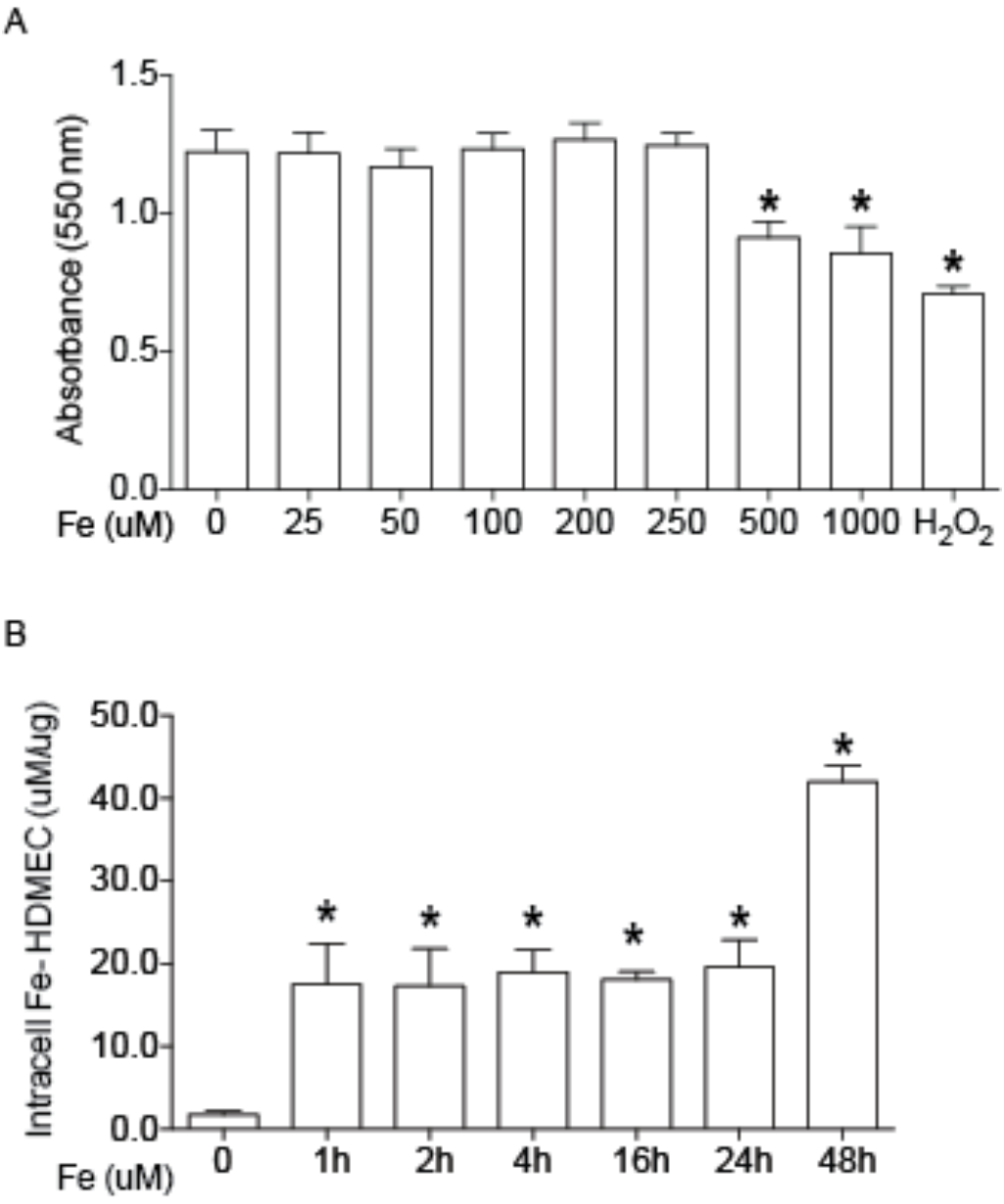

Figure 1: *Characterizing the HDMEC IO model. A) Determining treatment dose. Different doses of iron was applied to HDMEC. MTT is a dye which is reduced into a purple dye by AD(P)H-dependent oxidoreductase in a living cell. Hydrogen Peroxide was used as positive control for cell death. 250 uM is the concentration used for further experiments. B) Determining treatment time. Time-course showing accumulation of intracellular iron. HDMECs were treated with 250 uM of iron over a period of 48 hrs to determine treatment time. Amount of iron was normalized to protein concentration of the cell lysate. We determined HDMEC would be treated for 48 hrs to create an IO model. Data are expressed as mean values ± SEM (n = 3). Two-way ANOVA was used comparing treatment group to control (fig. A) or at* t_0 *(fig. B). * indicates significant difference* ($p \leq 0.05$) *from control group.*

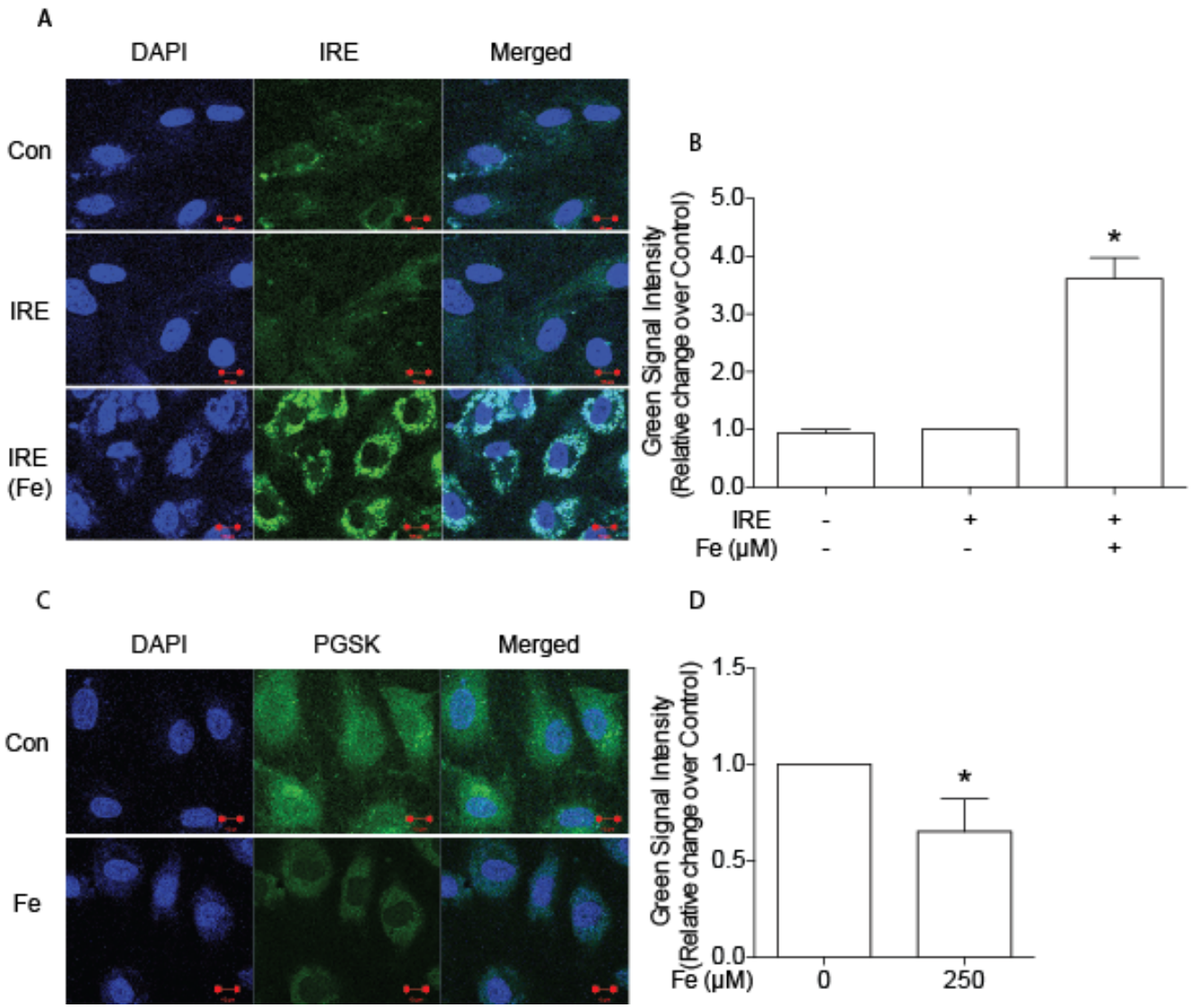

Figure 2: *Further confirmation of the IO HDMEC model using iron response element (IRE) and Phen Green SK (PGSK). A) Confirmation of IO in HDMEC by IRE-CFP construct. Representative images for HDMEC transfected with IRE-CFP. Cells were transfected with IRE-CFP construct then treated with iron. Fluorescent signal was normalized to transfected- control group. Exposing the cells to iron increased CFP fluorescence. B) Quantification of (A). C) Representative images for PGSK. PGSK is a fluorescent dye that accumulates intracellularly and gets quenched by iron. D) Quantification obtained from total green fluorescence per field of view. 5-10 images*

*were used per n number. Data are expressed as mean values ± SEM (n = 3). Two-way ANOVA and Student's t-test were used. * indicates significant difference ($p \leq 0.05$) from control group.*

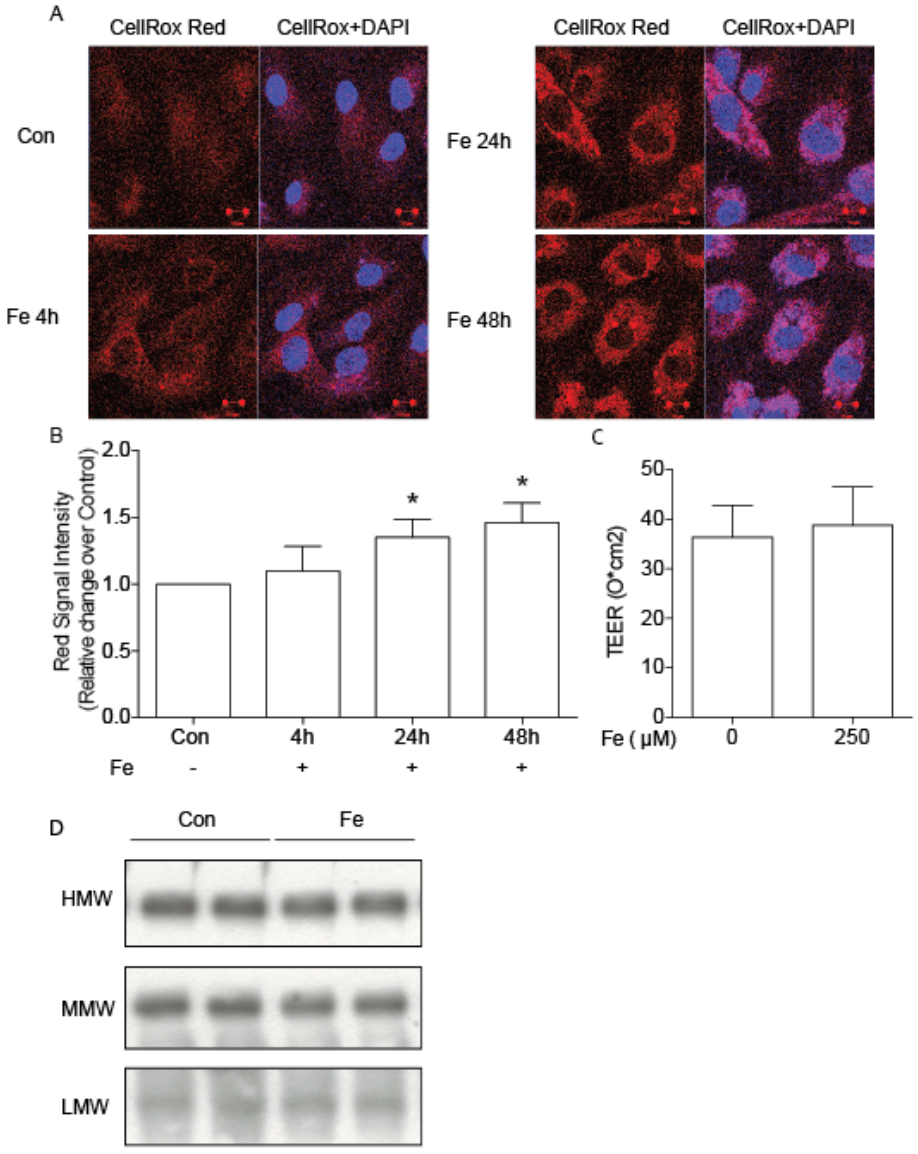

Figure 3: *The effects of iron on HDMEC monolayer. A) Representative image of reactive oxygen species (ROS) upon iron treatment. CellRox Red is a dye that becomes fluorescent upon oxidation by ROS. 5 uM of CellRox Deep Red reagent was added half an hour before*

*iron. B) Quantification of A. Total red signal in the field of view was normalized to total DAPI signal in that field of view. 5-10 images were used per n number. C) TEER after 48 hrs iron treatment. E) adiponectin flux after 48 hrs iron treatment by western blots. Data are expressed as mean values ± SEM (n = 3-4). Two-way ANOVA and Student's t-test were used. * indicates significant difference ($p \leq 0.05$) from control group.*

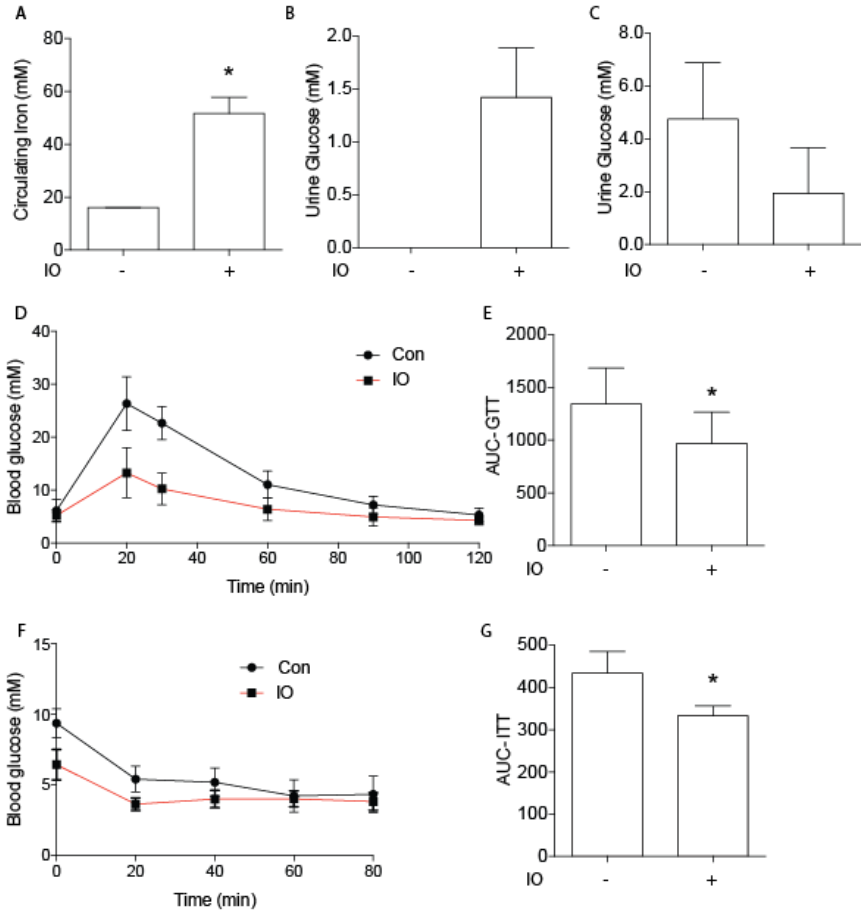

Figure 4: *Characterizing IO mouse model. Mice were intraperitoneally (i.p.) injected with iron for 4 weeks, 5 days per week at 10mg/ 25g of body weight to generate the IO model. Control mice were i.p injected with 10% dextrose. A) Circulating iron. Serum was used to test for circulating iron. B) Secreted glucose (non- fasted) determined in urine. C) Secreted glucose (fasted) determined in urine. D) Glucose Tolerance Test (GTT). Mice were i.p*

*injected with glucose at 2g/ kg of body weight. Blood glucose was recorded over period of 120 minutes at indicated times. E) Quantification of GTT, area under the curve. F) Insulin Tolerance Test (ITT). Mice were i.p injected with insulin at 1 unit/kg of body weight. Blood glucose was recorded over period of 80 minutes at indicated times. G) Quantification of ITT, area under the curve. Data are expressed as mean values ± SEM (n = 3-9). * indicates significant difference ($p \leq 0.05$) from control group. Student's t-test was used.*

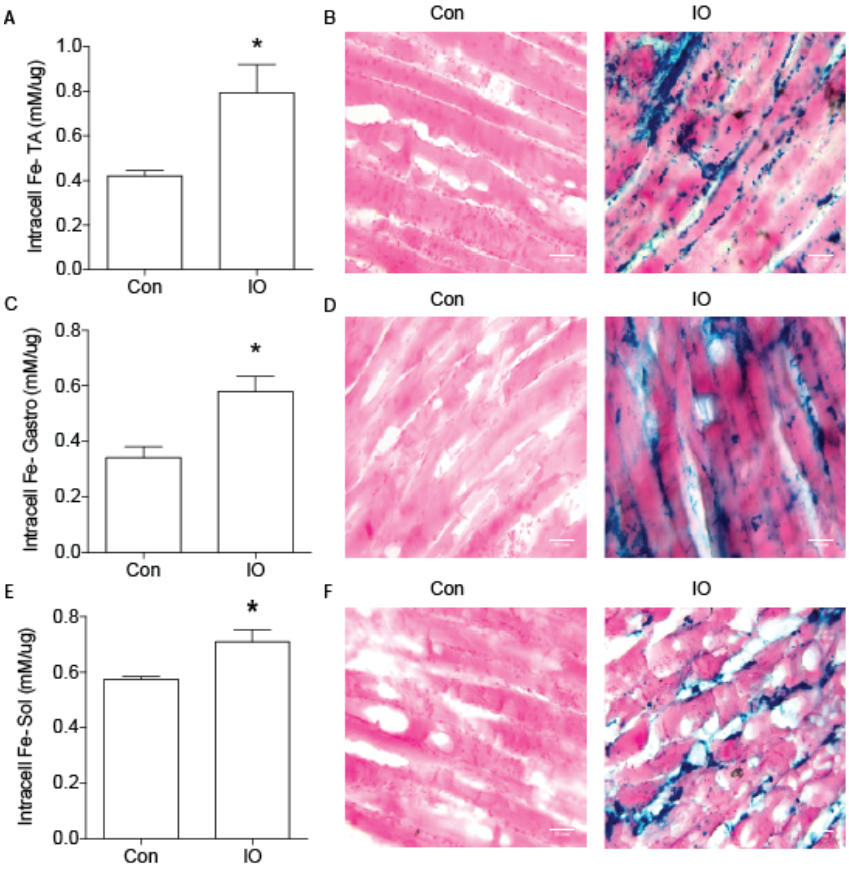

Figure 5: *Iron accumulation in IO mouse skeletal muscles. Tissues were isolated after 4 weeks injection with or without iron. Tissue lysates were used to detect intracellular iron. Amount of iron was normalized to protein concentration. A) Iron accumulation in tibialis anterior (TA) muscle. C) Iron accumulation in gastrocnemius (gastro). E) Iron*

*accumulation in soleus (sol). B,D, F) Representative images for Prussian blue staining in TA, gastro and sol. Data are expressed as mean values ± SEM (n = 3). * indicates significant difference (p ≤ 0.05) from control group. Student's t-test was used.*

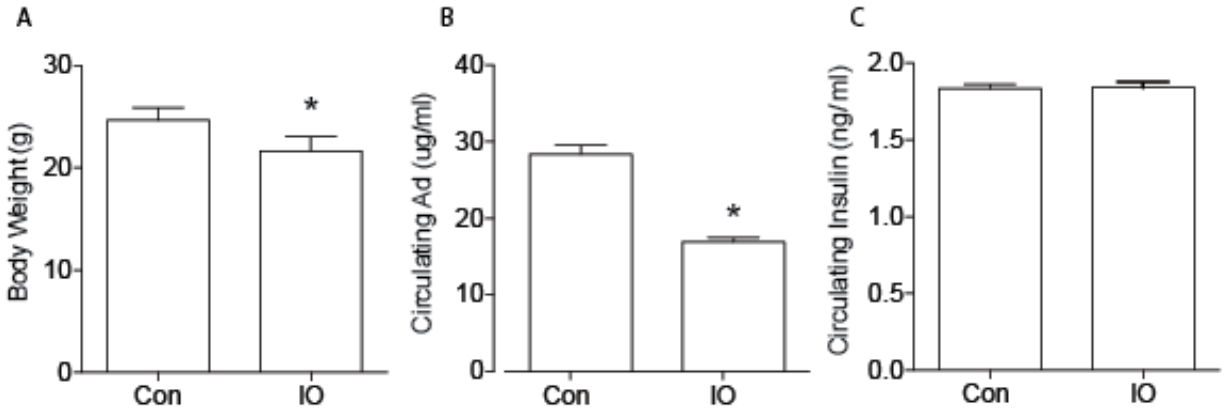

Figure 6: *Hormonal changes in IO mice. A) Mouse body weight after 4 weeks of dextrose (Con) or iron injection. B) Circulating fAd. Mouse adiponectin (fAd) ELISA kit was used to detect serum fAd. C) Circulating insulin. Mouse insulin ELISA kit was used to detect serum insulin. Data are expressed as mean values ± SEM (n = 3-9). * indicates significant difference (P ≤ 0.05) from control group. Student's t-test was used.*

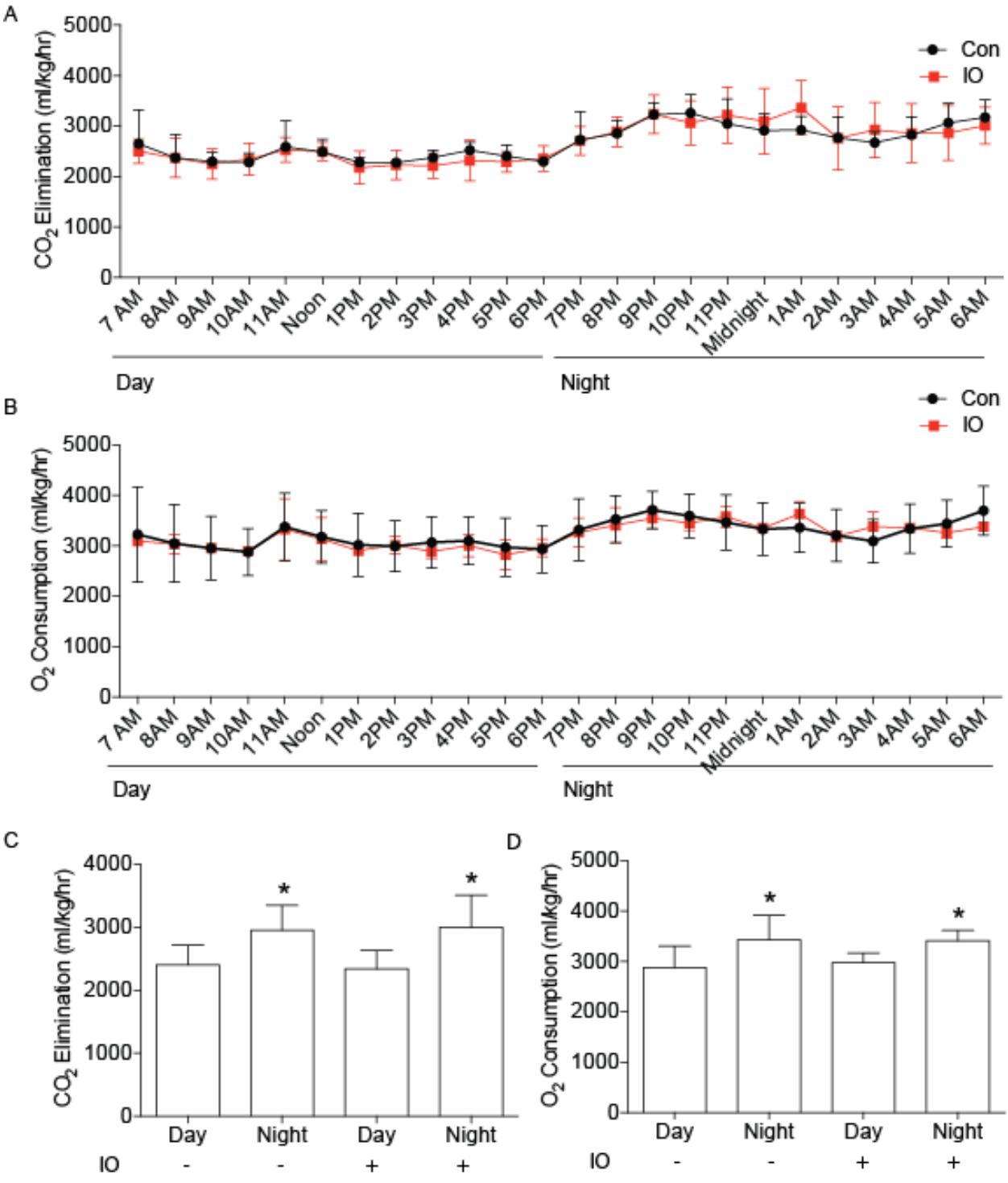

Figure 7: *Characterizing IO mouse respiration. Individual mice were kept in the comprehensive lab animal monitoring system (metabolic cage) for 3 days for measurement*

*of numerous metabolic parameters. Night time data were recorded between 7:00 PM and 6:00 AM, day time data collected between 7:00 AM and 6:00 PM. A) Oxygen (O_2) consumption. Data were collected as total amount of oxygen consumed by individual mice per hour then expressed as an average per hour for all 3 days for all animals. B) Carbon dioxide (CO_2) elimination. Data were collected as total amount of carbon dioxide eliminated by individual mice per hour then expressed as an average per hour for all 3 days for all animals. C) Quantification of O_2 consumption. Data expressed as an average of total O_2 consumed for all 3 days. D) Quantification of CO_2 elimination. Data expressed as an average of total CO_2 eliminated for all 3 days. Data are expressed as mean values ± SEM (n = 6-7). Two-way ANOVA was used comparing during day or night between groups. * indicates significant difference ($p \leq 0.05$) from control group.*

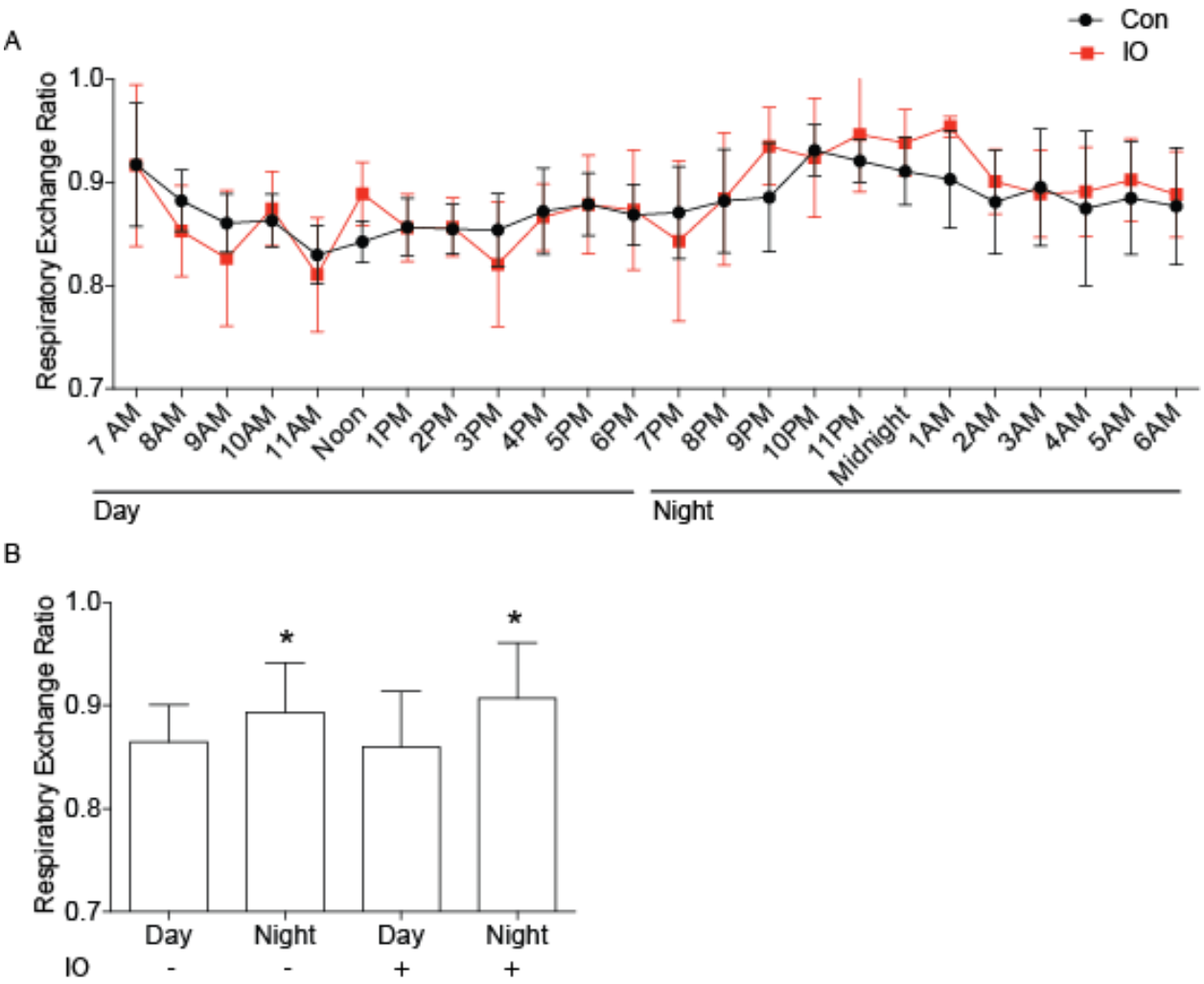

Figure 8: *IO mouse Respiratory Exchange Ratio. A) Respiratory Exchange Ratio. Data were calculated by taking the ratio of total carbon dioxide eliminated over oxygen consumed by individual mice per hour then expressed as an average per hour for all 3 days for all animals. B) Quantification of respiratory exchange ratio. Data expressed as averaged ratio over 3 days. Data are expressed as mean values ± SEM (n = 6-7). Two-way ANOVA was used comparing during day or night between groups. * indicates significant difference ($p \leq 0.05$) from control group.*

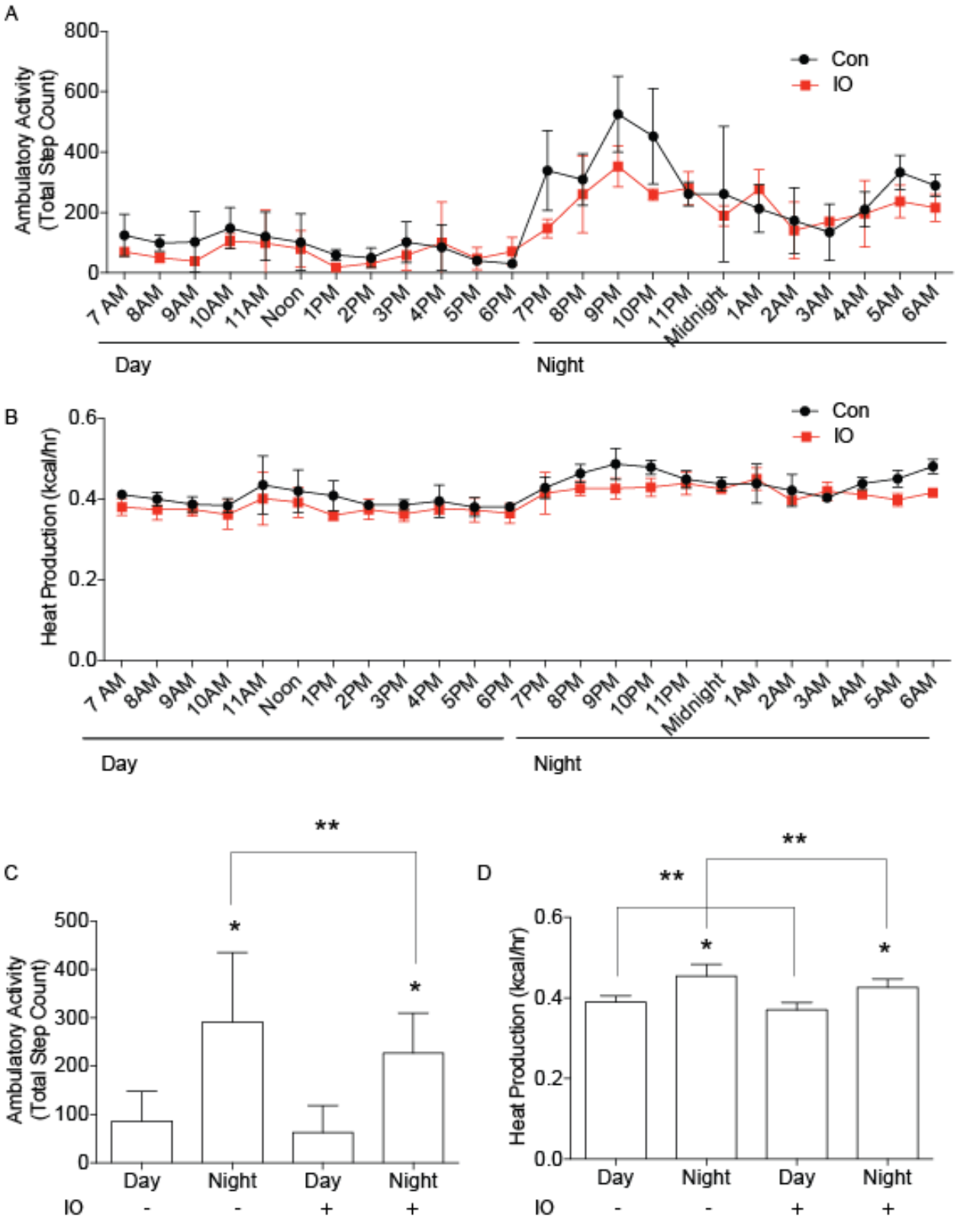
A
Ambulatory Activity (Total Step Count)
800
600
400
200
0
Con
IO
7 AM
8AM
9AM
10AM
11AM
Noon
1PM
2PM
3PM
4PM
5PM
6PM
7PM
8PM
9PM
10PM
11PM
Midnight
1AM
2AM
3AM
4AM
5AM
6AM
Day
Night
B
Heat Production (kcal/hr)
0.6
0.4
0.2
0.0
Con
IO
Day
Night
C
Ambulatory Activity (Total Step Count)
500
400
300
200
100
0
**
*
*
Day
Night
Day
Night
IO
-
-
+
+
D
Heat Production (kcal/hr)
0.6
0.4
0.2
0.0
**
**
*
*
Day
Night
Day
Night
IO
-
-
+
+

Figure 9: *Characterizing IO mouse phenotype. Individual mice were kept in the comprehensive lab animal monitoring system (metabolic cage) for 3 days for measurement of numerous metabolic parameters. A) Total ambulatory activity. Data were collected as total number of beam breaks (step counts) by individual mice per hour. This was then expressed as an average per hour from all animals for all 3 days. B) Heat production. Data was collected as total heat production per hour by individual mice, then expressed as an average per hour for all 3 days for all animals. C) Quantification of total ambulatory activity. Data expressed as an average of total step counts for all 3 days. D) Quantification of heat production. Data expressed as an average of total heat production for all 3 days for all animals. Data are expressed as mean values ± SEM (n = 6-7). Two-way ANOVA was used comparing during day or night between groups. * indicates significant difference ($p \leq 0.05$) from control group.*

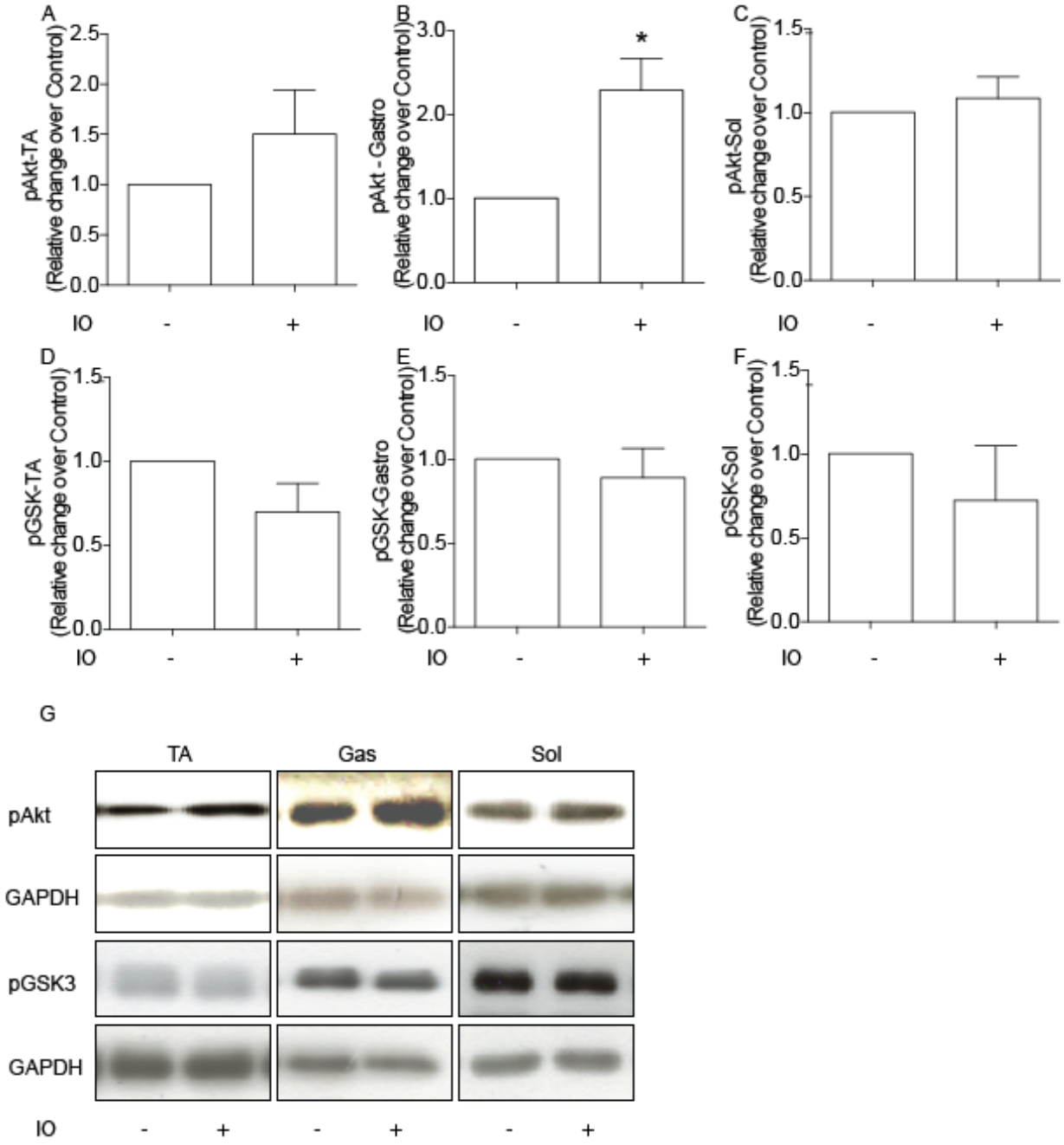

Figure 10*: Insulin signaling under IO conditions. Tissues were isolated after 4 weeks of iron injection. Mice were injection with 4U/ kg of insulin 5 minutes prior isolation of tissues. A-C) pAkt expression. A) TA. B) Gastroc. C) Soleus. D-F) pGSK expression. D) TA. E) Gastroc. F) Soleus. G) Representative western blots. Data are expressed as mean*

*values ± SEM (n = 3). * indicates significant difference (p ≤ 0.05) from control group. Student's t-test was used.*

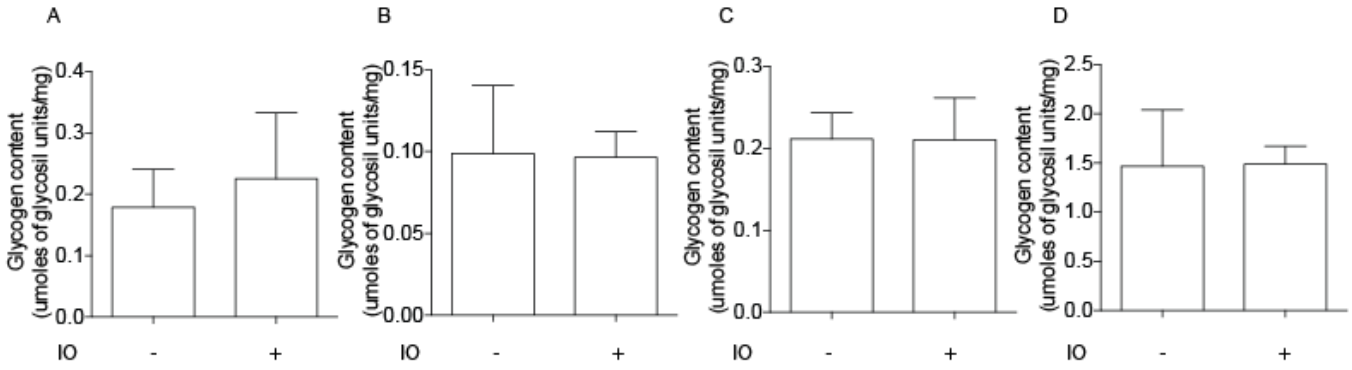

Figure 11*: Glycogen content in skeletal muscles and liver. A) TA. B) Gastroc. C) Soleus. D) Liver. Data are expressed as mean values ± SEM (n = 3-5). Data are expressed as mean values ± SEM (n = 3). * indicates significant difference (p ≤ 0.05) from control group. Student's t-test was used.*

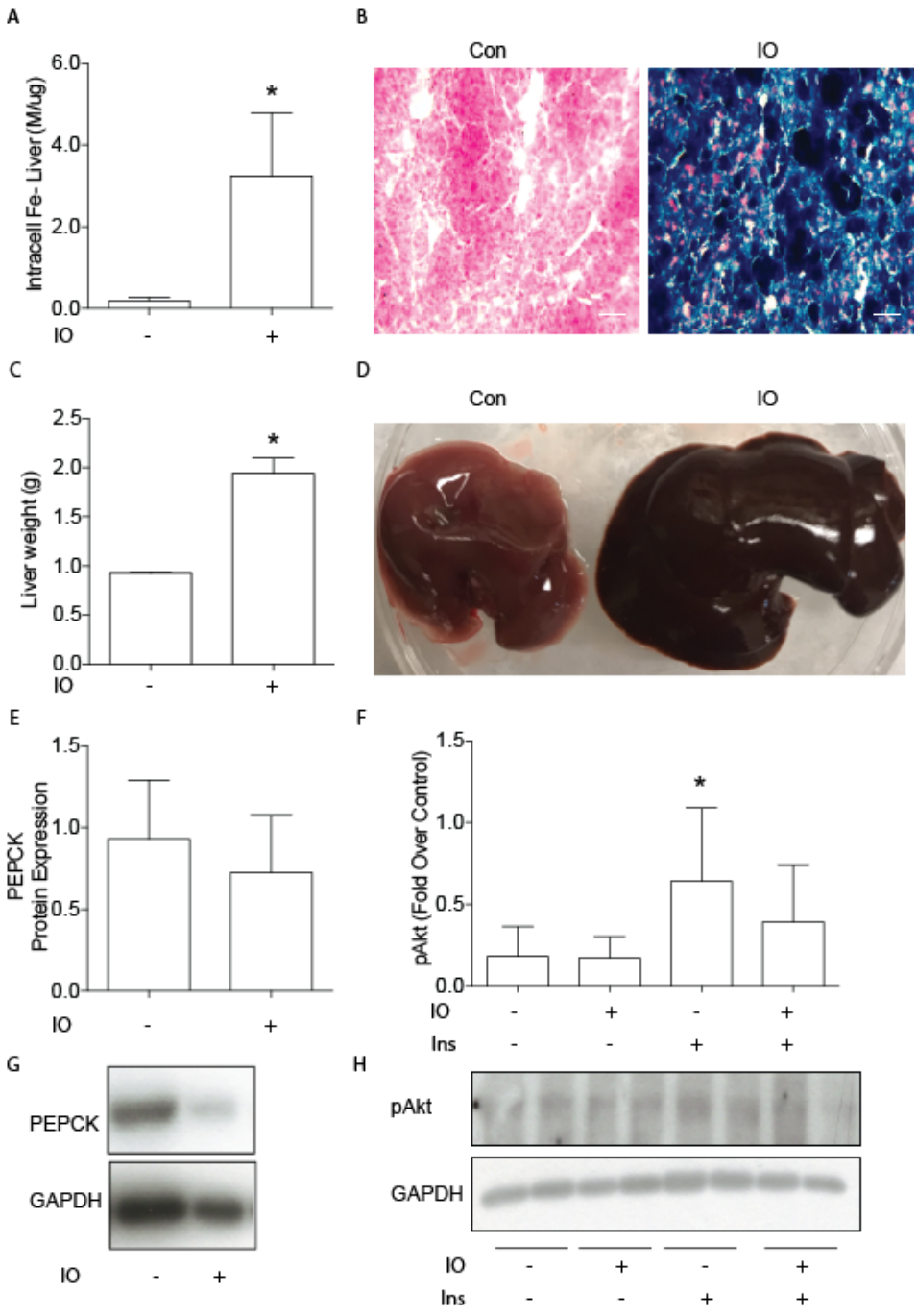

Figure 12: *Effects of iron on the liver. A) Intracellular liver iron content. B) Prussian blue staining for iron. C) Isolated liver weight. D) Isolated liver. E) PEPCK protein abundance. F) pAkt308 protein abundance G) representative blots for PEPCK protein. H) representative blot for pAkt308. Data are expressed as mean values ± SEM (n = 6-7). Data*

*are expressed as mean values ± SEM (n = 3). * indicates significant difference ($p \leq 0.05$) from control group. Student's t-test and two-way ANOVA were used.*

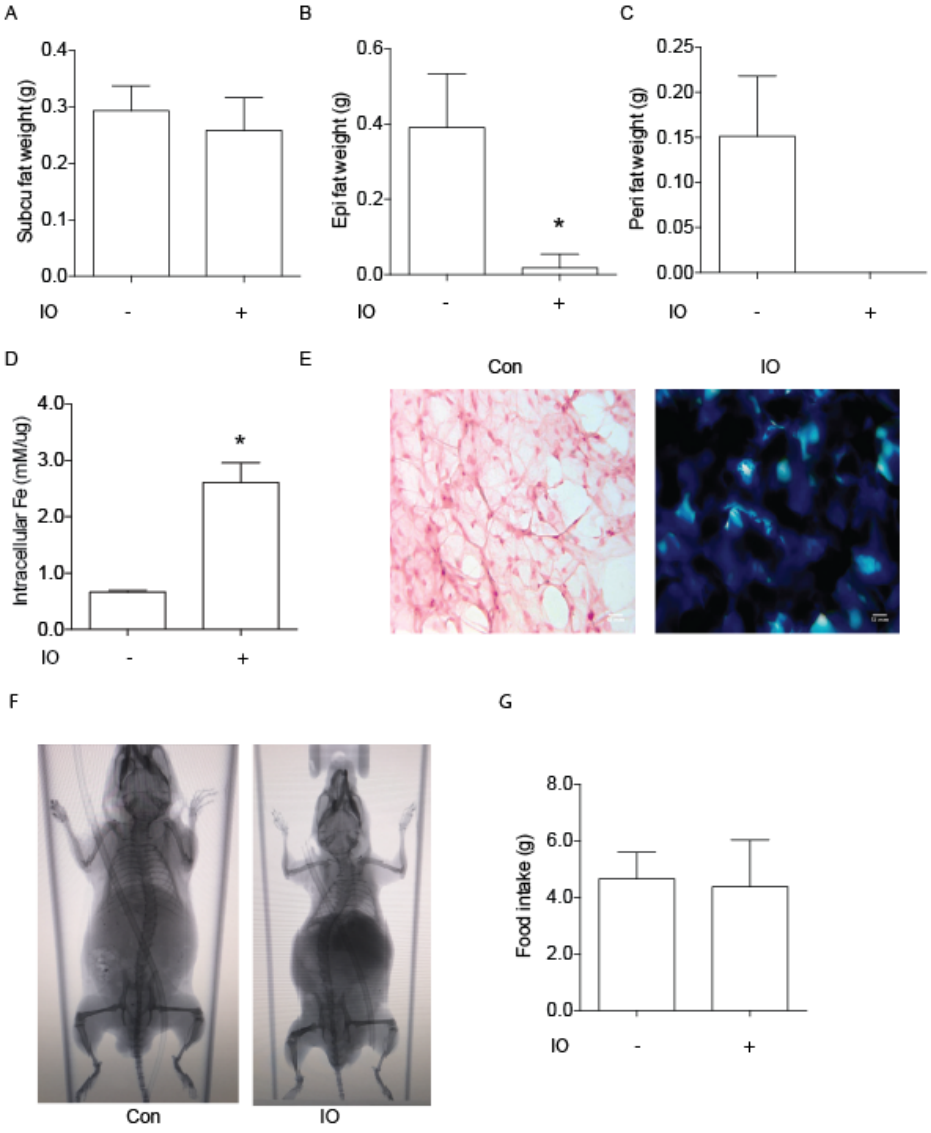

Figure 13: *Effects of iron on fat content. A) Weight of isolated subcutaneous fat from the inguinal region. B) Visceral fat- epididymal (epi) weight. C) visceral fat- perirenal (peri) weight. D) intracellular iron. E) Prussian blue staining for iron detection. F) micro-CT scan images. G) micro-CT scan quantification H) food intake. Data are expressed as mean*

*values ± SEM (n = 3-4). * indicates significant difference (p ≤ 0.05) from control group. Student's t-test was used.*

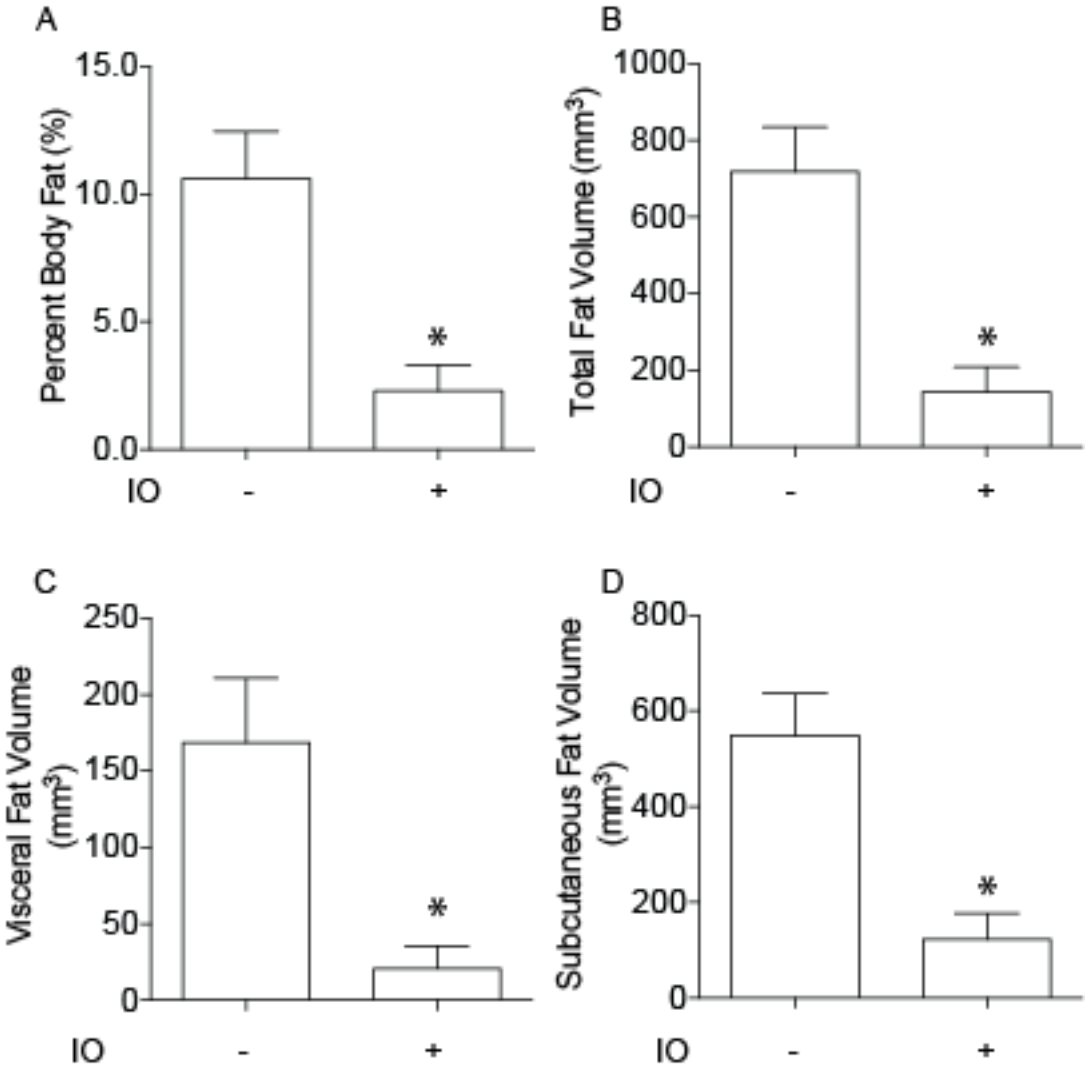

Figure 14*: Micro-CT quantification. Threshold was determined using whole mice to find the total body and fat volume using CT. Visceral fat was determined by manually highlighting the regions inside the mouse around the organs. Subcutaneous fat was calculated by subtracting visceral fat from the total fat. A) total percentage body fat. B) Total fat volume. C) Visceral fat volume. D) Subcutaneous fat volume. Data are expressed*

*as mean values ± SEM (n = 3). * indicates significant difference ($p \leq 0.05$) from control group. Student's t-test was used.*

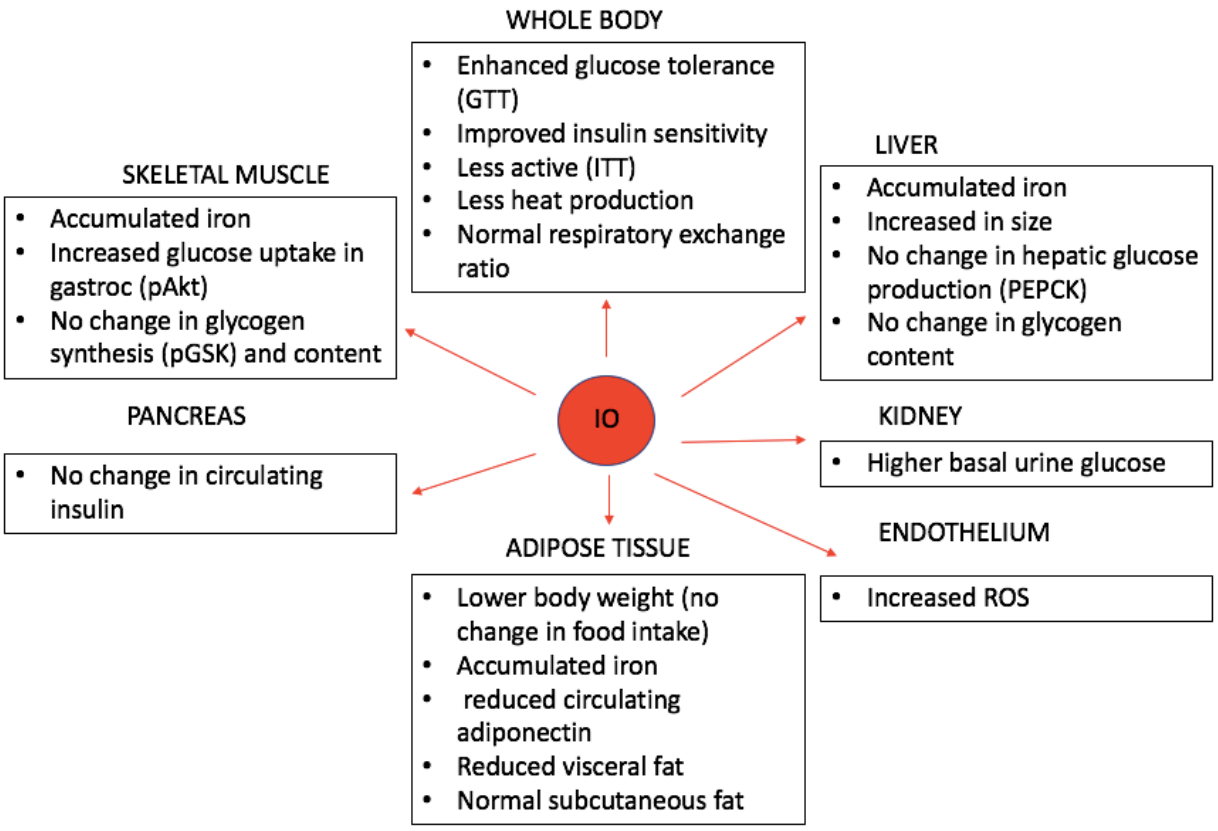

Figure 15*: Summary the effects of iron on different tissues.*

3.5 Discussion

We validated the HDMEC IO model using multiple methods including PGSK and IRE-CFP, and used this model for monitoring alterations in Ad movement (fig. 2). We concluded from our study, which consisted of 48 hrs of iron treatment, that transport of hormones did not alter, because there was no change in TEER or movement of Ad across the endothelium (fig. 3D,E). We further elucidated whether iron has an impact on metabolism in an animal model by creating an IO mouse model to investigate the effect of iron on metabolism. This model mimicked genetic HH disease. We successfully elevated iron levels in the blood (Fig. 4A) and iron accumulation in various skeletal muscles and fat (fig. 5). Our observation by GTT and ITT was that IO mice had better glucose clearance (fig. 4D,F). This contradicted previous findings that chronic IO results in decreased glucose clearance (Dongiovanni et al., 2013; Yu et al., 2015). Insulin signalling was enhanced in gastroc, as determined by pAkt activation that was stimulated by insulin (fig. 10B). Akt is involved in the regulation of many cellular functions including energy metabolism, cell proliferation, and apoptosis. The PI3K pathway is a key component in the regulation of glucose metabolism. Currently, there are no reports of enhancing pAkt activation in skeletal muscle under IO condition. However, in mouse hippocampal neurons, studies have shown the presence of iron caused an increase in the phosphorylation level of Akt in a PI3K-dependent manner. Additionally, nuclear localization of PI3K and Akt increased upon iron treatment as shown by immunohistochemistry. In contrast, nuclear localization of GSK3β decreased in the presence of iron (Uranga et al., 2013). This could potentially explain why phosphorylated Akt was unable to activate GSK3β via direct phosphorylation. With the currently accepted model of Akt phosphorylation/activation in skeletal muscle,

Akt is translocated from the cytoplasm and activated at the inner leaflet of the plasma membrane, rather than in the nucleus as shown in mouse hippocampal neurons (Motti et al., 2004; Santi and Lee, 2010; Zhou et al., 2001), Hence, further immunohistochemistry could be performed to confirm the hypothesis of GSK translocation by using MAPK/ERK as nuclear and cytosolic markers. Despite the GSK translocation theory, a glycogen content assay is needed to further confirm the functional effect of iron on GSK-3β activity. We speculated the lower blood glucose level resulted in more glycogen production in both liver and muscles. Hence, we examined the effect of iron-induced protein kinase activation on glycogen metabolism. Previous studies show that chelation reversed iron's effect on insulin signaling by increasing pAkt and GSK-3β, therefore enhancing glycogen synthesis in the liver (Dongiovanni et al., 2008). Interestingly, there was no change in GSK-3β phosphorylation or glycogen content in either skeletal muscles or liver in the current study (fig. 11).

Mouse activity level was tested as a potential contributor to lowered blood glucose levels, as blood glucose would decrease when the mice are active. Thus we hypothesized that enhanced glucose clearance observed in IO mice was due to higher physical activity. A group of researchers previously used genetic IO and found these mice had better glucose tolerance (Huang et al., 2007). The study concluded that increased glucose disposal does not result from increased insulin action. Instead, these mice demonstrated increased Ad levels and activation of AMPK. However, AMPK level can be closely associated to the activity of the mice; if the mice are more active, pAMPK increases (Huang et al., 2007). We utilized metabolic cages to confirm whether the IO mice are more active as compared to the control. If they have normal activity compared to control mice, we could explain the

phenotype using AMPK activity level (Huang et al., 2007). When they are more active, pAMPK is usually increased (Huang et al., 2007), hence decreasing blood glucose. Interestingly, IO mice did not exhibit higher activity compared to control mice (fig. 9).

Circulating levels of insulin did not change with IO (fig. 6C). Furthermore, circulating Ad was reduced by almost half (fig. 6B), potentially due to a significant reduction in visceral fat (fig.13B,C, 14C). Therefore, the observed effect in this study is limited.

There is a strong link between iron overload and kidney dysfunction. As reported from clinical studies, urine analysis of β-thalassemia patients had higher albumin and β2-macroglobulin, as well as higher NAG activity, which are positively correlated with serum ferritin and iron deposition (Koliakos et al., 2003). Hence, we tested whether iron affects glucose excretion. We observed an increased urine glucose level in mice in the non-fasted state after iron injection. Under basal conditions, iron-injected mice secreted more glucose, similar to the STZ-induced diabetic condition (Montilla et al., 2005). This observation suggested that iron treatment can have a diuretic effect and may eventually lead to iron-induced diabetic nephropathy in these mice if the injection was to continue further. Renal failure could possibly have contributed to lowered blood glucose levels. Furthermore, as kidneys play a major role in glucose homeostasis through reabsorption via the sodium glucose cotransporter (SGLT) (Kalra et al., 2016), down-regulation of SGLT could potentially explain the increased glucose excretion.

Phosphoenolpyruvate carboxylase (PEPCK), a protein that regulates blood glucose levels through hepatic glucose production, is supressed by an anti-diabetic substance (D_xylose), hence reducing glucose production in the liver on top of enhancing the

regeneration of pancreas tissues to increase insulin levels. Therefore, these mice have better glucose clearance by enhanced glucose uptake (Kim et al., 2016). The basal level of PEPCK after iron treatment did not change (fig. 12G). Therefore, the lower blood glucose (enhanced glucose clearance) was not due to supressing glucose production or secretion by the liver under IO conditions. The synthesis of glucose into glycogen in the liver contributes to the regulation of circulating glucose levels (Irimia et al., 2010). The improved glucose clearance might be a homeostatic strategy for the liver to compensate for the effects of excess iron. In mice with type 2 diabetes, treatment with obestatin showed improved insulin sensitivity and reduced liver mass, while glycogen content was higher in these obestatin treated mice (Kolodziejski et al., 2017).

Adipocytes are known for their function to store energy, and play an important role in energy balance. To further examine the role of adipocytes as regulators of energy balance in IO, we demonstrated that iron accumulated in fat tissue (fig. 12D,E), which may be due to an increase in hepcidin expression levels, as reported in cultured adipocytes (Andrews and Arredondo, 2012). IO mice induced a lipodystrophy-like condition, a heterogeneous autosomal recessive disorder that results in abnormal and degraded adipose tissues. Lipodystrophies are often associated with loss of subcutaneous adipose tissue and increase in visceral fat mass, and they exhibit pathophysiology of insulin resistance and abnormal triglyceride metabolism (Akpinar et al., 2015). However, the fat loss observed in IO mice was limited to the visceral depot, which is the opposite of lipodystrophy. Hence, lipolysis is likely a more accurate word to describe the observation. A similar observation was reported in cultured adipocytes, where iron increased lipolysis (Rumberger et al., 2004). The fat loss induced by IO was partial/selective rather than whole body. Only visceral fat

was affected in these IO mice. There were reports that patients with lipodystrophy had higher circulating levels of free fatty acids. Under normal conditions, adipocytes enlarge and store more triglycerides (TG). However, in patients that lack adipocytes, the excess TG gets stored in liver and skeletal muscles. This abnormal TG storage will eventually lead to insulin resistance and its complications (Muniyappa et al., 2014; Petersen et al., 2002).

This loss in fat induced by iron is responsible for the reduction in circulating Ad, similar to previously reported data (Gabrielsen et al., 2012). The elevated iron level might impair the Ad signalling pathway, hence leading to the onset of diabetes. Iron chelation therapy with desferrioxamine and deferiprone has significantly increased Ad levels in β-thalassaemia patients (Chaliasos et al., 2010).

In summary, acute IO did not affect circulating insulin levels. However, Ad levels were reduced by half. This phenotype might be an indicator of impaired Ad signalling induced by excessive iron. This IO model can be a potential tool for studying the underlying mechanisms in the progression of diabetes induced by iron. In adipose tissue, the DNA-binding protein high mobility group box 1 (HMGB1) was shown to be a pro-inflammatory mediator by releasing cytokines such as tumor necrosis factor-α (TNF-α) and promoting immune cell activation. Activated immune cells including macrophages secrete additional HMGB1 to further recruit additional immune cells. It has been demonstrated in obese mice that immune cell infiltration in adipose tissue contributes to the development of type 2 diabetes by supressing insulin-stimulated Akt phosphorylation (Feuerer et al., 2009; Winer et al., 2009). Adipose tissue dysfunction is considered as one of the main causes of diabetes. Future experiments to understand macrophage infiltration are needed, as it has been demonstrated that increased inflammatory cells in visceral adipose tissue impair adipocyte

function by reducing lipogenesis and increasing lipolysis (McGillicuddy et al., 2009; Souza et al., 2003). Current experiments may explain the observable decrease in fat tissue. Furthermore, the phenotype could be explained by six transmembrane protein of prostate 2 (STAMPS), a protein that is well known for its anti-inflammatory role and maintaining normal glucose level. Previous studies have shown overexpression of STAMPS reduced adipocyte size in obese mice (Wang et al., 2017). Hence, measuring adipocyte size can also be a good indicator for the progression of diabetes in these IO mice.

Lastly, previous research has shown the antioxidant role of activated Akt against oxidative stress that is induced by iron via an increase in ROS production. Such cells exhibited higher ROS levels when treated with a combination of iron and LY294002 (an Akt inhibitor), as opposed to treatment with iron alone. Conversely, using a cell line overexpressing Akt, it was possible to observe a reduction in ROS, hence protecting the cells from oxidative stress (Uranga et al., 2013). Oxidative stress has been considered a main contributor to impaired insulin signaling. Multiple experimental approaches have lead to the suggestion that the PI3K/Akt pathway is the initial response in preventing the negative effect of increasing cellular ROS levels generated by iron exposure. The mice under iron treatment will potentially progress to insulin and adiponectin resistance. Hence, early protection against excessive iron is required to arrest the progression and the deleterious effects. Such prevention can include the use of iron chelator, as clinical studies have demonstrated the effectiveness of iron chelation on the maintenance of normal glucose tolerance (Cooksey et al., 2010).

Chapter 4: Conclusion

4.1 Summary of research

I started my Masters research using HUVECs as a model. They are considered to have a leaky endothelium due to its venous derivation, and have been used in many studies to examine the effect of Dex (Goodwin et al., 2013; Wang et al., 2015). More recently, we used what we believe is a more physiologically relevant model, HDMEC. Since the microvascular complications of diabetes such as diabetic retinophaty, are well-known (Sacks et al., 2014). As HDMEC is also a tighter endothelium model compared to HUVEC, we hypothesized that we would be better able to see a change if iron causes the endothelium to be leakier. Regardless, they both are good representative models of endothelium.

Our study indicated that glucocorticoid-mediated tightening of endothelium can reduce flux of Ad across endothelial monolayers, and that this may be due to alterations in the expression profile of tight junction proteins. Furthermore, in a rat model of diabetes induced by exogenous glucocorticoids, we observed reduced interstitial and intracellular levels of Ad in skeletal muscle. Thus, we propose that reduced Ad action in target tissues, as a consequence of reduced endothelial flux from circulation to interstitial space, may contribute to the diabetic phenotype occurring after glucocorticoid treatment. Since glucocorticoids are one of the most commonly prescribed medications, our discovery of reduced Ad transport in response to glucocorticoids is a particularly important and novel finding with potentially far-reaching consequences, leading to the rationale for a second project to study whether iron could regulate endothelium Ad movement, hence altering glucose metabolism. Using a more physiologically-relevant iron overload HDMEC model, we have found that iron did not change the endothelium tightness nor Ad movement to the

target tissues, despite the elevated ROS production. To further elucidate the effect of iron on whole body glucose metabolism, we have successfully created an IO mouse model. I have found these mice have better glucose clearance compared to the control mice. We proposed that the underlying mechanism involved an upregulation of pAkt and constant excretion of glucose through in the urine as a compensatory mechanism to lower blood glucose. Additionally, we have shown that circulating Ad is reduced by half whereas insulin level was not affected by iron treatment.

4. 2 Future directions

Iron overload has been well established as a contributor to the development of insulin resistance and impairment of glucose metabolism, which is characteristic of metabolic disorders such as type 2 diabetes (Rumberger et al., 2004). In addition, research has shown the antioxidant role of activated Akt against oxidative stress induced by iron via the increase in ROS production. The cells showed much higher ROS levels when using a combination of iron and LY294002 (an Akt inhibitor) compared to treatment with iron alone. However, using a cell line overexpressing Akt, they were able to observe a reduction in ROS, hence protecting cells from oxidative stress (Uranga et al., 2013). Oxidative stress has been long considered a main contributor to impaired insulin signaling. This group also used multiple approaches to show the protective role of the PI3K/ Akt pathway as the initial response in preventing the negative effect of increased cellular ROS levels generated by iron exposure. These mice will potentially progress to insulin and Ad resistance if iron treatment is sustained, hence an early prevention is required (Uranga et al., 2013). Clinical studies have shown the effectiveness of using an iron chelator as treatment in obese mice, allowing maintenance of normal glucose tolerance (Cooksey et al., 2010). Hence, given

the importance of pAkt, I would like to repeat Western blots for pAkt to confirm previous protein abundance observations. Furthermore, total Akt is required as loading control to see the effect of iron on basal Akt. Also, I would like to check GLUT4 translation using immunofluorescence, as this is the key protein involved in intracellular insulin signalling, downstream of pAkt (Takenaka et al., 2014). Finally, I would like to evaluate glucose uptake in this mouse model using radioactive tracer (Ishino et al., 2017).

An additional finding in my study was that Ad levels are reduced by half, in association with diminished fat content. The same observation was reported in cultured adipocytes where iron increased lipolysis (Rumberger et al., 2004). Furthermore, iron overload reduced the abundance of adipocyte iron export channel (ferroportin), leading to decreased Ad and insulin resistance. Hence, for future studies, a time course iron treatment (1, 2, 3 weeks) to study the effect of iron on adipocytes and insulin resistance, characterized by mRNA and protein abundance, can be highly beneficial. This future study will help address and target the key stages in preventing the deleterious effect of excess iron.

Finally, kidneys isolated from IO mice could be an important target, as kidneys play a major role in glucose homeostasis through glucose reabsorption via sodium glucose cotransporter (SGLT). In diabetic patients, the SGLTs gene is upregulated (Kalra et al., 2016). Therefore, SGLT protein abundance may confirm the underlying mechanism that is responsible for glucose excretion.

4.3 Concluding remarks

In conclusion, my *in vitro* and *in vivo* studies present the importance of Ad access to target tissues in altering glucose metabolism. My studies have suggested the mechanism

through which iron enhanced glucose clearance via upregulation of Akt phosphorylation and glucose excretion. With the future plans, I hope to provide more insight into the underlying mechanism that is responsible for the enhanced glucose clearance, as well as identify potential targets for diabetes therapies.

Chapter 5 References

Abraham, D., Rogers, J., Gault, P., Kushner, J.P., and McClain, D.A. (2006). Increased insulin secretory capacity but decreased insulin sensitivity after correction of iron overload by phlebotomy in hereditary haemochromatosis. Diabetologia *49*, 2546-2551.

Agarwal, A., Sarwar, S., Sepah, Y.J., and Nguyen, Q.D. (2015). What have we learnt about the management of diabetic macular edema in the antivascular endothelial growth factor and corticosteroid era? Current opinion in ophthalmology *26*, 177-183.

Aguirre, V., Uchida, T., Yenush, L., Davis, R., and White, M.F. (2000). The c-Jun NH(2)-terminal kinase promotes insulin resistance during association with insulin receptor substrate-1 and phosphorylation of Ser(307). The Journal of biological chemistry *275*, 9047-9054.

Aird, W.C. (2007a). Phenotypic heterogeneity of the endothelium: I. Structure, function, and mechanisms. Circulation research *100*, 158-173.

Aird, W.C. (2007b). Phenotypic heterogeneity of the endothelium: II. Representative vascular beds. Circulation research *100*, 174-190.

Akpinar, F., Demir, E., and Apa, D.D. (2015). Membranous lipodystrophy: case report and review of the literature. Anais brasileiros de dermatologia *90*, 115-117.

Andrews, M., and Arredondo, M. (2012). Hepatic and adipocyte cells respond differentially to iron overload, hypoxic and inflammatory challenge. Biometals : an international journal on the role of metal ions in biology, biochemistry, and medicine *25*, 749-759.

Arita, Y., Kihara, S., Ouchi, N., Maeda, K., Kuriyama, H., Okamoto, Y., Kumada, M., Hotta, K., Nishida, M., Takahashi, M.*, et al.* (2002). Adipocyte-derived plasma protein adiponectin acts as a platelet-derived growth factor-BB-binding protein and regulates growth factor-induced common postreceptor signal in vascular smooth muscle cell. Circulation *105*, 2893-2898.

Ashwell, J.D., Lu, F.W., and Vacchio, M.S. (2000). Glucocorticoids in T cell development and function*. Annual review of immunology *18*, 309-345.

Backer, J.M. (2010). The regulation of class IA PI 3-kinases by inter-subunit interactions. Current topics in microbiology and immunology *346*, 87-114.

Bandyopadhyay, G., Standaert, M.L., Galloway, L., Moscat, J., and Farese, R.V. (1997). Evidence for involvement of protein kinase C (PKC)-zeta and noninvolvement of diacylglycerol-sensitive PKCs in insulin-stimulated glucose transport in L6 myotubes. Endocrinology *138*, 4721-4731.

Bandyopadhyay, G., Standaert, M.L., Sajan, M.P., Karnitz, L.M., Cong, L., Quon, M.J., and Farese, R.V. (1999). Dependence of insulin-stimulated glucose transporter 4 translocation on 3-phosphoinositide-dependent protein kinase-1 and its target threonine-410 in the activation loop of protein kinase C-zeta. Molecular endocrinology (Baltimore, Md) *13*, 1766-1772.

Barrett, E.J., Wang, H., Upchurch, C.T., and Liu, Z. (2011). Insulin regulates its own delivery to skeletal muscle by feed-forward actions on the vasculature. American journal of physiology Endocrinology and metabolism *301*, E252-263.

Beaudry, J.L., D'Souza A, M., Teich, T., Tsushima, R., and Riddell, M.C. (2013). Exogenous glucocorticoids and a high-fat diet cause severe hyperglycemia and

hyperinsulinemia and limit islet glucose responsiveness in young male Sprague-Dawley rats. Endocrinology *154*, 3197-3208.
Beaudry, J.L., Dunford, E.C., Leclair, E., Mandel, E.R., Peckett, A.J., Haas, T.L., and Riddell, M.C. (2015). Voluntary exercise improves metabolic profile in high-fat fed glucocorticoid-treated rats. Journal of applied physiology (Bethesda, Md : 1985) *118*, 1331-1343.
Beaudry, J.L., Dunford, E.C., Teich, T., Zaharieva, D., Hunt, H., Belanoff, J.K., and Riddell, M.C. (2014). Effects of selective and non-selective glucocorticoid receptor II antagonists on rapid-onset diabetes in young rats. PloS one *9*, e91248.
Bernal-Mizrachi, E., Wen, W., Stahlhut, S., Welling, C.M., and Permutt, M.A. (2001). Islet beta cell expression of constitutively active Akt1/PKB alpha induces striking hypertrophy, hyperplasia, and hyperinsulinemia. The Journal of clinical investigation *108*, 1631-1638.
Bjorntorp, P., and Rosmond, R. (2000). Obesity and cortisol. Nutrition (Burbank, Los Angeles County, Calif) *16*, 924-936.
Blackburn, D., Hux, J., and Mamdani, M. (2002). Quantification of the Risk of Corticosteroid-induced Diabetes Mellitus Among the Elderly. Journal of general internal medicine *17*, 717-720.
Blecharz, K.G., Drenckhahn, D., and Forster, C.Y. (2008). Glucocorticoids increase VE-cadherin expression and cause cytoskeletal rearrangements in murine brain endothelial cEND cells. Journal of cerebral blood flow and metabolism : official journal of the International Society of Cerebral Blood Flow and Metabolism *28*, 1139-1149.
Boden, G. (1997). Role of fatty acids in the pathogenesis of insulin resistance and NIDDM. Diabetes *46*, 3-10.
Bodenlenz, M., Schaupp, L.A., Druml, T., Sommer, R., Wutte, A., Schaller, H.C., Sinner, F., Wach, P., and Pieber, T.R. (2005). Measurement of interstitial insulin in human adipose and muscle tissue under moderate hyperinsulinemia by means of direct interstitial access. American journal of physiology Endocrinology and metabolism *289*, E296-300.
Booth, G., and Cheng, A.Y. (2013). Canadian Diabetes Association 2013 clinical practice guidelines for the prevention and management of diabetes in Canada. Methods. Canadian journal of diabetes *37 Suppl 1*, S4-7.
Braet, F., and Wisse, E. (2002). Structural and functional aspects of liver sinusoidal endothelial cell fenestrae: a review. Comparative hepatology *1*, 1.
Breiderhoff, T., Himmerkus, N., Stuiver, M., Mutig, K., Will, C., Meij, I.C., Bachmann, S., Bleich, M., Willnow, T.E., and Muller, D. (2012). Deletion of claudin-10 (Cldn10) in the thick ascending limb impairs paracellular sodium permeability and leads to hypermagnesemia and nephrocalcinosis. Proceedings of the National Academy of Sciences of the United States of America *109*, 14241-14246.
Bromhead, C., Miller, J.H., and McDonald, F.J. (2006). Regulation of T-cadherin by hormones, glucocorticoid and EGF. Gene *374*, 58-67.
Buren, J., and Eriksson, J.W. (2005). Is insulin resistance caused by defects in insulin's target cells or by a stressed mind? Diabetes/metabolism research and reviews *21*, 487-494.

Buren, J., Lai, Y.C., Lundgren, M., Eriksson, J.W., and Jensen, J. (2008). Insulin action and signalling in fat and muscle from dexamethasone-treated rats. Archives of biochemistry and biophysics *474*, 91-101.
Butler, A.E., Janson, J., Bonner-Weir, S., Ritzel, R., Rizza, R.A., and Butler, P.C. (2003). Beta-cell deficit and increased beta-cell apoptosis in humans with type 2 diabetes. Diabetes *52*, 102-110.
Ceddia, R.B., Somwar, R., Maida, A., Fang, X., Bikopoulos, G., and Sweeney, G. (2005). Globular adiponectin increases GLUT4 translocation and glucose uptake but reduces glycogen synthesis in rat skeletal muscle cells. Diabetologia *48*, 132-139.
Chaliasos, N., Challa, A., Hatzimichael, E., Koutsouka, F., Bourantas, D.K., Vlahos, A.P., Siamopoulou, A., Bourantas, K.L., and Makis, A. (2010). Serum adipocytokine and vascular inflammation marker levels in Beta-thalassaemia major patients. Acta haematologica *124*, 191-196.
Chen, Y., Pitzer, A.L., Li, X., Li, P.L., Wang, L., and Zhang, Y. (2015). Instigation of endothelial Nlrp3 inflammasome by adipokine visfatin promotes inter-endothelial junction disruption: role of HMGB1. Journal of cellular and molecular medicine *19*, 2715-2727.
Chiu, J.D., Kolka, C.M., Richey, J.M., Harrison, L.N., Zuniga, E., Kirkman, E.L., and Bergman, R.N. (2009). Experimental hyperlipidemia dramatically reduces access of insulin to canine skeletal muscle. Obesity (Silver Spring, Md) *17*, 1486-1492.
Chiu, J.D., Richey, J.M., Harrison, L.N., Zuniga, E., Kolka, C.M., Kirkman, E., Ellmerer, M., and Bergman, R.N. (2008). Direct administration of insulin into skeletal muscle reveals that the transport of insulin across the capillary endothelium limits the time course of insulin to activate glucose disposal. Diabetes *57*, 828-835.
Clark, A.R., and Belvisi, M.G. (2012). Maps and legends: the quest for dissociated ligands of the glucocorticoid receptor. Pharmacology & therapeutics *134*, 54-67.
Cole, T.J., Blendy, J.A., Monaghan, A.P., Krieglstein, K., Schmid, W., Aguzzi, A., Fantuzzi, G., Hummler, E., Unsicker, K., and Schutz, G. (1995). Targeted disruption of the glucocorticoid receptor gene blocks adrenergic chromaffin cell development and severely retards lung maturation. Genes & development *9*, 1608-1621.
Cooksey, R.C., Jones, D., Gabrielsen, S., Huang, J., Simcox, J.A., Luo, B., Soesanto, Y., Rienhoff, H., Abel, E.D., and McClain, D.A. (2010). Dietary iron restriction or iron chelation protects from diabetes and loss of beta-cell function in the obese (ob/ob lep-/-) mouse. American journal of physiology Endocrinology and metabolism *298*, E1236-1243.
Cooksey, R.C., Jouihan, H.A., Ajioka, R.S., Hazel, M.W., Jones, D.L., Kushner, J.P., and McClain, D.A. (2004). Oxidative stress, beta-cell apoptosis, and decreased insulin secretory capacity in mouse models of hemochromatosis. Endocrinology *145*, 5305-5312.
D'Souza A, M., Beaudry, J.L., Szigiato, A.A., Trumble, S.J., Snook, L.A., Bonen, A., Giacca, A., and Riddell, M.C. (2012). Consumption of a high-fat diet rapidly exacerbates the development of fatty liver disease that occurs with chronically elevated glucocorticoids. American journal of physiology Gastrointestinal and liver physiology *302*, G850-863.
Dadson, K., Liu, Y., and Sweeney, G. (2011). Adiponectin action: a combination of endocrine and autocrine/paracrine effects. Frontiers in endocrinology *2*, 62.

Dagenais, G.R., Tancredi, R.G., and Zierler, K.L. (1976). Free fatty acid oxidation by forearm muscle at rest, and evidence for an intramuscular lipid pool in the human forearm. The Journal of clinical investigation *58*, 421-431.
Das, S.K., Wang, W., Zhabyeyev, P., Basu, R., McLean, B., Fan, D., Parajuli, N., DesAulniers, J., Patel, V.B., Hajjar, R.J.*, et al.* (2015). Iron-overload injury and cardiomyopathy in acquired and genetic models is attenuated by resveratrol therapy. Scientific reports *5*, 18132.
Davis, R.J., Corvera, S., and Czech, M.P. (1986). Insulin stimulates cellular iron uptake and causes the redistribution of intracellular transferrin receptors to the plasma membrane. The Journal of biological chemistry *261*, 8708-8711.
Dimitriadis, G., Leighton, B., Parry-Billings, M., Sasson, S., Young, M., Krause, U., Bevan, S., Piva, T., Wegener, G., and Newsholme, E.A. (1997). Effects of glucocorticoid excess on the sensitivity of glucose transport and metabolism to insulin in rat skeletal muscle. The Biochemical journal *321 (Pt 3)*, 707-712.
Ding, H., and Triggle, C.R. (2010). Endothelial dysfunction in diabetes: multiple targets for treatment. Pflugers Archiv : European journal of physiology *459*, 977-994.
Ding, L., Lu, Z., Foreman, O., Tatum, R., Lu, Q., Renegar, R., Cao, J., and Chen, Y.H. (2012). Inflammation and disruption of the mucosal architecture in claudin-7-deficient mice. Gastroenterology *142*, 305-315.
Dongiovanni, P., Ruscica, M., Rametta, R., Recalcati, S., Steffani, L., Gatti, S., Girelli, D., Cairo, G., Magni, P., Fargion, S.*, et al.* (2013). Dietary iron overload induces visceral adipose tissue insulin resistance. The American journal of pathology *182*, 2254-2263.
Dongiovanni, P., Valenti, L., Ludovica Fracanzani, A., Gatti, S., Cairo, G., and Fargion, S. (2008). Iron depletion by deferoxamine up-regulates glucose uptake and insulin signaling in hepatoma cells and in rat liver. The American journal of pathology *172*, 738-747.
Fain, J.N., Madan, A.K., Hiler, M.L., Cheema, P., and Bahouth, S.W. (2004). Comparison of the release of adipokines by adipose tissue, adipose tissue matrix, and adipocytes from visceral and subcutaneous abdominal adipose tissues of obese humans. Endocrinology *145*, 2273-2282.
Feder, J.N., Gnirke, A., Thomas, W., Tsuchihashi, Z., Ruddy, D.A., Basava, A., Dormishian, F., Domingo, R., Jr., Ellis, M.C., Fullan, A.*, et al.* (1996). A novel MHC class I-like gene is mutated in patients with hereditary haemochromatosis. Nature genetics *13*, 399-408.
Fediuc, S., Gaidhu, M.P., and Ceddia, R.B. (2006). Inhibition of insulin-stimulated glycogen synthesis by 5-aminoimidasole-4-carboxamide-1-beta-d-ribofuranoside-induced adenosine 5'-monophosphate-activated protein kinase activation: interactions with Akt, glycogen synthase kinase 3-3alpha/beta, and glycogen synthase in isolated rat soleus muscle. Endocrinology *147*, 5170-5177.
Felinski, E.A., and Antonetti, D.A. (2005). Glucocorticoid regulation of endothelial cell tight junction gene expression: novel treatments for diabetic retinopathy. Current eye research *30*, 949-957.
Fernandez-Real, J.M., Lopez-Bermejo, A., and Ricart, W. (2002). Cross-talk between iron metabolism and diabetes. Diabetes *51*, 2348-2354.
Feuerer, M., Herrero, L., Cipolletta, D., Naaz, A., Wong, J., Nayer, A., Lee, J., Goldfine, A.B., Benoist, C., Shoelson, S.*, et al.* (2009). Lean, but not obese, fat is enriched for a

unique population of regulatory T cells that affect metabolic parameters. Nature medicine *15*, 930-939.
Ford, E.S. (2005). Prevalence of the metabolic syndrome defined by the International Diabetes Federation among adults in the U.S. Diabetes care *28*, 2745-2749.
Freidenberg, G.R., Suter, S., Henry, R.R., Nolan, J., Reichart, D., and Olefsky, J.M. (1994). Delayed onset of insulin activation of the insulin receptor kinase in vivo in human skeletal muscle. Diabetes *43*, 118-126.
Gabrielsen, J.S., Gao, Y., Simcox, J.A., Huang, J., Thorup, D., Jones, D., Cooksey, R.C., Gabrielsen, D., Adams, T.D., Hunt, S.C.*, et al.* (2012). Adipocyte iron regulates adiponectin and insulin sensitivity. The Journal of clinical investigation *122*, 3529-3540.
Gnana-Prakasam, J.P., Tawfik, A., Romej, M., Ananth, S., Martin, P.M., Smith, S.B., and Ganapathy, V. (2012). Iron-mediated retinal degeneration in haemojuvelin-knockout mice. The Biochemical journal *441*, 599-608.
Goddard, L.M., and Iruela-Arispe, M.L. (2013). Cellular and molecular regulation of vascular permeability. Thrombosis and haemostasis *109*, 407-415.
Goodwin, J.E., Feng, Y., Velazquez, H., and Sessa, W.C. (2013). Endothelial glucocorticoid receptor is required for protection against sepsis. Proceedings of the National Academy of Sciences of the United States of America *110*, 306-311.
Gozzelino, R., and Arosio, P. (2016). Iron Homeostasis in Health and Disease. International journal of molecular sciences *17*.
Gunzel, D., and Fromm, M. (2012). Claudins and other tight junction proteins. Comprehensive Physiology *2*, 1819-1852.
Gunzel, D., and Yu, A.S. (2013). Claudins and the modulation of tight junction permeability. Physiological reviews *93*, 525-569.
Handa, P., Morgan-Stevenson, V., Maliken, B.D., Nelson, J.E., Washington, S., Westerman, M., Yeh, M.M., and Kowdley, K.V. (2016). Iron overload results in hepatic oxidative stress, immune cell activation, and hepatocellular ballooning injury, leading to nonalcoholic steatohepatitis in genetically obese mice. American journal of physiology Gastrointestinal and liver physiology *310*, G117-127.
Hashimoto, T., Cook, W.S., Qi, C., Yeldandi, A.V., Reddy, J.K., and Rao, M.S. (2000). Defect in peroxisome proliferator-activated receptor alpha-inducible fatty acid oxidation determines the severity of hepatic steatosis in response to fasting. The Journal of biological chemistry *275*, 28918-28928.
Hayashi, T., Hirshman, M.F., Fujii, N., Habinowski, S.A., Witters, L.A., and Goodyear, L.J. (2000). Metabolic stress and altered glucose transport: activation of AMP-activated protein kinase as a unifying coupling mechanism. Diabetes *49*, 527-531.
Herkner, H., Klein, N., Joukhadar, C., Lackner, E., Langenberger, H., Frossard, M., Bieglmayer, C., Wagner, O., Roden, M., and Muller, M. (2003). Transcapillary insulin transfer in human skeletal muscle. European journal of clinical investigation *33*, 141-146.
Hu, E., Liang, P., and Spiegelman, B.M. (1996). AdipoQ is a novel adipose-specific gene dysregulated in obesity. The Journal of biological chemistry *271*, 10697-10703.
Huang, J., Gabrielsen, J.S., Cooksey, R.C., Luo, B., Boros, L.G., Jones, D.L., Jouihan, H.A., Soesanto, Y., Knecht, L., Hazel, M.W.*, et al.* (2007). Increased glucose disposal and AMP-dependent kinase signaling in a mouse model of hemochromatosis. The Journal of biological chemistry *282*, 37501-37507.

Huang, J., Jones, D., Luo, B., Sanderson, M., Soto, J., Abel, E.D., Cooksey, R.C., and McClain, D.A. (2011). Iron overload and diabetes risk: a shift from glucose to Fatty Acid oxidation and increased hepatic glucose production in a mouse model of hereditary hemochromatosis. Diabetes *60*, 80-87.
Hug, C., Wang, J., Ahmad, N.S., Bogan, J.S., Tsao, T.S., and Lodish, H.F. (2004). T-cadherin is a receptor for hexameric and high-molecular-weight forms of Acrp30/adiponectin. Proceedings of the National Academy of Sciences of the United States of America *101*, 10308-10313.
Hull, R.L., Kodama, K., Utzschneider, K.M., Carr, D.B., Prigeon, R.L., and Kahn, S.E. (2005). Dietary-fat-induced obesity in mice results in beta cell hyperplasia but not increased insulin release: evidence for specificity of impaired beta cell adaptation. Diabetologia *48*, 1350-1358.
Irimia, J.M., Meyer, C.M., Peper, C.L., Zhai, L., Bock, C.B., Previs, S.F., McGuinness, O.P., DePaoli-Roach, A., and Roach, P.J. (2010). Impaired glucose tolerance and predisposition to the fasted state in liver glycogen synthase knock-out mice. The Journal of biological chemistry *285*, 12851-12861.
Ishino, S., Sugita, T., Kondo, Y., Okai, M., Tsuchimori, K., Watanabe, M., Mori, I., Hosoya, M., Horiguchi, T., and Kamiguchi, H. (2017). Glucose uptake of the muscle and adipose tissues in diabetes and obesity disease models: evaluation of insulin and beta3-adrenergic receptor agonist effects by 18F-FDG. Annals of nuclear medicine *31*, 413-423.
Itoh, Y., Kawamata, Y., Harada, M., Kobayashi, M., Fujii, R., Fukusumi, S., Ogi, K., Hosoya, M., Tanaka, Y., Uejima, H*., et al.* (2003). Free fatty acids regulate insulin secretion from pancreatic beta cells through GPR40. Nature *422*, 173-176.
Kadowaki, T., Yamauchi, T., Kubota, N., Hara, K., Ueki, K., and Tobe, K. (2006). Adiponectin and adiponectin receptors in insulin resistance, diabetes, and the metabolic syndrome. The Journal of clinical investigation *116*, 1784-1792.
Kalra, S., Singh, V., and Nagrale, D. (2016). Sodium-Glucose Cotransporter-2 Inhibition and the Glomerulus: A Review. Advances in therapy *33*, 1502-1518.
Keaney, J., and Campbell, M. (2015). The dynamic blood-brain barrier. The FEBS journal *282*, 4067-4079.
Kelley, D.E., Goodpaster, B., Wing, R.R., and Simoneau, J.A. (1999). Skeletal muscle fatty acid metabolism in association with insulin resistance, obesity, and weight loss. The American journal of physiology *277*, E1130-1141.
Kelley, D.E., He, J., Menshikova, E.V., and Ritov, V.B. (2002). Dysfunction of mitochondria in human skeletal muscle in type 2 diabetes. Diabetes *51*, 2944-2950.
Kersten, S., Seydoux, J., Peters, J.M., Gonzalez, F.J., Desvergne, B., and Wahli, W. (1999). Peroxisome proliferator-activated receptor alpha mediates the adaptive response to fasting. The Journal of clinical investigation *103*, 1489-1498.
Kessing, L.V., Thomsen, A.F., Mogensen, U.B., and Andersen, P.K. (2010). Treatment with antipsychotics and the risk of diabetes in clinical practice. The British journal of psychiatry : the journal of mental science *197*, 266-271.
Khan, Z.A., Barbin, Y.P., Cukiernik, M., Adams, P.C., and Chakrabarti, S. (2004). Heme-oxygenase-mediated iron accumulation in the liver. Canadian journal of physiology and pharmacology *82*, 448-456.

Kim, E., Kim, Y.S., Kim, K.M., Jung, S., Yoo, S.H., and Kim, Y. (2016). D-Xylose as a sugar complement regulates blood glucose levels by suppressing phosphoenolpyruvate carboxylase (PEPCK) in streptozotocin-nicotinamide-induced diabetic rats and by enhancing glucose uptake in vitro. Nutrition research and practice *10*, 11-18.
Kim, H.B., Kong, M., Kim, T.M., Suh, Y.H., Kim, W.H., Lim, J.H., Song, J.H., and Jung, M.H. (2006). NFATc4 and ATF3 negatively regulate adiponectin gene expression in 3T3-L1 adipocytes. Diabetes *55*, 1342-1352.
Kim, S.P., Ellmerer, M., Van Citters, G.W., and Bergman, R.N. (2003). Primacy of hepatic insulin resistance in the development of the metabolic syndrome induced by an isocaloric moderate-fat diet in the dog. Diabetes *52*, 2453-2460.
Kloppel, G., Lohr, M., Habich, K., Oberholzer, M., and Heitz, P.U. (1985). Islet pathology and the pathogenesis of type 1 and type 2 diabetes mellitus revisited. Survey and synthesis of pathology research *4*, 110-125.
Koliakos, G., Papachristou, F., Koussi, A., Perifanis, V., Tsatra, I., Souliou, E., and Athanasiou, M. (2003). Urine biochemical markers of early renal dysfunction are associated with iron overload in beta-thalassaemia. Clinical and laboratory haematology *25*, 105-109.
Kolka, C.M., and Bergman, R.N. (2012). The barrier within: endothelial transport of hormones. Physiology (Bethesda, Md) *27*, 237-247.
Kolka, C.M., Harrison, L.N., Lottati, M., Chiu, J.D., Kirkman, E.L., and Bergman, R.N. (2010). Diet-induced obesity prevents interstitial dispersion of insulin in skeletal muscle. Diabetes *59*, 619-626.
Kolodziejski, P.A., Pruszynska-Oszmalek, E., Strowski, M.Z., and Nowak, K.W. (2017). Long-term obestatin treatment of mice type 2 diabetes increases insulin sensitivity and improves liver function. Endocrine *56*, 538-550.
Krause, M.P., Liu, Y., Vu, V., Chan, L., Xu, A., Riddell, M.C., Sweeney, G., and Hawke, T.J. (2008). Adiponectin is expressed by skeletal muscle fibers and influences muscle phenotype and function. American journal of physiology Cell physiology *295*, C203-212.
Krug, S.M., Gunzel, D., Conrad, M.P., Lee, I.F., Amasheh, S., Fromm, M., and Yu, A.S. (2012). Charge-selective claudin channels. Annals of the New York Academy of Sciences *1257*, 20-28.
Kubota, N., Yano, W., Kubota, T., Yamauchi, T., Itoh, S., Kumagai, H., Kozono, H., Takamoto, I., Okamoto, S., Shiuchi, T.*, et al.* (2007). Adiponectin stimulates AMP-activated protein kinase in the hypothalamus and increases food intake. Cell metabolism *6*, 55-68.
Kubota, T., Kubota, N., Kumagai, H., Yamaguchi, S., Kozono, H., Takahashi, T., Inoue, M., Itoh, S., Takamoto, I., Sasako, T.*, et al.* (2011). Impaired insulin signaling in endothelial cells reduces insulin-induced glucose uptake by skeletal muscle. Cell metabolism *13*, 294-307.
Kusminski, C.M., McTernan, P.G., Schraw, T., Kos, K., O'Hare, J.P., Ahima, R., Kumar, S., and Scherer, P.E. (2007). Adiponectin complexes in human cerebrospinal fluid: distinct complex distribution from serum. Diabetologia *50*, 634-642.
Lee, J.R., Hahn, H.S., Kim, Y.H., Nguyen, H.H., Yang, J.M., Kang, J.S., and Hahn, M.J. (2011). Adaptor protein containing PH domain, PTB domain and leucine zipper (APPL1) regulates the protein level of EGFR by modulating its trafficking. Biochemical and biophysical research communications *415*, 206-211.

Lee, M.H., Klein, R.L., El-Shewy, H.M., Luttrell, D.K., and Luttrell, L.M. (2008). The adiponectin receptors AdipoR1 and AdipoR2 activate ERK1/2 through a Src/Ras-dependent pathway and stimulate cell growth. Biochemistry *47*, 11682-11692.
Lemke, U., Krones-Herzig, A., Berriel Diaz, M., Narvekar, P., Ziegler, A., Vegiopoulos, A., Cato, A.C., Bohl, S., Klingmuller, U., Screaton, R.A.*, et al.* (2008). The glucocorticoid receptor controls hepatic dyslipidemia through Hes1. Cell metabolism *8*, 212-223.
Leung, L. (2016). Diabetes mellitus and the Aboriginal diabetic initiative in Canada: An update review. Journal of family medicine and primary care *5*, 259-265.
Lin, K.T., and Wang, L.H. (2016). New dimension of glucocorticoids in cancer treatment. Steroids *111*, 84-88.
Liu, Y., Chewchuk, S., Lavigne, C., Brule, S., Pilon, G., Houde, V., Xu, A., Marette, A., and Sweeney, G. (2009). Functional significance of skeletal muscle adiponectin production, changes in animal models of obesity and diabetes, and regulation by rosiglitazone treatment. American journal of physiology Endocrinology and metabolism *297*, E657-664.
Liu, Y., Retnakaran, R., Hanley, A., Tungtrongchitr, R., Shaw, C., and Sweeney, G. (2007). Total and high molecular weight but not trimeric or hexameric forms of adiponectin correlate with markers of the metabolic syndrome and liver injury in Thai subjects. The Journal of clinical endocrinology and metabolism *92*, 4313-4318.
Liu, Z., Xiao, T., Peng, X., Li, G., and Hu, F. (2017). APPLs: More than just adiponectin receptor binding proteins. Cellular signalling *32*, 76-84.
Lowell, B.B., and Shulman, G.I. (2005). Mitochondrial dysfunction and type 2 diabetes. Science (New York, NY) *307*, 384-387.
Maeda, N., Takahashi, M., Funahashi, T., Kihara, S., Nishizawa, H., Kishida, K., Nagaretani, H., Matsuda, M., Komuro, R., Ouchi, N.*, et al.* (2001). PPARgamma ligands increase expression and plasma concentrations of adiponectin, an adipose-derived protein. Diabetes *50*, 2094-2099.
Maggs, D.G., Jacob, R., Rife, F., Lange, R., Leone, P., During, M.J., Tamborlane, W.V., and Sherwin, R.S. (1995). Interstitial fluid concentrations of glycerol, glucose, and amino acids in human quadricep muscle and adipose tissue. Evidence for significant lipolysis in skeletal muscle. The Journal of clinical investigation *96*, 370-377.
Makimura, H., Mizuno, T.M., Isoda, F., Beasley, J., Silverstein, J.H., and Mobbs, C.V. (2003). Role of glucocorticoids in mediating effects of fasting and diabetes on hypothalamic gene expression. BMC physiology *3*, 5.
Matsuda, K., Fujishima, Y., Maeda, N., Mori, T., Hirata, A., Sekimoto, R., Tsushima, Y., Masuda, S., Yamaoka, M., Inoue, K.*, et al.* (2015). Positive feedback regulation between adiponectin and T-cadherin impacts adiponectin levels in tissue and plasma of male mice. Endocrinology *156*, 934-946.
McClain, D.A., Abraham, D., Rogers, J., Brady, R., Gault, P., Ajioka, R., and Kushner, J.P. (2006). High prevalence of abnormal glucose homeostasis secondary to decreased insulin secretion in individuals with hereditary haemochromatosis. Diabetologia *49*, 1661-1669.
McGillicuddy, F.C., Chiquoine, E.H., Hinkle, C.C., Kim, R.J., Shah, R., Roche, H.M., Smyth, E.M., and Reilly, M.P. (2009). Interferon gamma attenuates insulin signaling,

lipid storage, and differentiation in human adipocytes via activation of the JAK/STAT pathway. The Journal of biological chemistry *284*, 31936-31944.
Meehan, H.A., and Connell, G.J. (2001). The hairpin loop but not the bulged C of the iron responsive element is essential for high affinity binding to iron regulatory protein-1. The Journal of biological chemistry *276*, 14791-14796.
Messina, M.F., Lombardo, F., Meo, A., Miceli, M., Wasniewska, M., Valenzise, M., Ruggeri, C., Arrigo, T., and De Luca, F. (2002). Three-year prospective evaluation of glucose tolerance, beta-cell function and peripheral insulin sensitivity in non-diabetic patients with thalassemia major. Journal of endocrinological investigation *25*, 497-501.
Mirzaei, A., Chen, Z., Haghighat, F., and Yerushalmi, L. (2017). Removal of pharmaceuticals from water by homo/heterogonous Fenton-type processes - A review. Chemosphere *174*, 665-688.
Montilla, P., Barcos, M., Munoz, M.C., Bujalance, I., Munoz-Castaneda, J.R., and Tunez, I. (2005). Red wine prevents brain oxidative stress and nephropathy in streptozotocin-induced diabetic rats. Journal of biochemistry and molecular biology *38*, 539-544.
Mootha, V.K., Lindgren, C.M., Eriksson, K.F., Subramanian, A., Sihag, S., Lehar, J., Puigserver, P., Carlsson, E., Ridderstrale, M., Laurila, E.*, et al.* (2003). PGC-1alpha-responsive genes involved in oxidative phosphorylation are coordinately downregulated in human diabetes. Nature genetics *34*, 267-273.
Moreno, M., Ortega, F., Xifra, G., Ricart, W., Fernandez-Real, J.M., and Moreno-Navarrete, J.M. (2015). Cytosolic aconitase activity sustains adipogenic capacity of adipose tissue connecting iron metabolism and adipogenesis. FASEB journal : official publication of the Federation of American Societies for Experimental Biology *29*, 1529-1539.
Mori, Y., Otabe, S., Dina, C., Yasuda, K., Populaire, C., Lecoeur, C., Vatin, V., Durand, E., Hara, K., Okada, T.*, et al.* (2002). Genome-wide search for type 2 diabetes in Japanese affected sib-pairs confirms susceptibility genes on 3q, 15q, and 20q and identifies two new candidate Loci on 7p and 11p. Diabetes *51*, 1247-1255.
Motti, M.L., De Marco, C., Califano, D., Fusco, A., and Viglietto, G. (2004). Akt-dependent T198 phosphorylation of cyclin-dependent kinase inhibitor p27kip1 in breast cancer. Cell cycle (Georgetown, Tex) *3*, 1074-1080.
Muller, S., Martin, S., Koenig, W., Hanifi-Moghaddam, P., Rathmann, W., Haastert, B., Giani, G., Illig, T., Thorand, B., and Kolb, H. (2002). Impaired glucose tolerance is associated with increased serum concentrations of interleukin 6 and co-regulated acute-phase proteins but not TNF-alpha or its receptors. Diabetologia *45*, 805-812.
Munck, A., Guyre, P.M., and Holbrook, N.J. (1984). Physiological functions of glucocorticoids in stress and their relation to pharmacological actions. Endocrine reviews *5*, 25-44.
Muniyappa, R., Brown, R.J., Mari, A., Joseph, J., Warren, M.A., Cochran, E.K., Skarulis, M.C., and Gorden, P. (2014). Effects of leptin replacement therapy on pancreatic beta-cell function in patients with lipodystrophy. Diabetes care *37*, 1101-1107.
Nanayakkara, G., Kariharan, T., Wang, L., Zhong, J., and Amin, R. (2012). The cardio-protective signaling and mechanisms of adiponectin. American journal of cardiovascular disease *2*, 253-266.
Navarro, A., and Boveris, A. (2007). The mitochondrial energy transduction system and the aging process. American journal of physiology Cell physiology *292*, C670-686.

Nemeth, E., Tuttle, M.S., Powelson, J., Vaughn, M.B., Donovan, A., Ward, D.M., Ganz, T., and Kaplan, J. (2004). Hepcidin regulates cellular iron efflux by binding to ferroportin and inducing its internalization. Science (New York, NY) *306*, 2090-2093.
Neumeier, M., Weigert, J., Buettner, R., Wanninger, J., Schaffler, A., Muller, A.M., Killian, S., Sauerbruch, S., Schlachetzki, F., Steinbrecher, A.*, et al.* (2007). Detection of adiponectin in cerebrospinal fluid in humans. American journal of physiology Endocrinology and metabolism *293*, E965-969.
Niederau, C., Berger, M., Stremmel, W., Starke, A., Strohmeyer, G., Ebert, R., Siegel, E., and Creutzfeldt, W. (1984). Hyperinsulinaemia in non-cirrhotic haemochromatosis: impaired hepatic insulin degradation? Diabetologia *26*, 441-444.
Ouchi, N., Parker, J.L., Lugus, J.J., and Walsh, K. (2011). Adipokines in inflammation and metabolic disease. Nature reviews Immunology *11*, 85-97.
Pajvani, U.B., Hawkins, M., Combs, T.P., Rajala, M.W., Doebber, T., Berger, J.P., Wagner, J.A., Wu, M., Knopps, A., Xiang, A.H.*, et al.* (2004). Complex distribution, not absolute amount of adiponectin, correlates with thiazolidinedione-mediated improvement in insulin sensitivity. The Journal of biological chemistry *279*, 12152-12162.
Panthakalam, S., Bhatnagar, D., and Klimiuk, P. (2004). The prevalence and management of hyperglycaemia in patients with rheumatoid arthritis on corticosteroid therapy. Scottish medical journal *49*, 139-141.
Park, P.H., Huang, H., McMullen, M.R., Mandal, P., Sun, L., and Nagy, L.E. (2008). Suppression of lipopolysaccharide-stimulated tumor necrosis factor-alpha production by adiponectin is mediated by transcriptional and post-transcriptional mechanisms. The Journal of biological chemistry *283*, 26850-26858.
Patti, M.E., Butte, A.J., Crunkhorn, S., Cusi, K., Berria, R., Kashyap, S., Miyazaki, Y., Kohane, I., Costello, M., Saccone, R.*, et al.* (2003). Coordinated reduction of genes of oxidative metabolism in humans with insulin resistance and diabetes: Potential role of PGC1 and NRF1. Proceedings of the National Academy of Sciences of the United States of America *100*, 8466-8471.
Paz, K., Hemi, R., LeRoith, D., Karasik, A., Elhanany, E., Kanety, H., and Zick, Y. (1997). A molecular basis for insulin resistance. Elevated serine/threonine phosphorylation of IRS-1 and IRS-2 inhibits their binding to the juxtamembrane region of the insulin receptor and impairs their ability to undergo insulin-induced tyrosine phosphorylation. The Journal of biological chemistry *272*, 29911-29918.
Paz, K., Voliovitch, H., Hadari, Y.R., Roberts, C.T., Jr., LeRoith, D., and Zick, Y. (1996). Interaction between the insulin receptor and its downstream effectors. Use of individually expressed receptor domains for structure/function analysis. The Journal of biological chemistry *271*, 6998-7003.
Perneger, T.V., Whelton, P.K., and Klag, M.J. (1994). Risk of kidney failure associated with the use of acetaminophen, aspirin, and nonsteroidal antiinflammatory drugs. The New England journal of medicine *331*, 1675-1679.
Perretti, M., and Ahluwalia, A. (2000). The microcirculation and inflammation: site of action for glucocorticoids. Microcirculation (New York, NY : 1994) *7*, 147-161.
Peters, K.E., Beilby, J., Cadby, G., Warrington, N.M., Bruce, D.G., Davis, W.A., Davis, T.M., Wiltshire, S., Knuiman, M., McQuillan, B.M.*, et al.* (2013). A comprehensive investigation of variants in genes encoding adiponectin (ADIPOQ) and its receptors

(ADIPOR1/R2), and their association with serum adiponectin, type 2 diabetes, insulin resistance and the metabolic syndrome. BMC medical genetics *14*, 15.
Petersen, K.F., Oral, E.A., Dufour, S., Befroy, D., Ariyan, C., Yu, C., Cline, G.W., DePaoli, A.M., Taylor, S.I., Gorden, P.*, et al.* (2002). Leptin reverses insulin resistance and hepatic steatosis in patients with severe lipodystrophy. The Journal of clinical investigation *109*, 1345-1350.
Prentki, M., Joly, E., El-Assaad, W., and Roduit, R. (2002). Malonyl-CoA signaling, lipid partitioning, and glucolipotoxicity: role in beta-cell adaptation and failure in the etiology of diabetes. Diabetes *51 Suppl 3*, S405-413.
Pries, A.R., and Kuebler, W.M. (2006). Normal endothelium. Handbook of experimental pharmacology, 1-40.
Raj, D.S., Dominic, E.A., Pai, A., Osman, F., Morgan, M., Pickett, G., Shah, V.O., Ferrando, A., and Moseley, P. (2005). Skeletal muscle, cytokines, and oxidative stress in end-stage renal disease. Kidney international *68*, 2338-2344.
Rao, A., Pandya, V., and Whaley-Connell, A. (2015). Obesity and insulin resistance in resistant hypertension: implications for the kidney. Advances in chronic kidney disease *22*, 211-217.
Reaven, G.M., Hollenbeck, C., Jeng, C.Y., Wu, M.S., and Chen, Y.D. (1988). Measurement of plasma glucose, free fatty acid, lactate, and insulin for 24 h in patients with NIDDM. Diabetes *37*, 1020-1024.
Rhodes, C.J. (2005). Type 2 diabetes-a matter of beta-cell life and death? Science (New York, NY) *307*, 380-384.
Ritov, V.B., Menshikova, E.V., Azuma, K., Wood, R., Toledo, F.G., Goodpaster, B.H., Ruderman, N.B., and Kelley, D.E. (2010). Deficiency of electron transport chain in human skeletal muscle mitochondria in type 2 diabetes mellitus and obesity. American journal of physiology Endocrinology and metabolism *298*, E49-58.
Rochfort, K.D., and Cummins, P.M. (2015). The blood-brain barrier endothelium: a target for pro-inflammatory cytokines. Biochemical Society transactions *43*, 702-706.
Rodriguez, J.C., Gil-Gomez, G., Hegardt, F.G., and Haro, D. (1994). Peroxisome proliferator-activated receptor mediates induction of the mitochondrial 3-hydroxy-3-methylglutaryl-CoA synthase gene by fatty acids. The Journal of biological chemistry *269*, 18767-18772.
Rosella, L.C., Lebenbaum, M., Fitzpatrick, T., O'Reilly, D., Wang, J., Booth, G.L., Stukel, T.A., and Wodchis, W.P. (2016). Impact of diabetes on healthcare costs in a population-based cohort: a cost analysis. Diabetic medicine : a journal of the British Diabetic Association *33*, 395-403.
Rui, L., Fisher, T.L., Thomas, J., and White, M.F. (2001). Regulation of insulin/insulin-like growth factor-1 signaling by proteasome-mediated degradation of insulin receptor substrate-2. The Journal of biological chemistry *276*, 40362-40367.
Rumberger, J.M., Peters, T., Jr., Burrington, C., and Green, A. (2004). Transferrin and iron contribute to the lipolytic effect of serum in isolated adipocytes. Diabetes *53*, 2535-2541.
Rutkowski, J.M., Halberg, N., Wang, Q.A., Holland, W.L., Xia, J.Y., and Scherer, P.E. (2014). Differential transendothelial transport of adiponectin complexes. Cardiovascular diabetology *13*, 47.

Ruzzin, J., Wagman, A.S., and Jensen, J. (2005). Glucocorticoid-induced insulin resistance in skeletal muscles: defects in insulin signalling and the effects of a selective glycogen synthase kinase-3 inhibitor. Diabetologia *48*, 2119-2130.
Sacks, F.M., Hermans, M.P., Fioretto, P., Valensi, P., Davis, T., Horton, E., Wanner, C., Al-Rubeaan, K., Aronson, R., Barzon, I*., et al.* (2014). Association between plasma triglycerides and high-density lipoprotein cholesterol and microvascular kidney disease and retinopathy in type 2 diabetes mellitus: a global case-control study in 13 countries. Circulation *129*, 999-1008.
Santi, S.A., and Lee, H. (2010). The Akt isoforms are present at distinct subcellular locations. American journal of physiology Cell physiology *298*, C580-591.
Schoneveld, O.J., Gaemers, I.C., and Lamers, W.H. (2004). Mechanisms of glucocorticoid signalling. Biochimica et biophysica acta *1680*, 114-128.
Shields, M. (2006). Overweight and obesity among children and youth. Health reports *17*, 27-42.
Shikatani, E.A., Trifonova, A., Mandel, E.R., Liu, S.T., Roudier, E., Krylova, A., Szigiato, A., Beaudry, J., Riddell, M.C., and Haas, T.L. (2012). Inhibition of proliferation, migration and proteolysis contribute to corticosterone-mediated inhibition of angiogenesis. PloS one *7*, e46625.
Shpilberg, Y., Beaudry, J.L., D'Souza, A., Campbell, J.E., Peckett, A., and Riddell, M.C. (2012). A rodent model of rapid-onset diabetes induced by glucocorticoids and high-fat feeding. Disease models & mechanisms *5*, 671-680.
Shulman, G.I. (2000). Cellular mechanisms of insulin resistance. The Journal of clinical investigation *106*, 171-176.
Sjostrand, M., Holmang, A., and Lonnroth, P. (1999). Measurement of interstitial insulin in human muscle. The American journal of physiology *276*, E151-154.
Smoak, K.A., and Cidlowski, J.A. (2004). Mechanisms of glucocorticoid receptor signaling during inflammation. Mechanisms of ageing and development *125*, 697-706.
Somwar, R., Kim, D.Y., Sweeney, G., Huang, C., Niu, W., Lador, C., Ramlal, T., and Klip, A. (2001). GLUT4 translocation precedes the stimulation of glucose uptake by insulin in muscle cells: potential activation of GLUT4 via p38 mitogen-activated protein kinase. The Biochemical journal *359*, 639-649.
Souza, S.C., Palmer, H.J., Kang, Y.H., Yamamoto, M.T., Muliro, K.V., Paulson, K.E., and Greenberg, A.S. (2003). TNF-alpha induction of lipolysis is mediated through activation of the extracellular signal related kinase pathway in 3T3-L1 adipocytes. Journal of cellular biochemistry *89*, 1077-1086.
Storlien, L.H., Jenkins, A.B., Chisholm, D.J., Pascoe, W.S., Khouri, S., and Kraegen, E.W. (1991). Influence of dietary fat composition on development of insulin resistance in rats. Relationship to muscle triglyceride and omega-3 fatty acids in muscle phospholipid. Diabetes *40*, 280-289.
Symons, J.D., and Abel, E.D. (2013). Lipotoxicity contributes to endothelial dysfunction: a focus on the contribution from ceramide. Reviews in endocrine & metabolic disorders *14*, 59-68.
Takenaka, N., Yasuda, N., Nihata, Y., Hosooka, T., Noguchi, T., Aiba, A., and Satoh, T. (2014). Role of the guanine nucleotide exchange factor in Akt2-mediated plasma membrane translocation of GLUT4 in insulin-stimulated skeletal muscle. Cellular signalling *26*, 2460-2469.

Tanaka, H., Takechi, M., Kiyonari, H., Shioi, G., Tamura, A., and Tsukita, S. (2015). Intestinal deletion of Claudin-7 enhances paracellular organic solute flux and initiates colonic inflammation in mice. Gut *64*, 1529-1538.
Tanner, L.I., and Lienhard, G.E. (1989). Localization of transferrin receptors and insulin-like growth factor II receptors in vesicles from 3T3-L1 adipocytes that contain intracellular glucose transporters. The Journal of cell biology *108*, 1537-1545.
Tatum, R., Zhang, Y., Salleng, K., Lu, Z., Lin, J.J., Lu, Q., Jeansonne, B.G., Ding, L., and Chen, Y.H. (2010). Renal salt wasting and chronic dehydration in claudin-7-deficient mice. American journal of physiology Renal physiology *298*, F24-34.
Toborek, M., Wasik, T., Drozdz, M., Klin, M., Magner-Wrobel, K., and Kopieczna-Grzebieniak, E. (1992). Effect of hemodialysis on lipid peroxidation and antioxidant system in patients with chronic renal failure. Metabolism: clinical and experimental *41*, 1229-1232.
Toomajian, C., Ajioka, R.S., Jorde, L.B., Kushner, J.P., and Kreitman, M. (2003). A method for detecting recent selection in the human genome from allele age estimates. Genetics *165*, 287-297.
Ullrich, A., Gray, A., Tam, A.W., Yang-Feng, T., Tsubokawa, M., Collins, C., Henzel, W., Le Bon, T., Kathuria, S., Chen, E.*, et al.* (1986). Insulin-like growth factor I receptor primary structure: comparison with insulin receptor suggests structural determinants that define functional specificity. The EMBO journal *5*, 2503-2512.
Uranga, R.M., Katz, S., and Salvador, G.A. (2013). Enhanced phosphatidylinositol 3-kinase (PI3K)/Akt signaling has pleiotropic targets in hippocampal neurons exposed to iron-induced oxidative stress. The Journal of biological chemistry *288*, 19773-19784.
Valencak, T.G., Osterrieder, A., and Schulz, T.J. (2017). Sex matters: The effects of biological sex on adipose tissue biology and energy metabolism. Redox biology *12*, 806-813.
Vegiopoulos, A., and Herzig, S. (2007). Glucocorticoids, metabolism and metabolic diseases. Molecular and cellular endocrinology *275*, 43-61.
Verma, S.K., and Molitoris, B.A. (2015). Renal endothelial injury and microvascular dysfunction in acute kidney injury. Seminars in nephrology *35*, 96-107.
Vionnet, N., Hani, E.H., Dupont, S., Gallina, S., Francke, S., Dotte, S., De Matos, F., Durand, E., Lepretre, F., Lecoeur, C.*, et al.* (2000). Genomewide search for type 2 diabetes-susceptibility genes in French whites: evidence for a novel susceptibility locus for early-onset diabetes on chromosome 3q27-qter and independent replication of a type 2-diabetes locus on chromosome 1q21-q24. American journal of human genetics *67*, 1470-1480.
Wang, F., Han, L., Qin, R.R., Zhang, Y.Y., Wang, D., Wang, Z.H., Tang, M.X., Zhang, Y., Zhong, M., and Zhang, W. (2017). Overexpressing STAMP2 attenuates adipose tissue angiogenesis and insulin resistance in diabetic ApoE-/- /LDLR-/- mouse via a PPARgamma/CD36 pathway. Journal of cellular and molecular medicine.
Wang, H., Li, H., Jiang, X., Shi, W., Shen, Z., and Li, M. (2014). Hepcidin is directly regulated by insulin and plays an important role in iron overload in streptozotocin-induced diabetic rats. Diabetes *63*, 1506-1518.
Wang, X.Y., Chen, X.L., Wang, L., and Chen, H.W. (2015). High-dose glucocorticoids increases the expression of mineralocorticoid receptor in vascular endothelial cells. European review for medical and pharmacological sciences *19*, 4314-4323.

Wang, Y., Xu, A., Knight, C., Xu, L.Y., and Cooper, G.J. (2002). Hydroxylation and glycosylation of the four conserved lysine residues in the collagenous domain of adiponectin. Potential role in the modulation of its insulin-sensitizing activity. The Journal of biological chemistry *277*, 19521-19529.
Weatherall, D.J. (1998). Pathophysiology of thalassaemia. Bailliere's clinical haematology *11*, 127-146.
Weinstein, S.P., Wilson, C.M., Pritsker, A., and Cushman, S.W. (1998). Dexamethasone inhibits insulin-stimulated recruitment of GLUT4 to the cell surface in rat skeletal muscle. Metabolism: clinical and experimental *47*, 3-6.
Weisberg, S.P., McCann, D., Desai, M., Rosenbaum, M., Leibel, R.L., and Ferrante, A.W., Jr. (2003). Obesity is associated with macrophage accumulation in adipose tissue. The Journal of clinical investigation *112*, 1796-1808.
Wellen, K.E., and Hotamisligil, G.S. (2005). Inflammation, stress, and diabetes. The Journal of clinical investigation *115*, 1111-1119.
Wichmann, H., Vocke, F., Brinkhoff, T., Simon, M., and Richter-Landsberg, C. (2015). Cytotoxic Effects of Tropodithietic Acid on Mammalian Clonal Cell Lines of Neuronal and Glial Origin. Marine drugs *13*, 7113-7123.
Wilcox, G. (2005). Insulin and insulin resistance. The Clinical biochemist Reviews *26*, 19-39.
Winer, S., Chan, Y., Paltser, G., Truong, D., Tsui, H., Bahrami, J., Dorfman, R., Wang, Y., Zielenski, J., Mastronardi, F.*, et al.* (2009). Normalization of obesity-associated insulin resistance through immunotherapy. Nature medicine *15*, 921-929.
Witchel, S.F., and DeFranco, D.B. (2006). Mechanisms of disease: regulation of glucocorticoid and receptor levels--impact on the metabolic syndrome. Nature clinical practice Endocrinology & metabolism *2*, 621-631.
Witt, K.A., and Sandoval, K.E. (2014). Steroids and the blood-brain barrier: therapeutic implications. Advances in pharmacology (San Diego, Calif) *71*, 361-390.
Wolfe, F., and Marmor, M.F. (2010). Rates and predictors of hydroxychloroquine retinal toxicity in patients with rheumatoid arthritis and systemic lupus erythematosus. Arthritis care & research *62*, 775-784.
Won, S.M., Lee, J.H., Park, U.J., Gwag, J., Gwag, B.J., and Lee, Y.B. (2011). Iron mediates endothelial cell damage and blood-brain barrier opening in the hippocampus after transient forebrain ischemia in rats. Experimental & molecular medicine *43*, 121-128.
Wood, C.M., Gilmour, K.M., Perry, S.F., Part, P., and Walsh, P.J. (1998). Pulsatile urea excretion in gulf toadfish (Opsanus beta): evidence for activation of a specific facilitated diffusion transport system. The Journal of experimental biology *201*, 805-817.
Xu, A., Wang, Y., Keshaw, H., Xu, L.Y., Lam, K.S., and Cooper, G.J. (2003a). The fat-derived hormone adiponectin alleviates alcoholic and nonalcoholic fatty liver diseases in mice. The Journal of clinical investigation *112*, 91-100.
Xu, A., Yin, S., Wong, L., Chan, K.W., and Lam, K.S. (2004). Adiponectin ameliorates dyslipidemia induced by the human immunodeficiency virus protease inhibitor ritonavir in mice. Endocrinology *145*, 487-494.
Xu, H., Barnes, G.T., Yang, Q., Tan, G., Yang, D., Chou, C.J., Sole, J., Nichols, A., Ross, J.S., Tartaglia, L.A.*, et al.* (2003b). Chronic inflammation in fat plays a crucial role

in the development of obesity-related insulin resistance. The Journal of clinical investigation *112*, 1821-1830.
Yamauchi, T., and Kadowaki, T. (2013). Adiponectin receptor as a key player in healthy longevity and obesity-related diseases. Cell metabolism *17*, 185-196.
Yamauchi, T., Kamon, J., Minokoshi, Y., Ito, Y., Waki, H., Uchida, S., Yamashita, S., Noda, M., Kita, S., Ueki, K.*, et al.* (2002). Adiponectin stimulates glucose utilization and fatty-acid oxidation by activating AMP-activated protein kinase. Nature medicine *8*, 1288-1295.
Yamauchi, T., Kamon, J., Waki, H., Terauchi, Y., Kubota, N., Hara, K., Mori, Y., Ide, T., Murakami, K., Tsuboyama-Kasaoka, N.*, et al.* (2001). The fat-derived hormone adiponectin reverses insulin resistance associated with both lipoatrophy and obesity. Nature medicine *7*, 941-946.
Yang, Q., Graham, T.E., Mody, N., Preitner, F., Peroni, O.D., Zabolotny, J.M., Kotani, K., Quadro, L., and Kahn, B.B. (2005). Serum retinol binding protein 4 contributes to insulin resistance in obesity and type 2 diabetes. Nature *436*, 356-362.
Yang, Y.J., Hope, I.D., Ader, M., and Bergman, R.N. (1994). Importance of transcapillary insulin transport to dynamics of insulin action after intravenous glucose. The American journal of physiology *266*, E17-25.
Yang, Y.X., Lewis, J.D., Epstein, S., and Metz, D.C. (2006). Long-term proton pump inhibitor therapy and risk of hip fracture. Jama *296*, 2947-2953.
Yoon, M.J., Lee, G.Y., Chung, J.J., Ahn, Y.H., Hong, S.H., and Kim, J.B. (2006). Adiponectin increases fatty acid oxidation in skeletal muscle cells by sequential activation of AMP-activated protein kinase, p38 mitogen-activated protein kinase, and peroxisome proliferator-activated receptor alpha. Diabetes *55*, 2562-2570.
Yoon, N., Dang, T.Q., Chasiotis, H., Kelly, S.P., and Sweeney, G. (2014). Altered transendothelial transport of hormones as a contributor to diabetes. Diabetes & metabolism journal *38*, 92-99.
Yu, F., Hao, S., Yang, B., Zhao, Y., Zhang, R., Zhang, W., Yang, J., and Chen, J. (2015). Insulin resistance due to dietary iron overload disrupts inner hair cell ribbon synapse plasticity in male mice. Neuroscience letters *597*, 183-188.
Yuan, D., and He, P. (2012). Vascular remodeling alters adhesion protein and cytoskeleton reactions to inflammatory stimuli resulting in enhanced permeability increases in rat venules. Journal of applied physiology (Bethesda, Md : 1985) *113*, 1110-1120.
Yuan, D., Xu, S., and He, P. (2014). Enhanced permeability responses to inflammation in streptozotocin-induced diabetic rat venules: Rho-mediated alterations of actin cytoskeleton and VE-cadherin. American journal of physiology Heart and circulatory physiology *307*, H44-53.
Yusuf, S., Hawken, S., Ounpuu, S., Bautista, L., Franzosi, M.G., Commerford, P., Lang, C.C., Rumboldt, Z., Onen, C.L., Lisheng, L.*, et al.* (2005). Obesity and the risk of myocardial infarction in 27,000 participants from 52 countries: a case-control study. Lancet (London, England) *366*, 1640-1649.
Zhang, X., Wang, N., Schachat, A.P., Bao, S., and Gillies, M.C. (2014). Glucocorticoids: structure, signaling and molecular mechanisms in the treatment of diabetic retinopathy and diabetic macular edema. Current molecular medicine *14*, 376-384.

Zheng, B., Ohkawa, S., Li, H., Roberts-Wilson, T.K., and Price, S.R. (2010). FOXO3a mediates signaling crosstalk that coordinates ubiquitin and atrogin-1/MAFbx expression during glucocorticoid-induced skeletal muscle atrophy. FASEB journal : official publication of the Federation of American Societies for Experimental Biology *24*, 2660-2669.
Zhou, B.P., Liao, Y., Xia, W., Zou, Y., Spohn, B., and Hung, M.C. (2001). HER-2/neu induces p53 ubiquitination via Akt-mediated MDM2 phosphorylation. Nature cell biology *3*, 973-982.
Zhou, X., and He, P. (2011). Temporal and spatial correlation of platelet-activating factor-induced increases in endothelial [Ca(2)(+)]i, nitric oxide, and gap formation in intact venules. American journal of physiology Heart and circulatory physiology *301*, H1788-1797.

Appendix A: List of publications

6.1 Altered transendothelial transport of hormones as a contributor to diabetes

6.2 Transendothleial movement of adiponectin is restricted by glucocorticoid